INHIBITORY SYNAPTIC TRANSMISSION IN EARLY AUDITORY PROCESSING

By

Sidney P. Kuo

A DISSERTATION

Presented to the Neuroscience Graduate Program
and the Oregon Health and Science University
School of Medicine
in partial fulfillment of the
requirements for the degree of

Doctor of Philosophy

April 2011

School of Medicine
Oregon Health & Science University

CERTIFICATE OF APPROVAL

This is to certify that the Ph.D. dissertation of
SIDNEY KUO
has been approved on April 20, 2011

Advisor, Laurence Trussell, PhD

Member and Chair, Peter Gillespie, PhD

Member, Craig Jahr, PhD

Member, William Taylor, PhD

Member, John Williams, PhD

TABLE OF CONTENTS

ACKNOWLEDGEMENTS

I am indebted to many individuals who contributed to this work.

First, I am grateful to my mentor, Larry Trussell, for always providing thoughtful guidance and support and for encouraging me to think deeply about science. I could not have asked for a better teacher to introduce me to cellular neurophysiology and I feel very fortunate to have had the opportunity to learn from Larry.

I also thank the many past and present members of the Trussell lab that I had the pleasure to work with. I am particularly grateful to Kevin Bender and Michael Roberts, who were essentially secondary mentors and who were a constant source of advice, help and friendship. I also thank Trillium Blackmer, Hai Huang, Yuil Kim and Tao Lu for providing technical advice and suggestions which made this work possible.

I thank my parents for their encouragement.

I thank my son, Eddie Kuo, for being himself and for making the past year a joyful one.

Finally and most of all, I thank my wife, Lizzie Brodeen-Kuo. I cannot fully express how much her love, support and encouragement has meant as I have pursued this work, but none of this would have been possible without her.

ABSTRACT

The brainstem cochlear nuclei form the initial stage for sound processing in the brain. Synaptic inhibition has multiple roles in shaping the output of the neuronal circuits that comprise the cochlear nuclei, yet how inhibitory neurons contribute to cochlear nucleus function is incompletely understood. To identify some of the basic mechanisms that define how inhibition contributes to acoustic processing in the cochlear nuclei, the physiology of auditory brainstem inhibitory neurons and synapses was examined using patch-clamp electrophysiological recording techniques in *in vitro* brainstem slice preparations.

Birds have provided an important model system for investigating sound processing. In Chapter 1, inhibitory currents were compared between functionally distinct nuclei in the chick auditory brainstem. The time course of synaptic inhibition was different between nuclei specialized for relaying temporal information, comparing the timing of binaural inputs, or processing sound intensity information, despite a common presynaptic source for inhibitory input. Further, inhibitory currents in the sound intensity nucleus were mediated by both glycine and $GABA_A$ receptors, in contrast to purely GABAergic transmission in regions dedicated to temporal processing. These results indicated that postsynaptic mechanisms contribute to specialization of inhibitory transmission among functionally distinct avian brainstem nuclei.

Inhibitory inputs from multiple classes of interneuron converge upon principal neurons of the mammalian dorsal cochlear nucleus (DCN). In Chapter 2, intrinsic and synaptic features of vertical cells, the primary type of glycinergic neuron found in the DCN deep layer, were investigated. Vertical cells exhibited diverse action potential firing

characteristics, but were consistently able to sustain high rates of spiking, similar to other fast spiking neuron types in the brain. However, vertical cells provided unexpectedly weak input to principal neurons and single presynaptic vertical cells were not capable of strongly influencing principal neuron spike output. Thus, coordinated recruitment of multiple vertical cells is required to inhibit principal neuron activity.

In Chapter 3, inhibition mediated by the other major class of DCN glycinergic interneuron, cartwheel cells, was studied. In contrast to vertical neurons, cartwheel cells spontaneously fire action potentials, even without synaptic input. Thus, an important question is how stimulus-evoked inhibition mediated by cartwheel cells can be distinguished from inhibitory signals arising from spontaneous activity. By simultaneously reducing spontaneous inhibitory currents while strengthening stimulus-evoked cartwheel cell output, noradrenaline enhanced the signal-to-noise ratio for evoked cartwheel-cell mediated inhibition of principal neurons. Both effects were due to noradrenergic silencing of spontaneous cartwheel cell spiking. As firing decreased, spontaneous synaptic output was reduced and cartwheel cell synapses recovered from a tonically depressed state, which resulted in enhanced stimulus-evoked output. Thus, control of spontaneous spike rate provides a simple yet powerful mechanism to shift the balance between spontaneous and stimulus-evoked inhibition.

INTRODUCTION

Our senses form the basis for how we interact with the external world. Diverse physical stimuli are transduced by sensory organs into patterns of neuronal action potential firing in sensory afferent fibers, which convey all the information available to the brain about the environment. How are sensory signals encoded and represented in the brain? This basic question motivates studies that span the range of neuroscience research. An important issue is how excitatory and inhibitory signals are integrated to control the output of neural circuits that constitute the various sensory systems. The work presented in this thesis was focused upon understanding the cellular and synaptic features that define how neurons that release the inhibitory neurotransmitters glycine and/or γ-Aminobutyric acid (GABA) contribute to the representation of acoustic information in the brainstem cochlear nuclei, the first sites of auditory processing in the brain. These studies primarily utilized single cell patch-clamp electrophysiological recording techniques in brainstem slice preparations to investigate the physiology of inhibitory neurons and synapses in auditory circuits. Because examination of both avian and mammalian auditory systems has provided important insight into computational strategies for extracting meaningful information from the acoustic environment, I investigated inhibitory signaling in both the chicken auditory brainstem (Chapter 1) and the dorsal division of the mouse cochlear nucleus (Chapters 2 and 3).

Parallel processing is established in the cochlear nuclei

In common with other sensory systems, different features of acoustic signals are extracted and conveyed in multiple, parallel pathways in the auditory system. Segregation

of sound information begins in the cochlear nuclei, where unique cellular and synaptic properties establish circuits dedicated to particular aspects of sound stimuli (Oertel, 1999; Trussell, 1999). Information from sensory hair cells of the inner ear, which transduce the mechanical vibrations of sound pressure waves into electrical signals (Hudspeth, 1989), arrives in the cochlear nuclei via the auditory nerve and is encoded in the anatomical organization and firing pattern of inputs. Individual hair cells tuned to different frequencies are arranged within the cochlea in a spatial map of sound frequency (Fettiplace and Fuchs, 1999). This tonotopic arrangement is a fundamental organizing principle of the auditory system and is preserved in the projection pattern of auditory nerve fibers to the cochlear nuclei and through ascending levels of the auditory pathway (Smith, 2002). Phase-locking, in which action potentials occur at a consistent point in the period of a sound wave, can also convey frequency information at low sound frequencies (Rose et al., 1967). Sound intensity is represented in the average firing rate of auditory nerve fibers, with increasing sound level corresponding to higher firing rates (Sachs and Abbas, 1974)**.** Functional specialization within the cochlear nuclei is reflected in a diversity of responses to acoustic stimuli; the firing pattern of some cells mirrors that of auditory nerve fibers, whereas others transform their inputs to represent particular characteristics of sounds (Koppl and Carr, 2003; Rhode, 1992). The different response patterns of cochlear nuclei neurons convey specific attributes of acoustic information to higher auditory regions and form the initial basis for parallel processing in the auditory system. Knowledge of the cellular and synaptic mechanisms that determine how cochlear nucleus neurons respond to sound is therefore critical to understanding how the acoustic environment is represented in the brain. Although significant progress has been made in

understanding how anatomical specializations, intrinsic membrane properties, and features of excitatory synaptic transmission contributes to sound processing in cochlear nucleus neurons (Oertel, 1999; Trussell, 1999), relatively less is known regarding the role of inhibitory signaling.

Sound localization

A basic and critical function of the auditory system is to identify the location of sound sources. Across species, survival depends on the ability to identify from where in space behaviorally relevant sounds, such as those made by predators or prey, arise. Sound localization presents a unique challenge because, unlike in the visual system, where the locations of sensory inputs are mapped topographically in the activation pattern of retinal photoreceptors, spatial information is not explicitly encoded by cochlear hair cells. Instead, the auditory systems of both birds and mammals rely upon specific cues from the acoustic environment, including the differential timing and intensity of sounds arriving at the two ears (Joris and Yin, 2007; Konishi, 2003), to compute from where a sound arises. In both birds and mammals, neuronal circuits dedicated to the processing of timing and intensity cues are first established in the cochlear nuclei and their synaptic targets (Konishi, 2003). Monoaural cues derived from the frequency (spectral) content of sounds are thought to provide additional information used in sound localization, at least in mammals (Oertel and Young, 2004).

Avian cochlear nuclei

In birds, the auditory nerve innervates two anatomically distinct subdivisions of the cochlear nucleus, nucleus magnocellularis (nMag) and nucleus angularis (nAng) (Parks and Rubel, 1978). Nucleus magnocellularis and nAng are each organized in a tonotopic representation of sound frequency, but are specialized for different computational tasks; timing information is encoded in nMag whereas nAng is dedicated to sound intensity (Sullivan and Konishi, 1984; Takahashi et al., 1984). Nucleus magnocellularis neurons bilaterally relay, or even improve upon (Fukui et al., 2006), the precise temporal information contained in the phase-locked firing pattern of auditory nerve inputs to cells in nucleus laminaris (nLam). Nucleus laminaris neurons use this information to signal sub-millisecond differences in sound arrival time between each ear that arise when a sound originates closer to one side of the head than the other (Carr and Konishi, 1990). Termed interaural timing differences (ITDs), these cues are a principal mechanism for localizing sound sources in the horizontal plane.

Phase information is not well preserved in nAng (Koppl and Carr, 2003; Sullivan and Konishi, 1984). Rather, nAng is thought to represent the first stage in processing of sound intensity (Sullivan and Konishi, 1984; Takahashi et al., 1984). Understanding of nAng lags behind that of nMag and nLam, but unlike nMag, nAng is clearly a heterogeneous nucleus containing cells with diverse morphologies and response properties (Fukui and Ohmori, 2003; Koppl and Carr, 2003; Soares and Carr, 2001; Soares et al., 2002). This observation, considered along with extreme specialization for temporal coding in nMag, has led to the proposal that *all* non-temporal aspects of sound information ascend through nAng (Soares et al., 2002).

Inhibition in the avian auditory brainstem

Nucleus angularis and nMag, as well as nLam, each receive significant inhibitory synaptic input, the majority of which is thought to arise from the same ipsilateral source, the superior olivary nucleus (SON) (Figure 1.1) (Burger et al., 2005; Lachica et al., 1994; Monsivais et al., 2000). SON receives excitatory projections from nAng and nLam, giving rise to a feed-back inhibitory projection (Carr et al., 1989; Lachica et al., 1994). Immunohistochemical localization of glycine and GABA indicated inhibition in the chick auditory brainstem is predominantly GABAergic (Code and Rubel, 1989; Lachica et al., 1994; von Bartheld et al., 1989). Indeed, the idea of glycine as an inhibitory transmitter in the avian auditory system has been largely ignored.

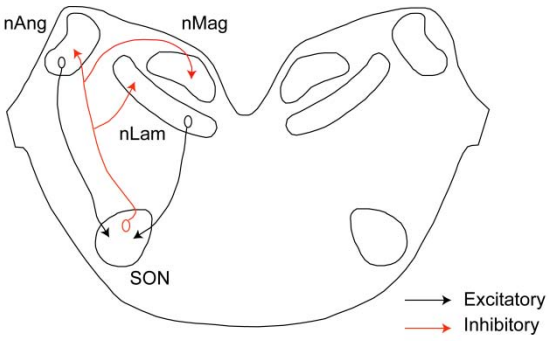

Figure 1. Proposed major inhibitory projections in chicken auditory brainstem. Diagram is representation of a coronal section through the chick brainstem. nAng, nMag and nLam receive inhibitory input (red) from ipsilateral SON. SON receives excitatory input (black) from ipsilateral nAng and nLam. Adapted from Burger et al., 2005.

Studies of inhibition in the avian auditory brainstem have focused almost exclusively on the timing pathway. In nMag and nLam, inhibitory input enhances timing sensitivity by introducing a shunting membrane conductance that narrows the temporal integration window for excitatory inputs and increases the amount of current required to reach spike threshold (Funabiki et al., 1998; Howard et al., 2007; Howard and Rubel, 2010; Monsivais and Rubel, 2001; Monsivais et al., 2000). Additionally, SON input may function to preserve ITD coding across sound levels by opposing increased nMag cell activity in response to loud sounds that might otherwise allow monoaural input alone to drive firing in nLam cells (Burger et al., 2005).

The properties of synaptic inhibition underlying these functions have primarily been examined in nMag. In contrast to the extremely rapid kinetics of AMPA receptor-mediated excitatory postsynaptic currents (EPSCs) in nMag, evoked and spontaneous inhibitory postsynaptic currents (IPSCs) are relatively long in duration (decay time constant ~30 ms at 35ºC) (Lu and Trussell, 2000; Lu et al., 2005). Bicuculline and SR-95531, selective $GABA_A$ receptor antagonists, block IPSCs in nMag and nLam (Lu and Trussell, 2000; Lu et al., 2005). Additionally, the reversal potential for GABAergic inputs (E_{GABA}) is depolarized (E_{GABA} ~ -35 to -25 mV) relative to resting membrane potential (~ -60 mV)**,** even in mature chicks (Howard et al., 2007; Lu and Trussell, 2001; Monsivais and Rubel, 2001). Depolarizing inhibition is thought to effectively reduce excitability in nMag by activating a low threshold K^+ conductance and inactivating voltage-gated Na^+ channels (Howard et al., 2007; Howard and Rubel, 2010; Monsivais and Rubel, 2001). SON inputs are not likely to phase-lock to acoustic stimuli (Yang et al., 1999) and evoked IPSCs exhibit profound asynchrony of release at high stimulus frequencies (Lu and Trussell, 2000). Thus, inhibitory transmission in nMag is long lasting and temporally imprecise. Inhibition has not previously been directly studied in nAng, but *in vivo* response properties of some nAng neurons exhibit clear inhibitory influences (Koppl and Carr, 2003). While the role of inhibition is not clear, the distinct function and cellular response characteristics of nAng raise the possibility that inhibitory mechanisms may be different than in nMag, despite a shared source of inhibitory input. We examined this hypothesis in the study described in Chapter 1 by making whole-cell patch-clamp recordings of inhibitory synaptic currents from neurons in nMag, nLam and nAng in acutely prepared brainstem slices from late-stage chick embryos.

Anatomy of the mammalian dorsal cochlear nucleus

In mammals, the auditory nerve bifurcates to tonotopically innervate the anteroventral cochlear nucleus (AVCN) rostrally and the posteroventral and dorsal cochlear nuclei (PVCN and DCN) caudally (Ryugo and May, 1993). The DCN, which does not appear to have an avian counterpart, has a laminar organization with three primary layers oriented parallel to the surface of the nucleus (Figure 2) (Oertel and Young, 2004). As with other auditory regions, the innervation pattern of auditory inputs targeting the DCN are arranged tonotopically into a spatial map of sound frequency. The main principal neurons of the DCN, termed fusiform cells, reside within the middle, fusiform cell layer. Fusiform cells extend spiny apical dendrites into the outermost, molecular layer and smooth basal dendrites into the deep layer (Blackstad et al., 1984; Rhode et al., 1983; Smith and Rhode, 1985; Zhang and Oertel, 1994). These dendrites are oriented parallel to isofrequency laminae (Blackstad et al., 1984), which likely underlies their narrow frequency tuning (Rhode et al., 1983). Giant cells are the other principal neuron type in the DCN and are found in the deep layer (Zhang and Oertel, 1993b). Fusiform and giant cells constitute the sole pathway through which the DCN conveys information to its targets in the inferior colliculus (Joris, 1998; Oertel and Young, 2004; Young, 1980).

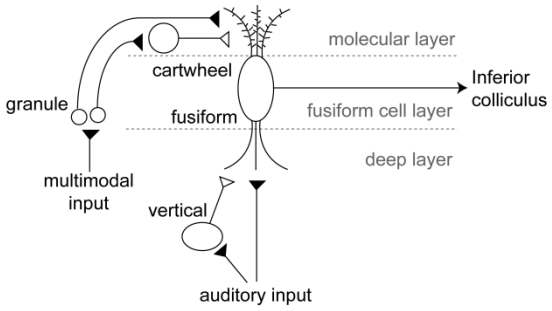

Figure 2. Simplified diagram of DCN circuitry. Vertical cells provide feed-forward inhibition associated with deep layer auditory inputs that transmit information from the cochlea. Cartwheel cells provide feed-forward inhibition associated with granule cell parallel fiber inputs in the molecular layer, which convey multimodal information. Filled triangles represent glutamatergic synapses. Open triangles represent glycinergic synapses. Gray dotted lines represent boundaries of different layers.

Acoustic information from the cochlea enters the DCN through the deep layer. Auditory nerve fibers, as well as axons from VCN T-stellate cells, innervate giant cells and the basal dendrites and somata of fusiform cells (Doucet and Ryugo, 1997; Oertel et al., 1990; Rubio and Juiz, 2004; Ryugo and May, 1993; Smith and Rhode, 1985). These excitatory inputs also contact vertical cells (Rubio and Juiz, 2004) (also termed tuberculoventral or corn cells), which are the most abundant cell type in the deep layer (Lorente de No, 1981). Similar to fusiform neurons, vertical cell dendrites are restricted to isofrequency bands and are thus narrowly tuned (Rhode, 1999; Zhang and Oertel, 1993c). Vertical cells are glycinergic (Kolston et al., 1992; Saint Marie et al., 1991) and project local axon collaterals within the deep layer as well as into the VCN (Lorente de No, 1981; Zhang and Oertel, 1993c). Vertical cell axons synapse upon fusiform cells (Rhode, 1999) and cross-correlation analysis of simultaneous *in vivo* extracellular recordings of tone-evoked responses in vertical and principal neurons indicated vertical cells inhibit fusiform cells (Voigt and Young, 1990). Indeed, vertical cells are hypothesized to have a central role in shaping the acoustic response properties of DCN principal neurons (Young and Davis, 2002) (see below).

The DCN is unique among the mammalian cochlear nuclei in that it receives significant non-auditory input. DCN granule cells, which reside in the fusiform cell layer and in granule cell regions between DCN and VCN, are contacted by excitatory mossy fiber endings that convey information from multiple sources, including vestibular, somatosensory, and higher auditory regions (Ryugo et al., 2003; Shore and Zhou, 2006). The DCN granule cell system is analogous to that of the cerebellum (Mugnaini et al., 1980). Granule cell parallel fiber axons project through the DCN molecular layer, where

they make direct excitatory contact with apical dendrites of fusiform cells as well as with inhibitory interneurons including stellate, Golgi, and cartwheel cells (Mugnaini, 1985). Cartwheel cells are unique among DCN neurons in their ability to fire high frequency bursts of action potentials (usually 2-5 spikes at ~200 Hz), termed complex spikes (Manis et al., 1994; Zhang and Oertel, 1993a), and constitute the largest population of cells in the molecular layer (Lorente de No, 1981). Cartwheel cells form strong, predominantly glycinergic synapses on nearby fusiform cells and cartwheel cells with high connection probability (Mancilla and Manis, 2009; Roberts et al., 2008; Roberts and Trussell, 2010) and their activity can strongly filter the response properties of DCN principal neurons (Davis et al., 1996b; Davis and Young, 1997; Shore, 2005).

Role of the DCN

The role of the DCN is not well understood. However, one proposed function is to process and encode spectral cues used to localize sounds (Oertel and Young, 2004; Young and Davis, 2002). The shape of the head and the external ear (pinna) filters acoustic signals in a characteristic manner, termed the head-related transfer function (Musicant et al., 1990; Rice et al., 1992). Compared to sounds in free-field, sounds that reach the ear drum are altered such that some frequencies are emphasized while energy at other frequencies is diminished. The position of peaks and notches in the sound frequency spectrum depends upon the position of a sound source, thus providing a spectral cue for localization (Oertel and Young, 2004). Consistent with a role in sound localization, lesioning the dorsal acoustic stria, through which axons of DCN principal neurons project on their way to the inferior colliculus, results in deficits in the ability to

orient the head to sounds in cats (May, 2000; Sutherland et al., 1998). Examination of *in vivo* responses to sound stimuli indicates DCN principal cells are tuned to detect spectral peaks and thus could encode spectral cues used for localization in the vertical plane (Young and Davis, 2002). This specialization is hypothesized to depend upon the unique circuitry of the DCN and, in particular, upon the interaction of inhibitory interneurons with principal cells.

In vivo response properties of DCN principal neurons

The *in vivo* sound-evoked response characteristics of DCN principal cells are heterogeneous and depend on the experimental preparation used to acquire recordings. The basis for this heterogeneity is unknown although differential inhibitory influences may play a role. Extracellular recordings of single unit activity from DCN of either anesthetized or unanesthetized, decerebrate cats have provided most of the information regarding sound-evoked firing patterns of principal neurons. Two methods have been used to categorize data from these preparations. One scheme relies upon analysis of peristimulus time histograms (PSTHs), which represent the temporal spiking pattern of units in response to pure tones presented at a cell's most sensitive frequency (best frequency), and has been used primarily to analyze responses from anesthetized animals (Godfrey et al., 1975; Pfeiffer, 1966). The other approach, applied most frequently to recordings from decerebrate preparations, utilizes a response map classification system in which excitatory and inhibitory responses are characterized over a range of frequencies and intensities (Evans and Nelson, 1973).

The most commonly encountered unit types in barbiturate-anesthetized cat DCN are termed "pauser" and "buildup" responses based on the characteristic shape of their PSTHs (Godfrey et al., 1975; Rhode et al., 1983). Pauser units exhibit sharp increases in firing rate at stimulus onset, followed closely by a spike-free period after which firing slowly increases. Buildup units gradually increase in discharge rate over the course of tone stimuli. Intracellular labeling identified cells exhibiting both response types as fusiform cells (Rhode et al., 1983; Smith and Rhode, 1985). Pauser/buildup units exhibit excitatory responses at all levels of best frequency tone presentation. Previous studies suggested pauser and buildup behaviors arise from the intrinsic electrical properties of fusiform neurons, specifically the expression of a fast-inactivating K^+ current (Manis, 1990; Kanold and Manis, 1999). Whether inhibition might also contribute to the expression of these response patterns is not known. Notably, hyperpolarizations have been observed to occur during pause responses in *in vivo* intracellular recordings (Smith and Rhode, 1985).

In decerebrate cats, principal neurons exhibit several characteristic response patterns to sound, the most frequently observed of which is termed Type IV (Young, 1980; Young and Brownell, 1976). Type IV units are distinguished by a prominent contribution of inhibition to their response profile; low sound-level presentation of best frequency tones results in an increase in firing rate, but higher intensity best frequency tones (~20 decibels above threshold) result in inhibition of spontaneous firing. Type IV units exhibit "onset-inhibitory" PSTHs characterized by brief spiking at tone onset followed by silence, or "on-off" responses, which are similar, but fire briefly at tone offset (Shofner and Young, 1985). Type III responses, which have excitatory responses to

all sound levels of best frequency tones are also recorded in decerebrate cats, but less frequently than Type IV units. Type III units likely correspond to the pauser/buildup response patterns described above. Of note, Type III responses are more commonly recorded in both anesthetized and decerebrate gerbil preparations, although some Type IV responses are also observed (Davis et al., 1996a; Ding and Voigt, 1997; Hancock and Voigt, 2002). In an *in vivo* study in awake mice, principal neurons only showed Type III responses and Type IV responses were not observed (Roberts and Portfors, 2008).

The inhibitory responses observed for Type IV units clearly demonstrate inhibition plays an integral role in determining this response type. Additionally, focal application of the glycine receptor antagonist strychnine at the recording site eliminates inhibitory responses of Type IV cells to best frequency tones (Davis and Young, 2000). Tone-evoked glycinergic input to principal cells has been attributed to feed-forward inhibition from similarly tuned vertical cells (Nelken and Young, 1994; Voigt and Young, 1990; Young and Brownell, 1976; Young and Davis, 2002). Vertical cells, which are classified as Type II units in the response map classification scheme, are excited at all sound levels of best frequency tones (Rhode, 1999; Shofner and Young, 1985; Spirou et al., 1999; Zafra et al., 1995) and tone-evoked activity in Type II units is correlated with inhibition of spiking in Type IV cells (Voigt and Young, 1990). Additonally, the observation that vertical cells respond weakly to broadband noise, if at all (Rhode, 1999; Shofner and Young, 1985; Spirou et al., 1999; Zafra et al., 1995), is consistent with the excitatory responses produced at all sound levels of broadband noise stimulation in principal cells (Nelken and Young, 1994; Spirou and Young, 1991; Young and Brownell, 1976). Although *in vivo* evidence supports a role for vertical cells in shaping principal

neuron output, vertical cells have only rarely been studied using intracellular recordings and little is known regarding the cellular and synaptic mechanisms that underlie how vertical cells operate in the DCN. In the work described in Chapter 2, we used transgenic mice in which enhanced green fluorescent protein (EGFP) is expressed in glycinergic neurons to target vertical cells for whole-cell patch-clamp recordings in slices of mouse DCN.

Spontaneous cartwheel cell spiking

Cartwheel cells of the molecular layer provide an additional important source of inhibitory input to principal neurons. Because cartwheel cells receive excitatory input from parallel fibers (Mugnaini, 1985; Rubio and Juiz, 2004), cartwheel cell-mediated inhibition is thought to filter the auditory response properties of principal neurons according to activity in the diverse sensory regions that provide mossy fiber input to granule cells (Oertel and Young, 2004). By providing a substrate for the integration of spectral information with somatosensory and proprioceptive information about the orientation of the head and ears in space, in particular somatosensory inputs that signal the position of the pinna , the molecular layer circuitry in which cartwheel cells participate is hypothesized to contribute importantly to sound localization (Oertel and Young, 2004; Young and Davis, 2002). By analogy with similar cerebellum-like electrosensory structures in weakly electric fish, an additional proposal is that the DCN molecular layer circuitry functions as an adaptive filter to cancel sounds that are not behaviorally relevant, such as self- or movement-generated noise (Bell et al., 2008;

Oertel and Young, 2004). Notably, cartwheel cell-mediated inhibition is central to both proposed functions of the DCN molecular layer.

An important feature of cartwheel cells is that they fire action potentials spontaneously, both *in vivo* (Davis et al., 1996b; Davis and Young, 1997; Portfors and Roberts, 2007) and *in vitro* (Golding and Oertel, 1997; Kim and Trussell, 2007). This is distinct from vertical cells. In fact, lack of spontaneous activity is a distinguishing feature used to classify Type II (vertical cell) responses recorded *in vivo* (Joris, 1998; Shofner and Young, 1985; Spirou et al., 1999). Because they are spontaneously active, cartwheel cells provide fluctuating synaptic input to their postsynaptic targets, including principal neurons, even in the absence of external stimuli (Golding and Oertel, 1997; Roberts and Trussell, 2010). As briefly described in the preceding paragraph, cartwheel cell-mediated inhibition of principal neurons in response to parallel fiber activity is thought to be critical to DCN function. However, it is unclear whether mechanisms are in place to allow postsynaptic targets to distinguish between parallel fiber-evoked versus spontaneous cartwheel cell inhibition. In the work described in chapter 3, we elucidated a mechanism by which the neuromodulatory transmitter noradrenaline (NA) shifts the balance between spontaneous and evoked cartwheel cell-mediated inhibition to favor inhibition elicited by parallel fiber activity.

CHAPTER 1. HETEROGENEOUS KINETICS AND PHARMACOLOGY OF SYNAPTIC INHIBITION IN THE CHICK AUDITORY BRAINSTEM

Sidney P. Kuo[1, 2], Laura A. Bradley[2], and Laurence O. Trussell[1, 2]

[1]Neuroscience Graduate Program and [2]Oregon Hearing Research Center and Vollum Institute, Oregon Health and Science University, Portland, OR 97239

Abstract

Identification of shared features between avian and mammalian auditory brainstem circuits has provided much insight into the mechanisms underlying early auditory processing. However, previous studies have highlighted an apparent difference in inhibitory systems; synaptic inhibition is thought to be slow and GABAergic in birds, but to have fast kinetics and be predominantly glycinergic in mammals. Using patch-clamp recordings in chick brainstem slices, we found this distinction is not exclusively true. Consistent with previous work, inhibitory postsynaptic currents (IPSCs) in nucleus magnocellularis (nMag) were slow and mediated by $GABA_A$ receptors. However, IPSCs in nucleus laminaris (nLam) and a subset of neurons in nucleus angularis (nAng) had rapid time courses two to three-fold faster than those in nMag. Further, we found IPSCs in nAng were mediated by both glycine and $GABA_A$ receptors, demonstrating for the first time a role for fast glycinergic transmission in the avian auditory brainstem. Although nMag, nLam and nAng have unique roles in auditory processing, the majority of inhibitory input to each nucleus arises from the same source, ipsilateral superior olivary nucleus (SON). Our results demonstrate remarkable diversity of inhibitory transmission among the avian brainstem nuclei and suggest differential glycine and $GABA_A$ receptor activity tailors inhibition to the specific functional roles of nMag, nLam, and nAng despite common SON input. We additionally observed that glycinergic/GABAergic activity in nAng was usually depolarizing and could elicit spiking activity in nAng neurons. Because nAng projects to SON, these excitatory effects may influence the recruitment of inhibitory activity in the brainstem nuclei.

Introduction

The vertebrate auditory system utilizes several environmental cues to determine the location of sound sources, including the relative timing and intensity of acoustic signals between the two ears (Konishi, 2003). In both birds and mammals, specialized circuits devoted to these distinct sound characteristics are established in the brainstem. In birds, auditory nerve fibers diverge to innervate nucleus magnocellularis and nucleus angularis (Parks and Rubel, 1978). Neurons in nMag bilaterally relay precise timing information to targets in nucleus laminaris (Boord, 1968; Fukui et al., 2006; Parks and Rubel, 1975). nLam neurons rely on these signals to compute sub-millisecond differences in sound arrival time between each ear that arise when a sound originates closer to one side of the head, termed interaural timing differences (ITDs) (Carr and Konishi, 1990; Konishi, 2003). In contrast, nAng is thought to represent the first stage in the processing of sound intensity, as well as other non-timing aspects of auditory signals (MacLeod and Carr, 2007; Sullivan and Konishi, 1984; Takahashi et al., 1984).

Examination of the intrinsic properties of auditory brainstem neurons as well as their excitatory inputs have revealed similar anatomical and biophysical specializations in the avian and mammalian brainstem nuclei, indicating shared principles for encoding sound (Carr and Soares, 2002; Oertel, 1999; Trussell, 1999). However, investigations of inhibitory synaptic transmission suggested a striking distinction between birds and mammals. In mammals, inhibition undergoes a developmental switch from GABAergic in immature animals to predominantly glycinergic transmission in the adult (Awatramani et al., 2005; Kotak et al., 1998; Nabekura et al., 2004; Smith et al., 2000). Glycinergic currents in the mammalian brainstem typically have rapid kinetics, with decay time

constants of only a few milliseconds or less (Awatramani et al., 2004; Magnusson et al., 2005; Smith et al., 2000), and can retain the phase-locked temporal structure of auditory signals. By contrast, inhibition in the avian auditory brainstem is thought to be GABAergic throughout development (Code and Rubel, 1989; Lachica et al., 1994; von Bartheld et al., 1989). In nMag, where IPSCs have slow kinetics, GABA release becomes asynchronous at high rates of activity and IPSCs summate to mediate tonic inhibition (Lu and Trussell, 2000). The anatomy of inhibition is also unique in birds; inhibition to nMag, nLam, and nAng arises predominantly from the same source, ipsilateral superior olivary nucleus (Burger et al., 2005; Lachica et al., 1994; Monsivais et al., 2000), which is not thought to provide phase-locked inhibition to its targets (Lachica et al., 1994; Yang et al., 1999). SON receives excitatory projections from ipsilateral nLam and nAng. These distinctions have led to the suggestion that inhibition serves fundamentally different roles in birds and mammals (Grothe, 2003). We tested this generalization by examining inhibitory transmission in nMag, nLam and nAng neurons in slices of embryonic chick brainstem.

Methods

Tissue preparation

Coronal slices of brainstem (250 μm thick) were prepared from 17-20 day-old chick embryos (E17-E20). In experiments using hatchling chicks (post-hatch day 0), chicks were deeply anesthetized with isofluorane prior to sacrifice. Following decapitation, a portion of brainstem containing the auditory nuclei was blocked in the coronal plane and affixed to the stage of a vibratome (Leica VT1000S or VT1200S;

Wetzlar, Germany), then sectioned. During dissection and slicing, tissue remained immersed in an oxygenated saline solution containing (in mM): 140 NaCl, 5 KCl, 3 $CaCl_2$, 1 $MgCl_2$, 10 HEPES, 10 glucose; 300 mOsm, pH'd to 7.4 using NaOH, that was warmed to ~35ºC. After sectioning, slices were allowed to recover in the same solution at 35ºC for one hour then transferred to a recording chamber or maintained at room temperature (~22ºC) until use.

Electrophysiology

During recordings, slices were continuously perfused with oxygenated saline solution identical to that used for slice preparation, but with the addition of 6,7-dinitroquinoxaline-2,3-dione (DNQX; 20 μM) and DL-2-amino-5-phosphonopentanoic acid (DL-APV; 100 μM). For all experiments, bath solution was warmed to 35 $\pm$ 1ºC using an in-line heater (Warner Instruments; Hamden, CT). Bath temperature was constantly monitored with a thermister positioned at the tip of the microscope objective. Cells were visualized for recordings on the stage of an upright microscope (Olympus BX51W; Center Valley, PA) using infrared Dodt interference contrast optics and a 60X magnification objective. Neurons in nMag, nLam and nAng were identified by cellular morphology and location within the slice. Recordings from nMag and nLam were obtained from the caudal 1/3rd of the nuclei, corresponding to the middle to low characteristic frequency regions (Rubel and Parks, 1975). In this study, we did not explore whether tonotopic variation in IPSC properties exists in nMag and nLam. In nAng, cells were recorded throughout the extent of the nucleus. For whole-cell voltage-clamp experiments, patch pipettes were filled with one of two CsCl-based internal

solutions. One contained (in mM): 130 CsCl, 2 $MgCl_2$, 10 TEA-Cl, 10 HEPES, 4 BAPTA-Cs_4, 4 Mg-ATP; 290 mOsm, pH'd to 7.2 with CsOH. The other consisted of (in mM): 120 CsCl, 1.4 $MgCl_2$, 10 TEA-Cl, 0.4 Na_2-GTP, 10 $Tris_2$-phosphocreatine, 4 Mg-ATP, 10 HEPES, 4 BAPTA-Cs_4; 290 mOsm, pH'd to 7.2 with CsOH. QX-314 (1 mM) was sometimes included in the internal solution. IPSCs recorded with either internal solution and with or without QX-314 did not exhibit different decay kinetics or pharmacology, so data using the different CsCl-based internal solutions were pooled. To confirm strychnine blocked a Cl^- -mediated current in nAng neurons (see Results), some recordings were obtained using a low [Cl^-] internal solution containing (in mM): 108 $CsMeSO_3$, 5 CsCl, 1.4 $MgCl_2$, 0.4 Na-GTP, 15 $Tris_2$-phosphocreatine, 4 Mg-ATP, 10 HEPES, 8 BATPA-Cs_4; 290 mOsm, pH'd to 7.2 with CsOH. These measurements were not included in the reported averages. In order to assess the action potential firing phenotype of nAng neurons, recordings from a subset of nAng cells were acquired using a K^+-based internal solution containing (in mM): 81 K-gluconate, 32 KCl, 4.5 $MgCl_2$, 14 $Tris_2$-phosphocreatine, 4 Na_2-ATP, 0.3 Tris-GTP, 9 HEPES, 0.1 EGTA, 0.2 sucrose; 290 mOsm, pH'd to 7.2 with KOH. All recording pipettes were pulled from borosilicate glass (WPI, Sarasota, FL) and had a resistance of 1.5-3 MΩ when filled with CsCl-based internal solution. Reported membrane potential values were corrected for empirically determined junction potentials of -5.9 mV and -11.4 mV for CsCl-based and K^+-based internal solutions, respectively. IPSCs were evoked by locally applying electrical stimuli (<50 μm from soma; 20-60 V, 100-200 μs) through double-barreled glass pipettes (5-10 μm tip diameter) filled with bath solution. In experiments examining evoked IPSCs using the CsCl-based internal solutions, the recorded cell's membrane potential was held at -

35.9 mV. Evoked IPSCs were recorded at -71.4 mV in experiments using the K^+-based pipette solution. Spontaneously occurring IPSCs were measured while the recorded cell's membrane potential was maintained at -65.9 mV. For gramicidin perforated-patch recordings, pipettes were filled with a solution containing: 140 mM KCl, 10 mM NaCl, 10 mM HEPES, 60-100 μg gramicidin D, and 50 μM Alexa Fluor 488. After seal formation, series resistance (R_s) was monitored in voltage-clamp mode by applying a 10 mV voltage step across the pipette tip. Experiments were initiated once R_s declined to 20-50 MΩ, which typically took 20-30 minutes. The integrity of the membrane under the recording electrode was confirmed periodically by checking that Alexa Fluor 488 signal was excluded from the recording pipette. Gramicidin perforated-patch measurements were not corrected for junction potential (Kim and Trussell, 2007). Glycine (1 mM in bath solution) was pressure-applied using a picospritzer (Parker Instrumentation, Cleveland, OH; 100 ms, ~1-2 psi application; 1 psi = 6.89 kPa) through a patch pipette positioned adjacent to the soma of the recorded cell. SR-95531 and strychnine were applied by bath perfusion. Pharmacological agents were obtained from Ascent Scientific (Princeton, NJ) except for strychnine, which was from Sigma-Aldrich (St. Louis, MO). Extracellular and intracellular solution components were obtained from Sigma with the following exceptions: BAPTA-Cs_4 and Alexa Fluor 488 were from Invitrogen (Carlsbad, CA), and QX-314 was from Alomone (Jerusalem, Israel).

Electrophysiological data acquisition and analysis

Recordings were acquired using a MultiClamp 700B amplifier (Molecular Devices; Sunnyvale, CA) and pClamp 10.0 software. Signals were digitized at 20 kHz or

50 kHz using a Digidata 1322A (Molecular Devices) and low-pass filtered at 10 kHz. For whole-cell voltage-clamp experiments, series resistance (< 15MΩ) was compensated 60-80% during recordings. Series resistance was left uncompensated during perforated-patch recordings and was instead monitored continuously throughout the experiments by measuring the peak of the instantaneous current response to 5-10 mV voltage step commands. Membrane potential values for perforated-patch recordings were corrected off-line by subtracting the voltage error, calculated by multiplying holding current by series resistance, from the command holding potential. Analyses were conducted using Clampfit 10.0 (Molecular Devices) or custom procedures written in IgorPro (Wavemetrics; Lake Oswego, OR) (procedures written by M.T. Roberts). The decay phases of evoked IPSCs were fit with exponential functions with one, two, or three components. The best fit was selected by comparing the sum of squared errors between fits with different numbers of exponential components. We selected those fits that resulted in a sum of squared errors of less than half that of a fit with fewer components. Spontaneous IPSCs were detected and aligned using the variable-amplitude template function event detection feature of Axograph X (Sydney, Australia). Due to the small amplitudes of many of the spontaneous IPSCs, we determined their time courses by normalizing all events to their peak amplitudes and fitting a single exponential function to decay phases of the IPSCs. Fits obtained in this manner were visually inspected and events in which we were unable to satisfactorily fit the data, which represented a small minority of the total number of events, were removed. All reported values are mean $\pm$ S.D. Unless noted otherwise, statistical significance ($p < 0.05$) was tested using paired two-tailed Student's t-tests.

Immunohistochemistry

Chicks were transcardially perfused with warm (~40ºC) phosphate buffered saline (PBS) solution (0.1 M, pH 7.4) followed by ice cold 1% formaldehyde and 2% glutaraldehyde in PBS. The brains were removed from the skulls, rinsed in PBS and sectioned at 30 μm on a vibratome. After sectioning, the tissue was washed, then incubated in 1% sodium borohydride in PBS for 30 minutes at room temperature to reduce background glutaraldehyde fluorescence. After extensive washing, the tissue was incubated in block solution consisting of 2% normal goat serum, 1% bovine serum albumin (BSA), and 0.1% saponin in PBS for one hour at room temperature, followed by overnight 4ºC co-incubation with primary antibodies to glycine (rabbit anti-glycine; 1:200 or 1:1000; AB139, lots 0610044052 and LV1508357; Millipore; Temecula, CA) and GABA (mouse anti-GABA; 1:10,000; mAB 3A12, lot ps2; Swant; Bellinzona, Switzerland) diluted in block solution. Both antibodies were raised to their respective target neurotransmitter conjugated to BSA by glutaraldehyde and have been previously used in chick nervous tissue (Kalloniatis and Fletcher, 1993; Matute and Streit, 1986). After primary antibody incubation, sections were washed and incubated for two hours at room temperature with fluorescence-conjugated secondary antibodies (Alexa Fluor 488 goat anti-mouse and Alexa Fluor 568 or 633 goat anti-rabbit; 1:500; Invitrogen). After washing, sections were mounted on slides, dehydrated in ascending alcohols and delipidized in xylenes. The tissue was then rehydrated and coverslipped using Fluoromount G medium (Southern Biotech; Birmingham, AL).

Antibody specificity controls

Preadsorption control experiments were performed to confirm specificity of the anti-Gly and anti-GABA antibodies under the fixation and tissue preparation conditions used in this study (Supplementary Figure 1.1). Anti-Gly or anti-GABA antibodies were pre-incubated with glycine-BSA or GABA-BSA conjugates (Abcam; Cambridge, MA) for 24-48 hours at 4ºC prior to application to tissue sections. Preadsorption control tissue was compared in parallel with tissue from the same animal in which the antibodies were applied without preadsorption. Pre-incubation of anti-Gly antibody with a 100-fold molar excess of Gly-BSA protein eliminated glycine-like immunoreactivity (Figure 1.S1A, B). Likewise, preincubation of anti-GABA antibody with a 100-fold molar excess of GABA-BSA protein resulted in a greatly reduced GABA-like immunoreaction (Figure 1.S1E, F). When anti-Gly was pre-incubated with the same amount of GABA-BSA used to block the anti-GABA reaction, glycine-like labeling was preserved (Figure 1.S1C, D) and pre-incubation of anti-GABA with the same amount of gly-BSA used to block anti-Gly labeling did not inhibit anti-GABA labeling (Figure 1.S1G, H). Background fluorescence was assessed in all immunohistochemistry experiments by examining tissue processed identically to experimental samples but in which primary antibody was omitted.

Image acquisition and analysis

Fluorescence images were acquired using a confocal microscope (Olympus FV1000) by sequential scanning of Alexa Fluor 488 and Alexa Fluor 568 or Alexa Fluor 633 signals using an oil-immersion objective (60X magnification, nAng = 1.42). Lack of cross-talk between fluorescence channels was confirmed by examining tissue labeled

with only one of each of the secondary antibodies. Image analysis was conducted using ImageJ software (NIH; Bethesda, MD). Overlap between anti-Gly and anti-GABA signals was quantified in single confocal sections acquired at a depth of ~1.5-2 μm below the surface of the tissue from regions within each brainstem nucleus using methods similar to those previously employed by Muller et al. (2006). After applying a median filter to reduce noise, images from the different fluorescence channels were separately thresholded by eye. A binary mask was then applied to each thresholded image and overlapping regions between the binary images representing the different immunofluorescent signals were identified. The total area of overlap for each analyzed image was determined and expressed as a percentage of the total area of anti-GABA or anti-Gly signals.

Results

Evoked IPSCs exhibit region-specific decay kinetics

To compare inhibitory synaptic transmission between nMag, nLam and nAng, we obtained whole-cell voltage-clamp recordings from visually identified neurons within each region in tissue slices of auditory brainstem. IPSCs were evoked by extracellular stimulation and measured in the presence of ionotropic glutamate receptor antagonists (20 μM DNQX, 100 μM DL-APV).

The durations of stimulus-evoked IPSCs were distinct between the different nuclei. Although rise times were similar for IPSCs recorded in nMag, nLam and nAng (Table 1.1, only significant difference between nMag and nLam, $p=0.04$), the decay time courses were distinct among the different nuclei. IPSCs recorded in nMag decayed

approximately three-fold slower than those in nLam (Figure 1.1, Table 1.1). In nAng, IPSCs typically had a fast time course, similar to those recorded in nLam. However, slower currents with kinetics resembling nMag IPSCs were also observed (Figure 1.1, Table 1.1). The decay phases of nMag IPSCs were best fit by the sum of two (n= 4) or three exponentials (n= 7) (see Methods). Weighted time constants were not significantly different between biexponential and three component exponential fits ($p = 0.12$). The mean weighted time constant for IPSCs recorded in nMag neurons was 26.0 $\pm$ 5.0 ms. nLam IPSC decays were best fit by the sum of two exponentials with a weighted time constant of 8.1 $\pm$ 2.1 ms. Fast nAng IPSCs were similar in time course to nLam IPSCs, with a weighted decay time constant of 11.6 $\pm$ 9.0 ms. Slow nAng IPSCs (3/15 cells) were best fit by the sum of three exponentials and had a weighted time constant 23.1 $\pm$ 5.6 ms. Identical IPSC timecourses were also observed in tissue from hatchling chicks (P0). In hatchlings, the mean weighted decay time constants for IPSCs were 25.6 $\pm$ 6.2 ms in nMag (n=4), 8.8 $\pm$ 2.8 ms in nLam (n=4), and 12.0 $\pm$ 5.7 ms in nAng (n=5). Although maximal IPSC peak amplitudes varied widely within each nucleus, IPSCs in nAng were on average smaller than those in nMag and nLam (Table 1.1, $p<0.01$ for nAng compared to nMag or nLam), similar to previous observations of smaller excitatory currents in nAng compared to nMag and nLam (MacLeod and Carr, 2005; MacLeod et al., 2007).

Nucleus angularis is a heterogeneous nucleus composed of several types of neurons with distinct intrinsic firing characteristics (Fukui and Ohmori, 2003; Soares et al., 2002). We therefore recorded from some nAng neurons using a K^+-based pipette solution so that nAng neurons could be characterized in current-clamp configuration prior

to recording IPSCs. We divided neurons into two categories, those that fired only one or two spikes at the beginning of depolarizing current injection (hereafter termed "onset spiking") and those that fired multiple action potentials over the duration of positive current injection ("multiple spiking"). Previous work has subdivided repetitively firing nAng neurons into several categories (Soares et al., 2002), but we grouped all non-onset firing cells together as multiple spiking neurons because we observed they could exhibit different firing patterns depending on their initial membrane potential. Further, Fukui and Ohmori (2003) found nAng neurons could be classified as either tonically firing or onset firing neurons in tissue from post-hatch chicks. Evoked IPSCs recorded from onset firing or multiple spiking nAng neurons had different time courses (Figure 1.2). On average, onset spiking neurons had IPSCs that were significantly faster than those in multiple spiking neurons (weighted τ_{decay} 2.7 $\pm$ 0.8 ms and 16.7 $\pm$ 8.9 ms, respectively; $p < 0.001$). The population of multiple spiking neurons exhibited a range of IPSC decay times (weighted τ_{decay} ranged from 7.6 to 28.6 ms). Although the IPSC decay values cannot be directly compared between cells recorded using the CsCl-based internal solution and the K^+- based internal due to the different pipette solutions and holding potentials used (-35.9 mV for CsCl experiments, -71.4 mV for K^+-gluconate recordings), it is likely the slow IPSCs measured using the CsCl-based internal were recorded from multiple spiking neurons whereas the fast IPSCs were recorded from both onset and multiple spiking neurons.

Distinct pharmacology between the timing and intensity pathways

We tested the neurotransmitter phenotype of evoked IPSCs by bath application of SR-95531 (10-20 μM) and strychnine (0.5 μM), which are antagonists of $GABA_A$ and glycine receptors, respectively. For IPSCs recorded in nAng, we unexpectedly observed SR-95531 application only eliminated a fraction of the inhibitory current recorded in every nAng neuron tested (n = 12). Figure 1.3A shows an example cell in which IPSCs were evoked under control conditions (black trace), then in the presence of SR-95531 (red), then subsequently during application of strychnine after washout of SR-95531 (blue), and finally in the presence of both SR-95531 and strychnine (purple). Neither SR-95531 or strychnine application alone completely blocked evoked currents, but both drugs together eliminated IPSCs, demonstrating the existence of GABAergic and glycinergic components of the inhibitory currents. In addition to its well-characterized effect on glycine receptors, strychnine antagonizes some nicotinic acetylcholine receptor subtypes at the concentrations used in this study (Matsubayashi et al., 1998). To eliminate the possibility the strychnine-sensitive current in nAng neurons was mediated by nicotinic receptors, we performed some recordings using a low $[Cl^-]$ internal solution ($CsMeSO_3$-based solution, see Methods; predicted E_{Cl^-} = -82 mV). Outward currents were recorded at a holding potential of -30 mV both in the presence and absence of SR-95531 under these conditions (not shown, n = 4), consistent with both components of the evoked current being mediated by Cl^--conducting channels.

As summarized in Figure 1.3B, glycinergic and GABAergic components of IPSCs recorded in nAng neurons had distinct kinetics. The decay phases of the glycinergic component of evoked IPSCs, isolated by recording in the presence of SR-95531, were

best fit by the sum of two exponentials (τ_1 = 1.8 $\pm$ 0.4 ms, τ_2 = 5.0 $\pm$ 0.7 ms; % τ_1 = 41.7 $\pm$ 3.4%) except for two cells whose decays were fit adequately with a single exponential function (τ = 2.1 ms and 3.8 ms) (mean τ_{decay} for all cells = 3.1 $\pm$ 0.6 ms). The GABAergic component of evoked IPSCs, isolated pharmacologically using strychnine or by digital subtraction of traces acquired during SR-95531 application from control current traces, had decays best fit with the sum of two exponentials (τ_1 = 6.0 $\pm$ 1.4 ms, τ_2 = 35.1$\pm$ 4.2 ms; % τ_1 = 63.5 $\pm$ 8.6%) with a weighted time constant of 16.9 $\pm$ 3.8 ms.

In agreement with previous findings, evoked IPSCs in nMag and nLam were blocked $\geq$ 95% upon bath application SR-95531 (10-20 μM) (Figure 1.3C) (Funabiki et al., 1998; Howard et al., 2007; Lu and Trussell, 2000; Lu et al., 2005; Monsivais et al., 2000; Yang et al., 1999). In the five nAng neurons recorded with the CsCl-based pipette solution, SR-95531 reduced the peak amplitude of the control IPSC by 47.6 $\pm$ 14.2% (range 33.6% to 68.4 %) (Figure 1.3C).

Evidence for co-release of GABA and glycine in nAng

In nAng, the glycinergic and GABAergic components of evoked IPSCs we observed could arise from the simultaneous recruitment of distinct inhibitory fibers or from co-release of both neurotransmitters from the same presynaptic neuron (Awatramani et al., 2005; Jonas et al., 1998). To distinguish between these possibilities, we recorded spontaneously occurring IPSCs (sIPSCs) from nAng neurons under control conditions and in the presence of SR-95531 or strychnine. Because these sIPSCs represented a mixture of random vesicle fusion events (miniature IPSCs) and spontaneous action potential evoked release, this approach allowed us to monitor activity of single

presynaptic fibers and therefore address whether GABA and glycine can be released from the same presynaptic neuron. Figure 1.4A-C shows example peak amplitude-scaled control sIPSCs and those recorded during SR-95531 or strychnine application for one nAng neuron. A summary of IPSC decay kinetics for each condition from four nAng neurons is presented in Figure 1.4D. In control conditions, the mean decay time constants for sIPSCs ranged from 1.0 to 40.2 ms, with a mean time constant of 7.8 $\pm$ 2.9 ms (see Figure 1.4A, D). Glycinergic sIPSCs recorded in the presence of SR-95531 had fast decay kinetics (mean τ_{decay} = 2.9 $\pm$ 1.2 ms; range 0.9 to 8.9 ms) (Figure 1.4B, D). The duration of GABAergic sIPSCs isolated by strychnine application exhibited a range of values that were on average slower than glycinergic IPSCs (mean τ_{decay} = 11.7 ms $\pm$ 4.3 ms; range 1.6 to 43.6 ms) (Figure 1.4C, D). The broad distribution of sIPSC decay kinetics recorded in the presence of strychnine and overlap with decay kinetics of events recorded in SR-95531 prevented a quantitative assessment of the relative contributions of GABA and glycine-mediated transmission to spontaneous events. However, the significant shift in the overall population of τ_{decay} values recorded under control conditions to faster or slower values in the presence of SR-95531 or strychnine, respectively (Figure 1.4D; $p < 0.0001$; Kolmogorov-Smirnov test), indicates a considerable number of control sIPSCs arose from the release of both GABA and glycine from the same axon. If most IPSCs arose from release of GABA only or glycine only, under control conditions we should have observed two separate populations of decays with means matching those recorded in SR-95531 or strychnine, which would have appeared as a biphasic curve in the cumulative probability plot. The observation that SR-

95531 or strychnine application significantly reduced the amplitudes of sIPSCs (Figure 1.4E, $p<0.0001$, Kolmogorov-Smirnov test) also supports this interpretation.

As a complementary approach for investigating whether GABA and glycine arise from the same or different sources, we examined the expression patterns of these neurotransmitters in the chick auditory brainstem using immunohistochemistry. Double immunofluorescent labeling with a GABA-specific antibody in combination with a glycine-specific antibody revealed punctate expression of both neurotransmitters around cell bodies and in the neuropil of nAng (Figure 1.5A). These puncta likely correspond to inhibitory nerve terminals contacting nAng neurons. Bouton-like structures exhibiting only GABA-like immunoreactivity or only glycine-like immunoreactivity were observed (Figure 1.5A, double arrows and arrowheads, respectively), but many puncta also exhibited co-labeling for both neurotransmitters (Figure 1.5A, arrows). In nAng, 36.4 $\pm$ 5.2% of the glycine-like signal also exhibited GABA-like immunoreactivity (%GABA/Gly), while 36.8 $\pm$ 10.1% of GABA-like labeling also had glycine-like immunoreactivity (%Gly/GABA). Interestingly, glycine labeling was also observed in nMag and nLam (Figure 1.5B, C), despite the apparent lack of glycine receptor-mediated currents in these nuclei (Figure 1.3C). Similar overlap between GABA and glycine signals was observed in nMag (42.3 $\pm$ 16.6% %GABA/Gly, 47.5 $\pm$ 6.9% %Gly/GABA) and nLam (36.6 $\pm$ 12.9% %GABA/Gly, 33.9 $\pm$ 4.1% %Gly/GABA) ($p>0.05$ for all comparisons between nuclei; data from three different chicks, one image/brainstem region analyzed per animal). Taken together with our sIPSC recordings, these findings suggest GABA and glycine can be co-released from the same presynaptic axon in nAng, and possibly also in nMag and nLam.

Depolarizing Egly in nAng

A unique feature of inhibition in nMag is that GABAergic currents have a depolarizing effect on nMag neurons throughout development (Howard et al., 2007; Lu and Trussell, 2001; Monsivais and Rubel, 2001). GABAergic transmission remains inhibitory under most circumstances in mature animals due to high expression levels of low-threshold activated K^+ channels in nMag neurons (Howard et al., 2007). Because the majority of nAng neurons have fundamentally different intrinsic membrane properties compared to nMag neurons (Fukui and Ohmori, 2003; Soares et al., 2002) and less robust low-threshold K^+ conductances (Fukui and Ohmori, 2003), we examined the polarity of inhibition in nAng (Figure 1.6). To estimate the reversal potential for Cl^--mediated conductances, we measured currents in response to exogenously applied glycine using the gramicidin perforated-patch technique (Ebihara et al., 1995). In the majority of these recordings (9/12 cells), the reversal potential for glycine-induced currents (E_{gly}) was depolarized compared to resting membrane potential (mean E_{gly}= -41.5 $\pm$ 6.6 mV; mean resting membrane potential for all cells tested -61.9 $\pm$ 3.5 mV). A small subset of cells (3/12) was also observed with hyperpolarized E_{gly} values (-70.8 $\pm$ 3.5 mV). In the nAng neurons we studied, E_{gly} values did not seem to correlate with the age of tissue (E16-E20) or the action potential firing phenotype of the recorded cells. To confirm our results from gramicidin perforated-patch recordings, we also made extracellular recordings from several nAng neurons in the cell-attached configuration. In three out of four neurons, puff application of 1 mM glycine caused the cell to fire a single action potential (see example in Figure 1.6C). We also performed cell-attached recordings from four cells in the presence of the K^+-channel blocker 4-aminopyridine (4-AP; 30 μM), which was added to

enhance excitability in our slices. Again, action potentials were recorded in response to glycine application in three out of the four neurons examined. Two of these cells fired multiple action potentials in response to glycine (see Figure 1.6D for example), one cell fired a single action potential, and the last cell did not exhibit any spiking activity. Together, our results from gramicidin perforated-patch and cell-attached recordings indicate most nAng neurons in late embryonic chick tissue have depolarized Cl^- reversal potentials. Cell-attached recordings were additionally used to examine responses to glycine application in nAng neurons in tissue from hatchling chicks (P0). In hatchling tissue, four cells responded to glycine puffs with action potential firing (either from rest, or increased spiking above spontaneous firing) while three cells with spontaneous spiking activity responded with a decrease in spike output. Ten additional cells tested did not exhibit changes in action potential firing with glycine application.

Excitatory effects of GABA/glycine in nAng

Given that the depolarizing E_{gly} values measured for the majority of nAng neurons studied was above action potential threshold (-47.2 $\pm$ 1.4 mV in multiple spiking neurons, -51.1 $\pm$ 2.0 mV onset spiking cells), we examined whether GABAergic/glycinergic inputs to nAng neurons could exert an excitatory effect on these cells. To approximate the depolarizing E_{gly} values we measured using gramicidin perforated-patch recordings, whole-cell recordings were acquired using a K^+-based internal solution with a $[Cl^-]$ calculated to yield an E_{Cl^-} of -35 mV ($[Cl^-]$ = 41 mM). Immediately after acquiring whole-cell recordings, cellular firing characteristics of nAng neurons were assessed by current injection in current-clamp mode. After measuring

IPSCs in response to repetitive stimulation in voltage-clamp, recordings were switched back to current-clamp and responses the same stimulus pattern was investigated. Figure 1.7 shows example responses from an onset spiking cell (Figure 1.7A-C) and a multiple spiking neuron (Figure 1.7D-F). In both cell types, postsynaptic potentials recorded in the presence of glutamate receptor blockers could elicit action potentials. Out of four onset neurons tested, three fired at least one action potential over the course of ten stimuli applied at 100 Hz. Similarly, four out of five multiple spiking neurons fired action potentials in response to stimulation of inhibitory fibers.

Discussion

We found the time course and neurotransmitter phenotype of inhibitory currents were distinct between nMag, nLam, and nAng. These divergent properties may contribute to the unique computational tasks carried out in the different brainstem regions. Additionally, we observed glycinergic/GABAergic inputs could excite nAng neurons, which could have important implications for the recruitment of SON activity.

Implications for ITD coding

The approximately three-fold difference in IPSC decay kinetics we measured between nMag and nLam neurons indicates inhibition may have a more complex role in ITD processing than previously appreciated. Most proposals for how inhibition contributes to ITD coding assume a slow time course for GABAergic currents (Burger et al., 2005; Dasika et al., 2005; Funabiki et al., 1998; Grothe, 2003; Monsivais et al., 2000). In nMag, it is clear inhibitory inputs do not preserve temporal information, but

instead exert a tonic influence (Lu and Trussell, 2000). Our results raise the possibility inhibition may have more phasic effects in nLam compared to nMag. However, timing information is probably not retained in the activity of GABAergic inputs to nLam. SON neurons do not phase lock as well as nMag cells (Lachica et al., 1994) and do not appear to express intrinsic properties suited to preservation of timing information (Yang et al., 1999). However, heterogeneity in both tone-evoked response properties and anatomical features has been observed in SON neurons (Carr et al., 1989; Lachica et al., 1994). It is possible a sub-population of SON neurons may provide phase-locked inhibitory signals to nLam, although no evidence exists to suggest this may be the case. Further work will be needed to resolve whether precisely timed inhibition contributes to nLam function.

Previous studies did not observe fast kinetics for inhibition in nLam neurons from similarly aged chicks when recordings were performed at room temperature (Funabiki et al., 1998; Yang et al., 1999). Because our recordings were obtained closer to physiological temperature (41ºC in chickens), the measurements presented here likely more closely resemble *in vivo* inhibitory currents than those reported previously.

Glycinergic transmission in the avian auditory brainstem

Perhaps the most surprising finding of this study was glycinergic transmission contributes significantly to non-glutamatergic currents in all nAng neurons examined. Glycinergic transmission had not previously been believed to play an important role in the bird auditory system due to a lack of immunohistochemical evidence for significant glycine expression in the chicken auditory nuclei (Code and Rubel, 1989) as well as observations that inhibition in nMag and nLam could be completely abolished by

antagonists of $GABA_A$ receptors (Funabiki et al., 1998; Lu and Trussell, 2000). Our pharmacological and immunohistochemical evidence for glycinergic transmission raise the possibility that, at least within nAng, inhibition in the avian and mammalian auditory systems is more similar than originally believed. Because our study focused on late-stage embryos, it is possible the glycinergic currents we observed are not a permanent feature, but instead reflect a transient stage of nAng development. However, glycine-like immunoreactivity remains abundant in the nAng of hatchling chicks (P0) and hatchling nAng neurons still respond to glycine application (not shown). Thus, glycinergic transmission likely still persists at an age at which nAng neurons exhibit well-developed intrinsic properties (Fukui and Ohmori, 2003) and hearing is intact.

Interestingly, immunofluorescent labeling also revealed co-expression of GABA and glycine in nMag and nLam, despite the lack of glycinergic synaptic currents in these regions. Whether glycine release within nMag and nLam has any function in these nuclei despite the apparent lack of postsynaptic glycine receptors remains to be determined. Glycine could potentially modulate excitatory and/or inhibitory transmission by acting on presynaptic glycine receptors (Turecek and Trussell, 2001) or extrasynaptic receptors on nMag or nLam neurons. Co-released GABA was recently demonstrated to speed the decay of glycinergic currents by acting as a co-agonist at glycine receptors (Lu et al., 2008). An intriguing possibility is co-released glycine could act to modulate the response of postsynaptic GABA receptors on nLam and nMag neurons.

Depolarizing E_{Cl-} in nAng

An important caveat to our estimation of Cl^- reversal potential is that our experiments were performed in late-stage chick embryos. Although we did not observe any obvious relationship between tissue age and E_{Cl-} in the cells we tested, we cannot rule out the possibility our experiments were conducted prior to a developmental switch in the polarity of inhibition in nAng. Using cell-attached recordings, we found nAng neurons in tissue from hatchling chicks could fire action potentials in response to glycine application, demonstrating nAng neurons in more mature tissue can also have a depolarized E_{Cl}- value. However, inhibitory responses were also observed in some cells, and most cells did not respond to glycine puffs with spiking activity, although the lack of responses in these latter cells could be due to reduced excitability, perhaps due to higher low threshold K^+ channel expression (Fukui and Ohmori, 2003). Importantly, *in vivo* recordings have demonstrated clear inhibitory influences in the sound-evoked response properties of mature nAng units (Koppl and Carr, 2003; Warchol and Dallos, 1990). The obvious inhibition of spiking activity observed in some nAng cells in response to presentation of tone or noise stimuli may indicate GABAergic/glycinergic inputs are hyperpolarizing in at least some cell types in the mature animal.

Our current-clamp experiments indicate GABAergic/glycinergic postsynaptic potentials may exert an excitatory influence upon nAng neurons under certain conditions. It should be noted that we observed a range of depolarizing E_{gly} values, as well some instances where E_{gly} was hyperpolarizing. Differential expression or activity of $Na^+/K^+/Cl^-$ transporters and/or K^+/Cl^- transporters could underlie differences in E_{Cl-} (Payne et al., 2003). If SON neurons project to the same nAng neurons from which they

receive input, excitatory GABA/glycine influences in nAng could establish a positive feedback loop that would increase activity in both nuclei. This could in turn alter the level of inhibition to nMag and nLam neurons and thereby enhance the functional range of inhibitory signaling in the brainstem. Positive feedback could also enhance the range of sound intensity coding by nAng neurons by amplifying changes in the level of auditory nerve input to nAng. In this scenario, additional mechanisms such as synaptic depression, spike threshold accommodation, or metabotropic receptor activity (e.g. $GABA_B$ receptors), would be required to prevent overexcitability.

Sources of GABAergic/glycinergic input

Several anatomical studies have identified robust projections from ipsilateral SON to nMag, nLam and nAng (Lachica et al., 1994; Yang et al., 1999; Burger et al., 2005; Nishino et al., 2008), which has led to the prevailing view that the majority of GABAergic input to the timing and intensity pathways arises from SON. In partial support of this view, Nishino et al., (2008) recently demonstrated lesioning SON altered ITD coding in the ipsilateral nLam of chickens, presumably due to a loss of inhibitory input to nMag and nLam. Because our electrophysiological and immunohistochemical data indicates a significant amount of GABAergic and glycinergic innervation arises from a common source, we consider it likely that SON can provide mixed GABAergic/glycinergic input to the different brainstem nuclei. We occasionally observed a few GABA and/or glycine-like immunoreactive cell bodies within or around nAng (see Figure 1.5A) and in neurons between nMag and nLam (not shown), consistent with previous reports of GABAergic neurons adjacent to or within these nuclei (Carr et al.,

1989; Muller, 1987; von Bartheld et al., 1989). Thus, non-SON sources may also contribute some GABAergic and/or glycinergic input to nMag, nLam, and nAng, although this may represent a small fraction of the input to these nuclei.

Although we did not investigate the specific mechanisms underlying the unique features of GABAergic and glycineric currents in nMag, nLam and nAng, it is likely that postsynaptic factors had an important role. Differences in postsynaptic $GABA_A$ receptor subunit composition or receptor modulation probably accounts for the distinct decay kinetics between nMag and nLam. Differences in release time course are not likely to contribute to the observed differences in IPSC kinetics because in nMag, IPSCs evoked at the low stimulus frequencies used in this study have identical kinetics to miniature IPSCs, indicating that evoked release is highly synchronous in these cells at low stimulus frequency (Lu and Trussell, 2000). Because glycine appears to be expressed presynaptically not only in nAng, but also in nMag and nLam, the presence or absence of postsynaptic glycine receptors likely underlies the pharmacological differences between the sound intensity and timing pathways, similar to previous findings of postsynaptic selection of co-released GABA and glycine in the mammalian cerebellum (Dugue et al., 2005). Considering most of the inhibitory input to nMag, nLam and nAng likely arises from ipsilateral SON, the divergent properties of inhibitory transmission we observed suggest that postsynaptic specializations permit segregation of inhibitory influences between different functional pathways despite a common source.

Acknowledgements

This work was supported by NIH R01 DC004450 (L.O.T.) and a Cornelia H. Stevens Achievement Rewards for College Scientists scholarship (S.P.K.). We thank K. Bender, Y. Kim, C. Mello, K. Spinelli, T. Velho, and H. Zhao for advice and technical assistance, M. Roberts for providing Igor analysis procedures and advice, and P. Gillespie and Gillespie lab members for sharing equipment.

Figure 1.1

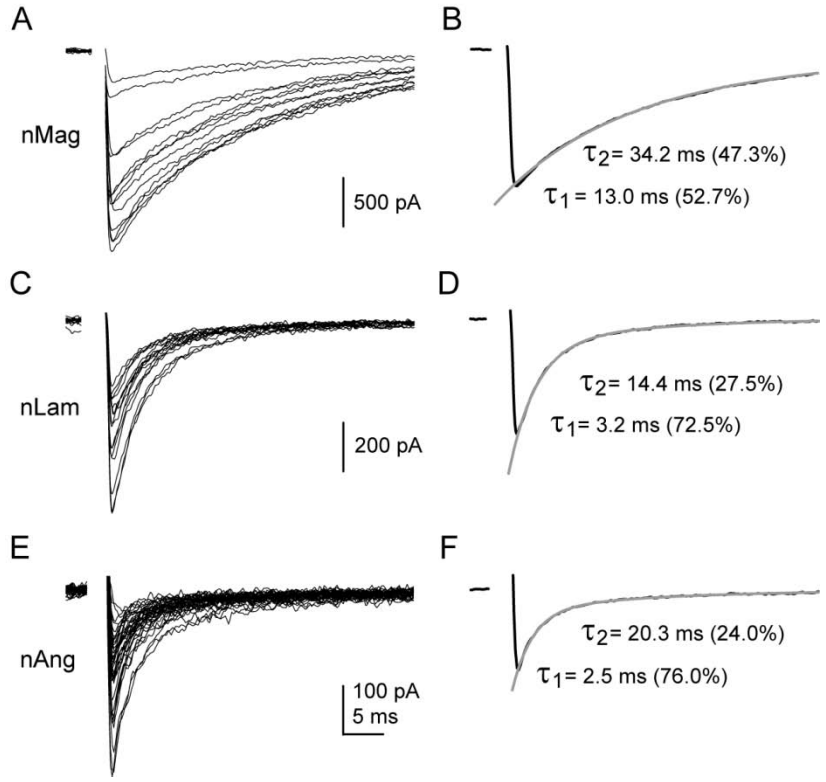

Figure 1.1. Divergent time courses of inhibition in chick auditory brainstem nuclei. Example stimulus-evoked IPSC recordings from neurons in nucleus magnocellularis (A-B), nucleus laminaris (C-D), and nucleus angularis (E-F). A, C, and E, individual, overlaid current traces from stimuli applied at 0.2 or 0.5 Hz. B, D, and F, averaged current traces (10-20 stimuli). Gray lines are biexponential fits to the current decay phases. Stimulus artifacts in this and subsequent figures have been blanked for clarity.

Table 1.1. Summary of IPSC properties in chick auditory brainstem

	Peak amplitude pA	20-80% rise time ms	Decay time constants					
			τ_1, ms	τ_2, ms	τ_3, ms	% τ_1	%τ_2	weighted τ ms
N. Magnocellularis (n=11)	-1536 ± 1293	0.27 ± 0.06						
three-component fit (n=7)			3.7 ± 1.9	21.5 ± 4.6	72.5 ± 36.3	12.8 ± 5.9	67.2 ± 12.6	27.8 ± 5.3
two-component fit (n=4)			11.5 ± 4.4	31.2 ± 5.1	---	41.6 ± 13.6	58.4 ± 13.6	22.9 ± 2.4
N. Laminaris (n = 11)	-782 ± 535	0.36 ± 0.11						
two-component fit			3.3 ± 1.0	19.0 ± 7.9	---	66.9 ± 10.4	33.1 ± 10.4	8.1 ± 2.1
N. Angularis (n = 15)	-244 ± 166	0.32 ± 0.14						
three-component fit (n=3)			1.9 ± 0.3	10.8 ± 1.2	91.5 ± 10.3	43.4 ± 16.4	36.7 ± 15.7	23.1 ± 5.6
two-component fit (n=12)			4.0 ± 2.6	29.9 ± 16.7	---	75.1 ± 11.5	24.9 ± 11.5	11.6 ± 9.0

Values are mean± SD. All measurements from cells filled held at -35.9 mV and using CsCl-based internal solutions. IPSC decay phases were fit with exponential functions with two or three components (see Methods).

Figure 1.2

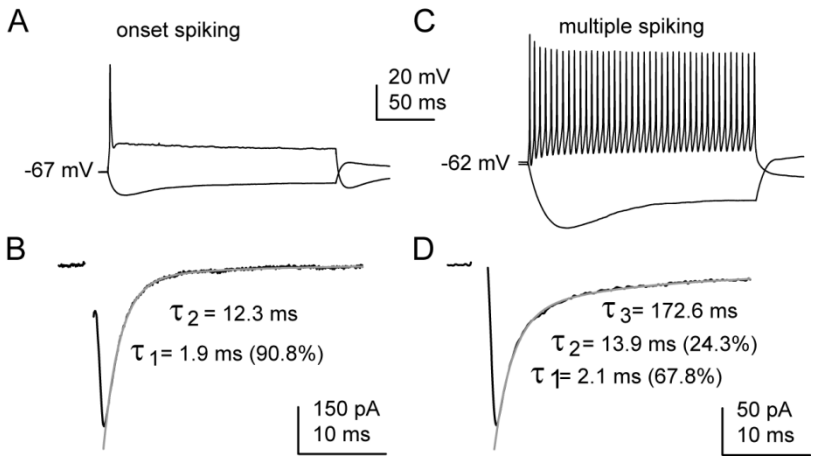

Figure 1.2. Unique IPSC decay kinetics between onset spiking and multiple spiking neurons in nAng. (A) response to -200 pA and +600 pA current injection in an example onset spiking neuron. (B) average evoked IPSC in same cell as in A. (C) multiple spiking neuron response to -200 pA and +600 pA injection. (D) evoked IPSC measured from same cell shown in (C) Gray lines in B and D show exponential fit to IPSC decay phase.

Figure 1.3

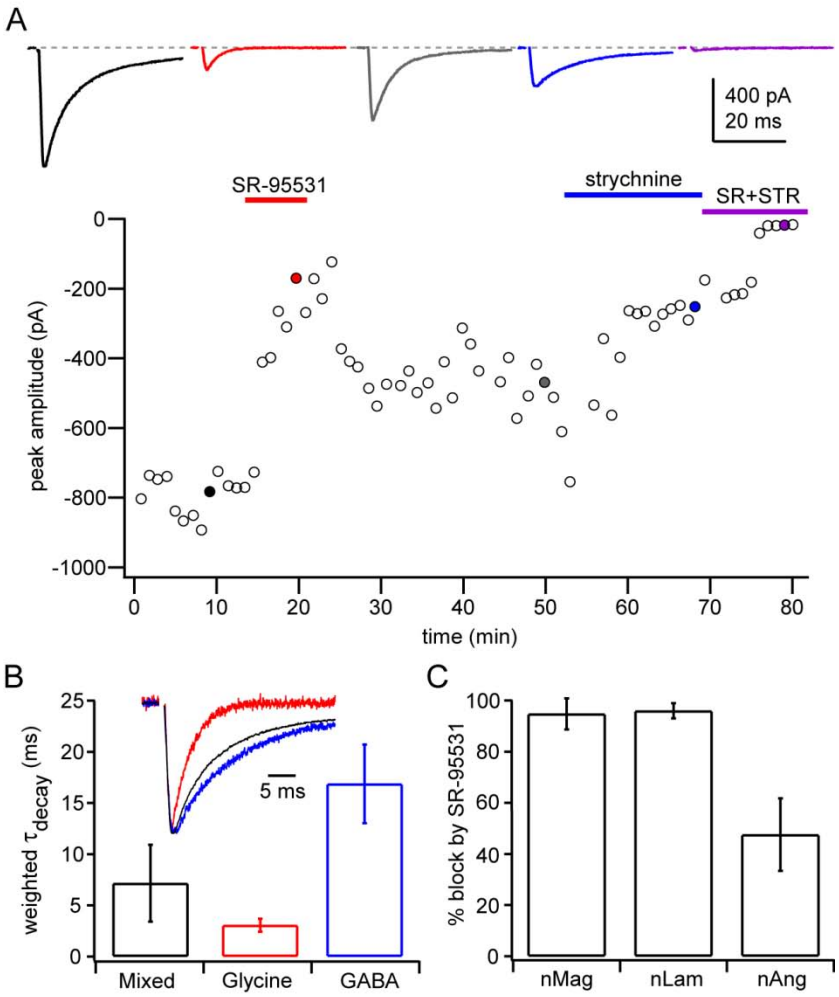

Figure 1.3. IPSCs recorded from nAng neurons have both GABAergic and glycinergic components. (A) example stimulus-evoked IPSCs recorded from an nAng neuron under control conditions (black), in the presence of SR-95531 (10 μM; red), following SR-95531 washout (gray), after application of strychnine (0.5 μM; blue), and in the presence of both SR-95531 and strychnine (purple) are shown above. The current traces show data from the time points indicated by the same color data points in the graph below. Each data point in the graph represents the average peak amplitude of six consecutive sweeps (data acquired at 0.1 Hz) from one example cell. (B) summary of weighted decay kinetics for IPSCs in nAng neurons for mixed

glycinergic/GABAergic IPSCs recorded under control conditions, glycinergic currents isolated by SR-95531 application, and GABAergic currents isolated by application of strychnine, or digital subtraction of currents recorded in SR-95531 from control IPSCs. Inset shows peak scaled IPSCs for same responses shown in A. (C) comparison of peak current of IPSCs in nMag (n = 4), nLam (n = 4) and nAng neurons (n = 5) before and during exposure to SR-95531 (10-20 μM).

Figure 1.4

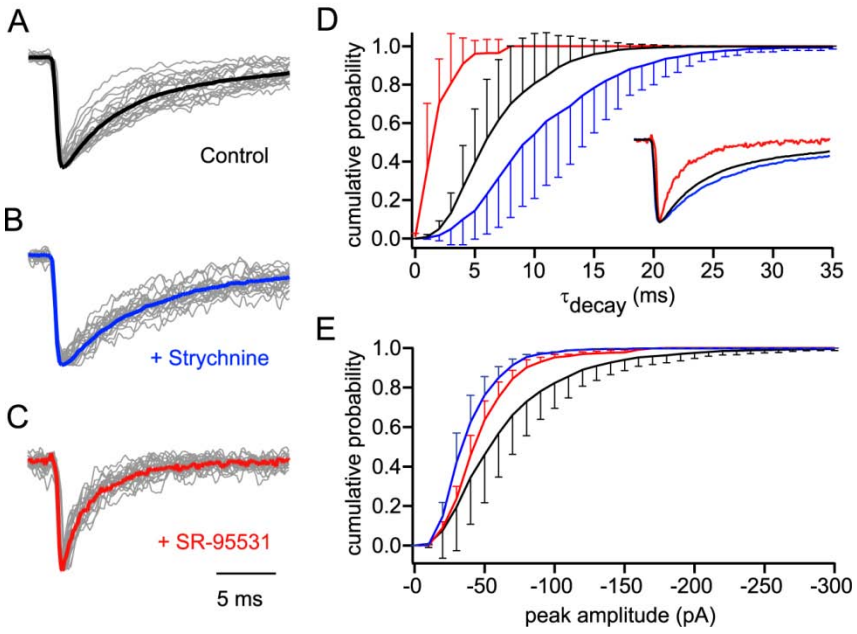

Figure 1.4. Spontaneous IPSCs in nAng indicate GABA and glycine are co-released. (A-C) peak-normalized average spontaneous IPSC (thick colored line) and 20 individual spontaneous IPSCs (gray lines) recorded in control conditions (A), and in the presence of strychnine (B), or SR-95531 (C) from the same nAng neuron (average IPSC from 540 events in A, 150 events in B, and 56 events in C). (D) cumulative histograms of IPSC decay times for sIPSCs recorded in control (black), strychnine (red), and SR-95531 (blue). Mean $\pm$ S.D. of distributions for each experimental condition from four nAng cells are shown. Inset shows peak-scaled average sIPSCs under the different conditions for the single nAng cell shown in A-C. sIPSC decay time distributions were significantly different between the conditions ($p<0.0001$, Kolmogorov-Smirnov test). (E) cumulative distributions of sIPSC peak amplitudes under control conditions (black), in the presence of strychnine (red), or SR-95531 (blue) (four cells, mean $\pm$ S.D.). Peak amplitudes of events in control conditions were significantly different from those in either drug ($p<0.0001$, Kolmogorov-Smirnov test).

Figure 1.5

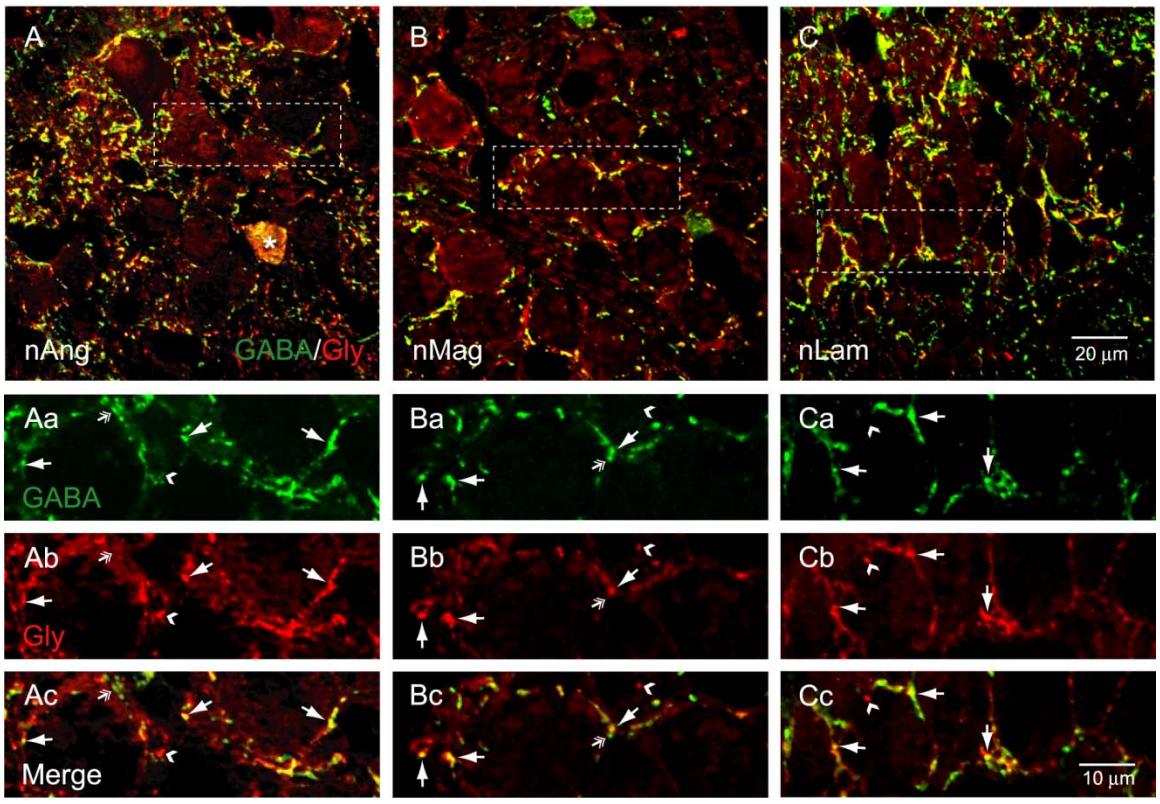

Figure 1.5. Co-localization of GABA and glycine in embryonic chick auditory brainstem. Immunofluorescent labeling of GABA (green) and glycine (red) in nAng (A), nMag (B), and nLam (C) of an E18 chick. A-C are merged stacks of confocal images acquired in 0.5 µm intervals in the z-axis (A, 18 sections; B, 5 sections; C, 5 sections). Aa-Ac, single confocal sections corresponding to dashed box in A showing GABA (Aa), glycine (Ab), and both fluorescent signals merged (Ac). Ba-Bc and Ca-Cc show same for nMag and nLam, respectively. Arrows indicate double labeled puncta. Arrowheads indicate bouton-like structures showing only glycine labeling. Double arrows show puncta with GABA labeling only. Asterisk in A denotes a cell body exhibiting labeling for GABA and glycine. Cell bodies exhibiting GABA-like and/or glycine-like immunoreactivity were infrequently observed within nAng (<3-4 cells when present, typically no cells observed). Scale bar in C applies to A-C. Scale bar in Cc applies to Aa-Cc.

Figure 1.6

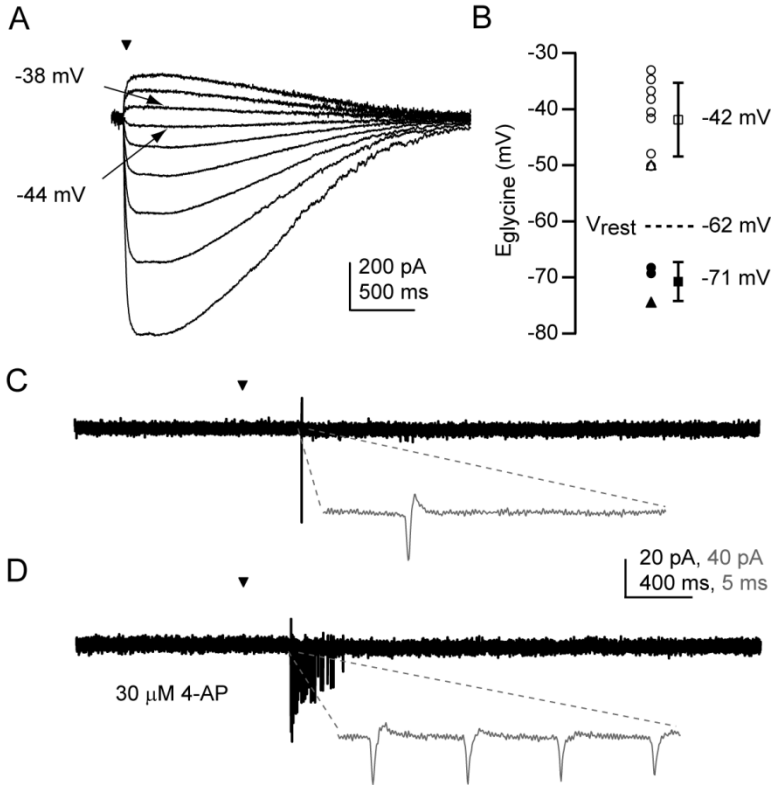

Figure 1.6. Depolarizing reversal potential for glycine-mediated currents in nAng. (A) example responses recorded from an nAng neuron using the gramicidin perforated-patch technique. Currents were recorded in response to a 100 ms puff of glycine (1 mM; inverted triangle indicates onset of application) at a series of holding potentials between -85 mV and -27 mV. (B) summary of reversal potentials for glycinergic currents (E_{glyine}) in nAng neurons. Circles show $E_{glycine}$ values for multiple spiking cells. Triangles show measurements for onset spiking cells. Squares show average values for depolarizing (open) and hyperpolarizing (filled in) $E_{glycine}$ values. (C) cell-attached recording from an nAng neuron. Glycine application elicited an action potential (see inset). (D) cell-attached recording from a different nAng neuron obtained in the presence of 30 μM 4-AP. Cell spiked multiple times in response to glycine exposure. In both C and D, 1 mM glycine was applied for 1 second starting at the time denoted by the inverted triangle.

Figure 1.7

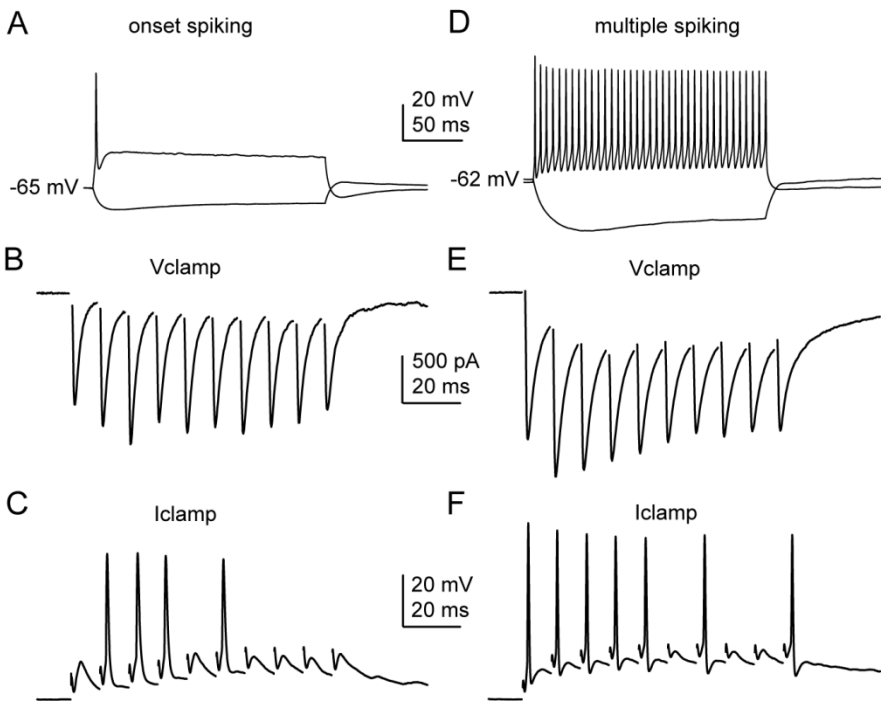

Figure 1.7. Excitatory effects of GABA/glycinergic input to nAng neurons. Whole cell recordings were made from nAng neurons using a pipette solution with a calculated E_{Cl}- of -35 mV. (A) response to current injection (-200 pA, +600 pA) in an onset spiking neuron. (B) IPSCs evoked at 100 Hz in the same cell as in A. (C) current-clamp measurements from the same cell in response to the same stimulus used in B. (D-F) same as in A-C, but for a multiple spiking neuron. Cells presented in this figure are different from those shown in Figure 1.2.

Figure 1.S1

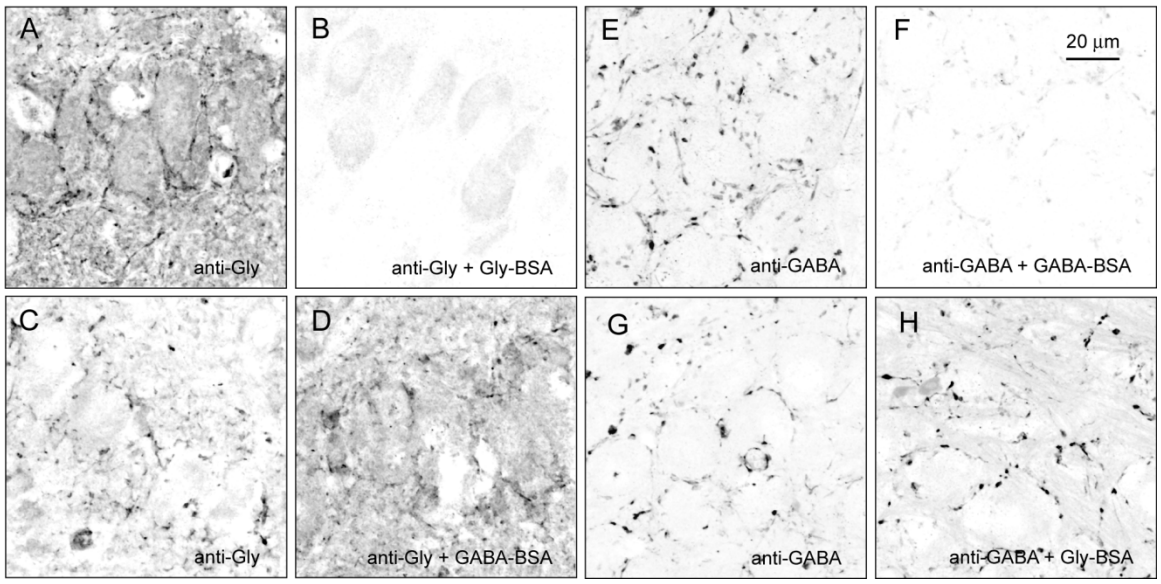

Figure 1.S1. Preadsorption controls. Anti-glycine (anti-Gly) and anti-GABA antibodies were tested for specificity to their respective antigens by pre-incubating the antibodies with glycine-BSA (Gly-BSA) or GABA-BSA glutaraldehyde conjugates prior to application to brain tissue. (A-B) tissue incubated with anti-Gly antibody (A) or anti-Gly pre-incubated with 100-fold molar excess of Gly-BSA (B). (C-D) glycine-like immunoreactivity in sections labeled with anti-Gly alone (C) or anti-Gly pre-incubated with GABA-BSA. E-F, tissue incubated with anti-GABA alone (E) or anti-GABA + 100-fold molar excess of GABA-BSA (F). (G-H) GABA-like immunoreactivity in sections labeled with anti-GABA alone (G) or anti-GABA + Gly-BSA (H). A-D, nucleus laminaris. E-H, nucleus magnocellularis. Sections shown in each set of comparison images were acquired from the same animal and processed identically with the exception of the preadsorption step. Comparison images were acquired with identical laser settings during the same imaging session and identical brightness and contrast settings were applied uniformly to each image pair. Scale bar in F applies to all images.

CHAPTER 2. INTRINSIC AND SYNAPTIC PROPERTIES OF VERTICAL CELLS OF THE MOUSE DORSAL COCHLEAR NUCLEUS.

Sidney P. Kuo and Laurence O. Trussell

Neuroscience Graduate Program and Oregon Hearing Research Center and Vollum Institute, Oregon Health and Science University, Portland, OR 97239

Abstract

Multiple classes of inhibitory interneuron shape the activity of principal neurons of the dorsal cochlear nucleus (DCN), a primary target of auditory nerve fibers in the mammalian brainstem. Feed-forward inhibition mediated by glycinergic vertical cells (also termed tuberculoventral or corn cells), is thought to contribute importantly to the sound-evoked response properties of principal neurons, but the cellular and synaptic properties that determine how vertical cells function are unclear. We used transgenic mice in which glycinergic neurons express GFP to target vertical cells for whole-cell patch-clamp recordings in acute slices of DCN. We found that vertical cells express diverse intrinsic spiking properties and could fire action potentials at high, sustained spiking rates. Using paired recordings, we directly examined synapses made by vertical cells onto fusiform cells, a primary DCN principal cell type. Vertical cell synapses produced unexpectedly small amplitude unitary currents in fusiform cells and additional experiments indicated that multiple vertical cells must be simultaneously active to inhibit fusiform cell spike output. Paired recordings also revealed that vertical cells make functional synapses upon other vertical cells with high probability. Our results indicate that the role of vertical cells within the DCN is likely more complex than previously proposed.

Introduction

The dorsal cochlear nucleus (DCN) is a mammalian auditory brainstem structure that contributes to sound localization (May, 2000; Sutherland et al., 1998). DCN principal neurons are proposed to detect spectral features of complex sounds that vary according to the position of sound sources with respect to the ears (Oertel and Young, 2004; Young and Davis, 2002). Sensitivity to spectral information is thought to arise from the interaction of excitatory and inhibitory signals within the deep layer of the DCN, where auditory nerve fibers form glutamatergic synapses upon basal dendrites of principal cell as well as glycinergic interneurons called vertical cells (also termed tuberculoventral or corn cells) (Rubio and Juiz, 2004). Evidence from *in vivo* electrophysiological recordings (Davis and Young, 2000; Nelken and Young, 1994; Rhode, 1999; Spirou et al., 1999; Voigt and Young, 1990) and anatomical work (Rhode, 1999) indicates vertical cells provide feed-forward inhibition that shapes the sound-evoked response properties of principal neurons. In fact, in some *in vivo* preparations, particularly decerebrate cats, principal neurons exhibit predominantly inhibitory responses to moderate and high intensity tones ("Type IV" units in the response map classification scheme (Young and Davis, 2002)), which has been attributed to vertical cell-mediated inhibition (Davis and Young, 2000; Spirou et al., 1999; Spirou and Young, 1991; Voigt and Young, 1990). Vertical cells are therefore hypothesized to contribute critically to the spectral analysis function of principal cells (Young and Davis, 2002). However, the cellular and synaptic properties that determine how vertical cells influence DCN output are not well understood.

We made use of transgenic mice in which glycinergic neurons express enhanced green fluorescent protein (EGFP) to target patch-clamp recordings of vertical cells in acute slices of DCN. We found previously unappreciated heterogeneity of intrinsic action potential firing properties in vertical cells. Additionally, paired recordings directly demonstrated functional synaptic connections between vertical cells and fusiform neurons, a primary type of principal neuron, as well as other vertical cells. However, postsynaptic targets received unexpectedly weak input from vertical cells and our experiments suggest activation of multiple vertical cells is necessary to influence the spiking output of fusiform cells.

Methods

Slice preparation

All animal care and handling procedures used in this study were approved by the OHSU Institutional Animal Care and Use Committee. Parasagittal slices (210 μm) were prepared from 17 to 23 day old heterozygous GlyT2-EGFP transgenic mice (Zeilhofer et al., 2005) or their wild-type littermates. GlyT2-EGFP mice were backcrossed into the C57BL/6J genetic background (Jackson Labs) and were genotyped and maintained as previously described (Roberts et al., 2008). To make slices, mice were deeply anesthetized, then killed by decapitation. After removing the skull to expose the brain, the brainstem was isolated by making a coronal cut just rostral to the cerebellum. A sagittal cut was then made down the midline of the brainstem, and one half of the brainstem was removed from the skull and glued cut side-down to the stage of a vibratome (Leica VT1200S). The ventral side of the brainstem was turned to face the vibratome blade and

was angled slightly downwards (6° angle with horizontal plane). During dissection and slicing, tissue was kept immersed in warm (~34°C) ACSF containing (in mM): 130 NaCl, 2.1 KCl, 1.7 $CaCl_2$, 1.0 $MgSO_4$, 1.2 KH_2PO_4, 20 $NaHCO_3$, 3 Na-HEPES, 11 glucose; saturated with 5% CO_2/ 95% O_2, ~300 mOsm. Following slicing, slices were allowed to recover in 34°C ACSF for one hour, then either transferred to a recording chamber or maintained in ACSF at room temperature (~22°C) until use.

Electrophysiology

During recordings, slices were constantly perfused with ACSF (1-2 mL/min) maintained at 33 ± 1°C using an in-line heater (Warner Instruments). Cells were visualized using a 60X magnification objective on the stage of an upright microscope (Olympus BX51W) equipped with infrared gradient contrast and fluorescence optics. GFP-expressing neurons were identified by briefly illuminating tissue via a mercury lamp light source and viewing fluorescence using a GFP filter set (Chroma). Vertical cells were initially identified based on location within the deep layer of DCN slices and GFP fluorescence in tissue from GlyT2-EGFP mice. With some experience, we could routinely target vertical cells for recordings based on location within the deep layer and somatic morphology (round or oval) and size (~10-15 μm diameter, see Figure 2.1B), even in wild-type tissue. Fusiform neurons were easily identified based upon location within the slice, lack of GFP expression in GlyT2-EGFP tissue, larger somatic size in comparison to vertical cells, and bipolar somatic morphology. Fusiform neurons had spiking properties consistent with previous reports (Tzounopoulos et al., 2004; Zhang and Oertel, 1994) and fusiform cells visualized using fluorescent dyes or biocytin labeling

had spiny apical dendrities extending through the molecular layer and long, smooth basal dendrites that projected into the deep layer (Blackstad et al., 1984; Tzounopoulos et al., 2004; Zhang and Oertel, 1994). Whole-cell recording electrodes (2-4 MΩ) were pulled from borosilicate glass (WPI) and filled with a solution containing (in mM): 113 K^+-Gluconate, 2.75 $MgCl_2$, 1.75 $MgSO_4$, 0.1 EGTA, 14 $Tris_2$-phosphocreatine, 4 Na_2-ATP, 0.3 Tris-GTP, 9 HEPES; osmolarity adjusted to ~290 mOsm with sucrose, pH adjusted to 7.25 with KOH. In some recordings, biocytin (0.3% weight/volume) was added to the internal solution. The red fluorescent dye AlexaFluor 555 (20 μM) was also routinely included in recording solutions. The composition of the internal solution was designed to give a calculated reversal potential of -84 mV for Cl^- conductances because previous work using gramicidin perforated-patch recordings established a reversal potential for glycine-elicited currents of -83.9 ± 0.7 mV in fusiform neurons (Kim and Trussell, 2009). All reported membrane potential values are corrected for a -10.2 mV junction potential that was measured between this internal solution and the ACSF solution. In a subset of paired recordings between vertical cells, the K^+-gluconate-based internal solution was supplemented with 20 mM glycine. Connections between cells recorded with the glycine-containing internal solution (3 total connections, one unidirectional, one reciprocal among three tested pairs (six tested connections)) were included in the calculation of connection probability, but were not included in the reported measurements of unitary IPSC properties. In two of the vertical cell and fusiform cell pairs, the postsynaptic fusiform cell was recorded using an internal solution containing (in mM): 108 $CsMeSO_3$, 5 CsCl, 1 $MgCl_2$, 4 Mg-ATP, 0.4 Tris-GTP, 14 $Tris_2$-phosphocreatine, 5 EGTA, 10 HEPES, 3 QX-314, pH adjusted to 7.3 with CsOH, 290 mOsm. For recordings of unitary

IPSCs (uIPSCs), postsynaptic cells were held at -60.2 mV, with the exception of the two recordings using the $CsMeSO_3$-based internal solution, in which postsynaptic fusiform cells were held at -30.2 mV. Extracellular stimulation of auditory fibers or vertical cell axons was achieved by applying voltage pulses (10-30V, 150-200 μsec) via ACSF-filled double-barreled glass electrodes (theta pipettes; lengthwise tip diameter ~5 μm; Sutter Instruments) placed in the deep layer within ~50 μm of the somas of recorded cells.

Electrophysiological data acquisition and analysis

Recordings were acquired using a Multiclamp 700B amplifier and pClamp 10 software (Molecular Devices). Signals were digitized at 50 kHz using a Digidata 1322A (Molecular Devices) and low-pass filtered at 10 kHz. For voltage-clamp experiments, pipette series resistance (<20 MΩ) was compensated by 80%. In current-clamp recordings, bridge balance was used to compensate series resistance. Membrane time constant ($\tau_{membrane}$) and input resistance (R_{input}) were measured in current-clamp from averaged voltage responses (10-20 sweeps) to 200 to 400 ms long -20 pA current steps delivered while vertical cells were at resting membrane potential (V_{rest}) (no bias current injection). R_{input} was determined by measuring the voltage change from resting membrane potential for the last 50 ms of current step and calculated using Ohm's law. $\tau_{membrane}$ was measured by fitting a single exponential function to the initial voltage response to the -20 pA current step. Action potential (AP) threshold was defined as the peak of the 3rd time-based derivative of the membrane voltage (V_m) before AP peak (Henze and Buzsaki, 2001). In eight of the 36 recordings in which action potential shape was determined, two deflections were clearly observable in phase-plane plots of V_m versus the time derivative

of V_m, likely due to initiation of spikes distal from the soma (i.e. in the axon initial segment) followed by initiation in the soma (Bean 2007). In these cells, the peak of the 3rd derivative of V_m usually corresponded to the more depolarized potential at which a rapid rise in membrane potential occurred, but downsampling the recordings to 25 kHz (from 50 kHz) reliably allowed us to determine the more hyperpolarized potential for spike initiation using the 3rd derivative method. AP height was defined as the difference between action potential peak and threshold. AP half-width was defined as the width of the action potential at V_m halfway between peak and threshold. Decay kinetics of spontaneous EPSCs and unitary IPSCs were determined by fitting biexponential or single exponential functions to the decay phase of currents, respectively. Spontaneous EPSCs were detected using the template function event detection feature of Axograph X. In paired recordings, latencies of uIPSCs were defined as the time difference between the peaks of presynaptic action potentials and current at which uIPSCs had achieved 20% of their peak amplitude. Unitary IPSC latencies and decay time constants were usually measured from the first uIPSC in a train, but were sometimes measured from the second or third uIPSC when the first uIPSC was obscured by spontaneous IPSCs or was very small. Conductance values for unitary events were calculated from the driving force for Cl^- currents (usually 23.8 mV) and peak current amplitudes relative to baseline current for the first uIPSC in a train. Unitary IPSC latency, decay time constant and peak amplitude were measured from averaged currents from 10-33 sweeps, with the exception of peak conductance values that exluded failures, in which averaged currents were from three or more sweeps. Failures were defined as trials in which a rapid outward current deflection rising above baseline noise levels was not observed within 1 ms after a

presynaptic AP. Correct identification of failures was confirmed by averaging together trials in which failures were counted. All data are presented as mean ± standard deviation (S.D.). Statistical significance ($p < 0.05$) was determined by ANOVA followed by Fischer's PLSD post-hoc tests unless noted otherwise.

Biocytin labeling

Following some recordings in which biocytin was included in the internal solution, slices were fixed overnight in a cold (4°C) phosphate-buffered saline (PBS) solution (0.1 M, pH 7.4) containing 4% formaldehyde. After fixation, slices were rinsed in PBS and stored for up to a week at 4°C in PBS until processing for biocytin labeling. After permeabilizing fixed tissue in 0.2% Triton-X100 solution (in PBS) for one hour at room temperature, slices were incubated in a PBS solution containing Alex Fluor 568-conjugated steptravidin (1:2500 dilution; Invitrogen) overnight at 4°C, then rinsed and mounted on glass slides. Slices were dehydrated in an ascending series of alcohols, delipidized in xylenes, then rehydrated and coverslipped using Fluoromount G (Southern Biotech). Fluoresence images were acquired using a confocal microscope (Olympus FV1000) by sequential scanning of GFP and Alexa Fluor 568 channels using a 40X oil-immersion objective.

Results

To study vertical cells, we made whole-cell patch-clamp recordings from GFP-expressing (GFP(+)) neurons located in the deep layer of the DCN in brainstem slices prepared from GlyT2-EGFP transgenic mice (Figure 2.1A-B). The neuronal glycine

transporter GlyT2 is a reliable marker of glycinergic neurons in mammals (Friauf et al., 1999; Zafra et al., 1995) and GFP is selectively expressed in almost all glycinergic neurons in GlyT2-EGFP mice (Zeilhofer et al., 2005). Many neurons in the DCN express GFP in GlyT2-EGFP mice (Figure 2.1A) (Zeilhofer et al., 2005), consistent with the large number of glycinergic neurons in the DCN. The morphology of recorded cells was routinely assessed by examining fluorescent signals from Alexa Fluor 555, which was usually included in pipette solutions. In a few recordings, deep GFP(+) cell morphology was also examined in cells filled with biocytin. Most GFP(+) neurons in the DCN deep layer had a few (~3-5) relatively unbranched, smooth (aspiny) dendrites extending from the cell body (Figure 2.1B), similar to previous anatomical descriptions of vertical cells (Lorente de No, 1981; Rhode, 1999; Zhang and Oertel, 1993c). Additionally, almost all deep layer GFP(+) neurons had intrinsic and synaptic properties consistent with those previously described for anatomically identified vertical cells. Specifically, action potentials elicited by depolarizing current steps were short in duration and could exhibit biphasic afterhyperpolarizations (Figure 2.1C), termed 'double undershoots' by Oertel and colleagues (Zhang and Oertel, 1993c), and spontaneous excitatory postsynaptic currents (EPSCs) recorded from GFP(+) neurons displayed rapid decay kinetics (Figure 2.1D; τ_{fast}= 0.27 ± 0.09 ms, 77.81 ± 10.74% of decay, τ_{slow}= 1.65 ± 0.41 ms; n= 5) (Gardner et al., 1999). Vertical cells were easily distinguishable from cartwheel cells, which are usually found in the molecular layer and fusiform cell layer and make up the other major population of glycinergic neurons in the DCN (Lorente de No, 1981). Cartwheel cells exhibit EPSCs with slower kinetics (Gardner et al., 1999), have spiny dendrites that branch extensively in the molecular layer (Figure 2.1A) (Mugnaini, 1985;

Zhang and Oertel, 1993a), and are unique among DCN neurons in their ability to fire high frequency bursts of APs ("complex spikes") (Manis et al., 1994; Zhang and Oertel, 1993a). Thus, targeting deep layer GFP(+) neurons provided a reliable approach for acquiring recordings from vertical cells.

Heterogeneous spiking behavior in vertical cells

We initially performed current-clamp recordings from deep GFP(+) cells to characterize the intrinsic spiking properties of vertical cells. Some recordings (33/122 total) were also acquired in tissue from wild-type littermates of GlyT2-EGFP transgenic mice to assess whether transgene expression altered vertical cell characteristics. No differences between wild-type and GlyT2-EGFP cells were observed, so results were pooled.

In contrast to cartwheel cells of the molecular layer, ~75% of which spike spontaneously under our slice conditions (Kim and Trussell, 2007), vertical cells very rarely exhibited spontaneous spiking. This is consistent with the *in vivo* behavior of Type II units (Shofner and Young, 1985; Spirou et al., 1999), which are presumed vertical cells (Rhode, 1999). In fact, lack of spontaneous activity *in vivo* is a defining feature used to classify Type II units (Young and Davis, 2002).

In our recordings, we observed several different action potential firing responses to hyperpolarizing and depolarizing somatic current steps (200 ms duration) that we classified into four general categories (Figure 2.2). In over half of recordings (54.1%; 66/122 cells), cells fired rebound spikes after the offset of hyperpolarizing current steps and membrane potential quickly returned to resting levels following the offset of

depolarizing current steps (Figure 2.2A). We termed these cells "rebound spiking" cells. In another subset of recordings (24.6%; 30/122 cells), cells also exhibited rebound spiking after hyperpolarizing current injection but depolarizing steps evoked plateau depolarizations in which membrane potential remained depolarized beyond the offset of current injection ("plateau and rebound spiking" cells; Figure 2.2B). In most cases, plateau depolarizations could support action potential firing beyond the offset of current steps. Another group of cells (9.0%; 11/122) exhibited plateau depolarizations but no rebound spiking ("plateau" cells; Figure 2.2C). Finally, 12.3% of cells (15/122) did not exhibit either plateau potentials or rebound spiking ("no plateau or rebound spiking" cells; Figure 2.2D). In some cells with rebound or plateau spiking, the spiking behavior following current injection offset could last up to several seconds, but more typically rebound and plateau depolarizations lasted 100-300 ms.

Despite differences in spiking behavior, cells among the different categories could not be clearly differentiated from each other based on intrinsic membrane properties (Table 2.1). Resting membrane potentials (V_{rest}) were not significantly different between spiking phenotypes except for slightly hyperpolarized V_{rest} values in "no plateau or rebound spiking" compared to "rebound spiking" cells. No significant differences were observed between groups for measurements (see Methods for details) of cell input resistance or membrane time constant.

Action potential characteristics, which were measured in a subset of cells in which 1 ms suprathreshold current steps were applied to trigger spikes, were also similar among the different spiking phenotypes. No significant differences were observed

between spiking phenotypes for action potential threshold, spike height, or spike half-width (Table 2.2) (see Methods for definitions).

All cells, regardless of spiking phenotype, exhibited sustained, repetitive firing during long depolarizing current steps. Figure 2.3A and 2.3B show plots of instantaneous spike frequencies during 200 ms current injections from 50 to 650 pA (50 pA increments) for different example cells that were near opposite ends of the range for spike frequencies observed in our recordings. As illustrated by these plots as well as the summary of mean spike frequencies versus current injection in Figure 2.3C, vertical cells responded to increasing levels of current injection with steadily higher firing rates. Mean firing rates were significantly higher in "plateau and rebound spiking" cells at current injection levels between 50-400 pA compared to "no plateau no rebound" cells or "rebound spiking" cells, and for currents between 50-250 pA compared to "plateau" cells. All other comparisons between groups were not significant with the exception of higher firing rates in "rebound spiking" cells compared to "no rebound no plateau" cells at 50 pA.

Vertical cell spiking remained remarkably consistent over the course of 200 ms current injections. In a subset of recordings, we compared instantaneous spike frequencies for APs during identical, 300 pA current steps across different vertical cell categories (Figure 2.4). Although a range of initial spike frequencies was observed at this current level, in general spike frequency changed very little by the end of 200 ms steps as compared to initial spike rates. This was quantified by calculating the ratio of mean instantaneous spike frequency for the last 20 ms versus the first 20 ms of the 200 ms current steps (adaptation index). Within each subtype of vertical cell, some cells showed slight spike frequency adaptation (adapatation index < 1) and others exhibited some spike

frequency acceleration (adaptation index > 1), but on average spike rate was similar at the end of current steps compared to the start and were not significantly different between vertical cell subtypes (adaptation indexes: "rebound spiking": 1.01 ± 0.18, n=21; "plateau and rebound spiking": 1.05 ± 0.17, n=13; "plateau": 1.15 ± 0.27, n= 7; "no plateau or rebound spiking": 1.26 ± 0.38, n= 9; p= 0.06) (Figure 2.4E). In response to 300 pA steps, cells with initial spike rates of <~250 Hz tended to exhibit spike frequency acceleration whereas those with initial rates >250 Hz generally exhibited little change in spike frequency over the course of 200 ms current steps (Figure 2.4F).

Short-term depression of excitatory inputs

Excitatory inputs to vertical cells were evaluated by making voltage-clamp recordings of currents in response to stimuli applied through an extracellular electrode positioned in the deep layer of DCN. In these experiments, inhibitory transmission was blocked by including 10 μM SR-95531 and 0.5 μM strychnine in the bath solution and NMDA receptors were blocked by including 50 μM D-APV. EPSCs were likely mediated by AMPA receptors because we did not observe inward currents (evoked or spontaneous) in the presence of NBQX (10 μM) and vertical cells were previously shown to express GluA2 subunit-lacking AMPA receptors (Gardner et al., 1999, 2001). Consistent with auditory inputs to fusiform cells (Irie and Ohmori, 2008), EPSC amplitudes depressed in response to repetitive stimulation in 11 of 12 vertical cells (Figure 2.5A-B). However, in these cells, depression at the end of stimulus trains ranged somewhat widely between 80%-20% of initial EPSC amplitudes (see Figure 2.5C). In several cells (see Figure 2.5C), EPSCs at the end of a ten stimuli train were depressed to

similar levels across a ten-fold range in stimulation frequencies (200 Hz EPSC10/EPSC1 vs. 20 Hz EPSC10/EPSC1 ratio >0.75 in 6/11 cells) so that the average depression of EPSCs was constant across stimulus frequencies in the eleven vertical cells with depressing excitatory synapses (Figure 2.5B-C). However, the lack of difference was also likely due in part to variability in the extent of depression across the sample of recorded cells.

Weak synaptic connections between vertical cells and postsynaptic targets

Vertical cell-mediated inhibition is hypothesized to strongly shape DCN principal neuron activity (Young and Davis, 2002). However, existing evidence that vertical cells provide inhibition to principal neurons is indirect and comes primarily from anatomical studies (Rhode, 1999) and cross-correlation analysis of paired extracellular recordings between principal neurons and vertical cells (Voigt and Young, 1990). We therefore directly tested for functional synaptic connections between vertical cells and fusiform neurons using dual whole-cell recordings.

Fusiform cells were identified based on their location within the fusiform cell layer, large, bipolar somata (see Figure 2.1A), large amplitude spikes (peak ~20 mV more depolarized than vertical cells), and lack of GFP expression in tissue from GlyT2-EGFP mouse tissue. We also usually visualized dendritic morphology of fusiform cells by including Alexa Fluor 555 in pipette solutions. In almost all recordings in which dendritic morphology was examined, dendrites were observed to be mostly intact in our sagittal slice preparations (Figure 2.1A shows cells in a coronal section). Fusiform cells had extensive spiny dendrites extending throughout the molecular layer and long, aspiny

and less branched dendrites extending over large areas of the deep layer. After establishing a recording from a fusiform cell, whole-cell recordings were acquired from vertical cells located both nearby the fusiform cell soma as well as along the fusiform cell basal dendrites up to ~150 μm distal to the soma to test for synaptic connections. Often, we sequentially recorded from several vertical cells while simultaneously recording from the same fusiform cell (1-5 vertical cells were tested for a given fusiform cell).

We found that action potentials in vertical cells elicited detectable postsynaptic currents in fusiform cells in 11/91 of tested pairs (12.1% connection probability). In ten connected pairs in which presynaptic vertical cell spiking responses to long current steps was examined, five presynaptic cells were "rebound spiking" cells, four were "plateau and rebound spiking", and one was a "plateau" cell. Thus, at least three of the four subtypes of vertical cell can form synapses upon fusiform cells.

Measurements of peak conductance, latency, decay kinetics and failure rate for unitary postsynaptic currents (uIPSCs) elicited by presynaptic vertical cell spiking are summarized in Table 2.3. Consistent with monosynaptic connections between vertical cells and fusiform cells, uIPSCs were evoked with short latencies following presynaptic vertical cell APs (Table 2.3). Unitary currents had fast decay kinetics (Table 2.3), similar to spontaneously occurring IPSCs, which likely arose primarily from cartwheel cells (Golding and Oertel, 1997; Roberts and Trussell, 2010), the majority of which spontaneously fire action potentials under our slice conditions (Kim and Trussell, 2007). Vertical cell-mediated uIPSCs recorded in fusiform neurons were usually small in amplitude and were often obscured by spontaneous IPSCs, which could exhibit peak amplitudes of several hundred pA. The weak vertical cell inputs were in sharp contrast to

the more than 10-fold larger amplitudes of cartwheel cell-mediated uIPSCs recorded in fusiform cells recorded from cartwheel cell and fusiform cell pairs under identical conditions (peak conductance 23.95 ± 17.83 nS, range 6.39- 63.25 nS, n= 11 pairs). Connections between presynaptic vertical cells and postsynaptic fusiform neurons were likely often mediated by only a few synapses, because presynaptic spikes frequently failed to evoke uIPSCs (Table 2.3). This was unexpected because evidence from *in vivo* recordings suggests vertical cells can powerfully inhibit principal cell output (Young and Davis, 2002).

The short-term dynamics of vertical cell synapses onto fusiform cells were examined in a subset of paired recordings in which spontaneous IPSCs were not too large and frequent to complicate measurement of uIPSC amplitudes in response to trains of presynaptic APs. In response to 100 Hz trains of presynaptic action potentials, uIPSCs in fusiform cells usually exhibited moderate short-term facilitation (Figure 2.6B-C), suggesting a low initial release probability from vertical synapses. The mild facilitation of vertical cell-mediated synaptic currents indicates vertical cells can provide sustained inhibitory input to fusiform cells.

Although vertical cells are hypothesized to receive inhibitory input from D-stellate cells of the ventral cochlear nucleus (Nelken and Young, 1994), sources of inhibition to vertical cells are not well known. We also used dual recordings to explore whether vertical cells synapse upon other vertical cells. Functional connections were detected in 16 out of 36 tested vertical cell pairs, with a bidirectional connection observed in one pair. We tested for connections in both directions in all but one vertical cell pair. Thus, a total of 71 possible connections were examined, which yields a connection

probability of 23.9% (17 connected/71 tested connections). In the seven connected pairs in which spiking phenotypes of presynaptic vertical cells were assessed, we observed four “rebound spiking” cells, one “plateau and rebound spiking”, one “plateau”, and one “no plateau or rebound spiking” cell. Of the twelve connected pairs in which spiking behavior in postsynaptic cells were determined, we found eight “rebound spiking” cells, two “plateau and rebound spiking” cells, and two “plateau” cells. Thus, all vertical cell subtypes can synapse upon other vertical cells and all spiking phenotypes besides “no plateau or rebound spiking” neurons were observed to receive synaptic input from other vertical cells.

Unitary IPSCs recorded in vertical cells were similar to those observed in fusiform cells in peak amplitude, decay kinetics, latency and failure rate (Tables 2.3, 2.4). However, uIPSCs elicited by presynaptic spiking were more clearly distinguishable from baseline currents because vertical cells received very little spontaneous IPSC input, likely because they are not contacted by cartwheel cells (see Figure 2.7B). On average, vertical cell uIPSCs elicited by 100 Hz trains of presynaptic spikes exhibited moderate short-term facilitation, although the behavior of individual connections ranged from depression to strong facilitation (Figure 2.7C).

Given previous *in vivo* work suggesting vertical cells provide robust inhibitory input to principal neurons, we were surprised to find that vertical cell-mediated uIPSCs were relatively weak, especially in comparison to cartwheel cell inputs. We therefore wondered whether glycinergic transmission was potentially compromised in tissue from GlyT2-EGFP transgenic mice due to transgene expression. However, uIPSCs between vertical cells were not different in paired recordings from wild-type animals compared to

those from GlyT2-EGFP mice (peak conductance 2.208 ± 3.036 nS vs 1.561 ± 1.716 nS, respectively; p= 0.62; wildtype n= 6 pairs, transgenic n= 8 pairs). It was suggested in a previous study that neuronal glycine content declines over time in acutely prepared DCN slices (Wickesberg et al., 1994). However, we did not notice systematic differences for connection probability or uIPSC amplitudes in relation to times when paired recordings were made after tissue preparation (up to ~7 hours post-slicing). Unitary IPSCs were also stable for up to ~1 hour in recordings between connected neurons. Further, we did not observe significantly different uIPSC amplitudes in additional paired recordings between vertical cells in which pipette solutions were supplemented with 20 mM glycine (1.496 ± 0.780 nS peak conductance without failures, range 0.953 to 2.390 nS, n=3 connections, p= 0.46 unpaired t-test). The large amplitudes of cartwheel cell mediated uIPSCs also argue against slicing-induced rundown of neuronal glycine content. Together, these results indicate that artifacts from transgene expression or tissue slice preparation do not account for the small amplitude of vertical cell synaptic connections we observed.

Control of fusiform cell spiking requires multiple vertical cell inputs

We next investigated the functional impact of vertical cell-mediated inhibition on principal neuron spike output. In a first set of experiments, we made simultaneous current-clamp recordings between synaptically connected vertical cells and fusiform neurons. Brief (3 ms) current steps were applied to postsynaptic fusiform cells via somatic patch pipettes in order to elicit spiking on ~4 out of 5 identical current injections (620-680 pA each, 20 Hz) while the presynaptic vertical cell was resting below spike threshold (Figure 2.8A). Trials without vertical cell activity were then alternated with

those in which a train of 50 spikes at 100 Hz was evoked in the presynaptic vertical cell by suprathreshold current steps starting 50 ms prior to the first current injection into the postsynaptic fusiform cell (Figure 2.8B). Comparison of fusiform cell spiking probability in response to identical current steps in either condition demonstrated a slight, but significant reduction in spike probability when presynaptic vertical cells fired trains of spikes (Figure 2.8C; spike probability 0.797 ± 0.078 vs 0.710 ± 0.115, respectively; $p < 0.05$, paired t-test). This experiment indicated that even with robust presynaptic activity, a single vertical cell does not strongly influence fusiform cell spiking. To examine whether activity in multiple vertical cells could have greater impact on postsynaptic spiking, we performed a similar experiment, but replaced the presynaptic recording pipette with an extracellular stimulating electrode positioned in the deep layer near to the recorded fusiform cells and blocked excitatory transmission with 10 μM NBQX and 50 μM D-APV (see Figure 2.8D-E, inset). In three cells, SR95531 (10 μM) was included in the bath solution while another three recordings did not include SR95531. Stimulus position and strength were adjusted to evoke detectable IPSPs in current-clamped fusiform cells (Figure 2.8E, inset). When currents were recorded in voltage-clamp, the same stimuli evoked IPSCs with ~100pA peak amplitude (average value), which should correspond to activity in ~3-5 vertical cells. Presumptive vertical cell-mediated IPSCs, which exhibited moderate facilitation in response to trains of stimuli, were easily distinguished from those likely arising from cartwheel cells because cartwheel inputs to fusiform cells exhibit short-term depression and are typically large in amplitude (Mancilla and Manis, 2009; our unpublished observations). Extracellular stimuli (50 stimuli at 100 Hz starting 10 ms prior to somatic current injections in fusiform cells) significantly reduced fusiform cell

spiking in comparison to control conditions without extracellular stimuli (spike probability in control: 0.808 ± 0.062, with stim: 0.286 ± 0.096; $p < 0.0001$, paired t-test). Thus, coordinated activity in several vertical cells can reduce fusiform cell output.

Discussion

Intrinsic properties of vertical cells

Vertical cells exhibited diverse firing responses to step current injections. We used the presence or absence of persistent activity lasting beyond the duration of hyperpolarizing or depolarizing steps (rebound spiking or plateau depolarizations) to group vertical cells into different subtypes. However, within each subcategory, the duration of rebound or plateau activity varied from ~20 ms to several seconds beyond the end of current injection. Further, vertical cells could not generally be distinguished from each other based upon intrinsic membrane properties or action potential shape. Also, repetitive firing of vertical cells during depolarizing current steps was not distinctive between subcategories, with the exception of higher firing rates in cells exhibiting both plateau depolarizations and rebound spiking compared to other subtypes. The different spiking patterns we observed therefore appear to reflect a continuous distribution of response properties across the vertical cell population.

An unexpected feature of many vertical cells was the ability to generate plateau potentials that outlasted the duration of depolarizing current steps. In other cell types, the generation of similar plateau depolarizations has generally been attributed to calcium-dependent activation of a non-specific cation conductance (Chang and Kim, 2004; Egorov et al., 2002; Lee and Tepper, 2007; Morisset and Nagy, 1999). Whether a similar

mechanism accounts for vertical cell plateau depolarizations is currently unclear. Although the non-specific cation channel antagonist flufenamic acid (100 μM) reduced plateau potentials in vertical cells (not shown), spiking during steps was also severely affected, likely due to non-specific actions of flufenamic acid (Ottolia and Toro, 1994; Poronnik et al., 1992; Yau et al., 2010).

The maximum firing rates of vertical cells (with 650 pA injected current mean firing rate was 431 ± 55 Hz, range 315 to 560 Hz; n= 47 cells across subtypes) was at the high end of reported maximum firing rates in several classes of cells that exhibit rapid spiking including hippocampal and cortical fast-spiking interneurons (McCormick et al., 1985), vestibular nucleus neurons (Bagnall et al., 2007), and chicken cochlear nucleus neurons (Fukui and Ohmori, 2003). In these other cell types, fast-spiking phenotypes have been shown to rely upon expression of Kv3 family K^+ channels (Erisir et al., 1999; Fukui and Ohmori, 2003; Gittis et al., 2010; Lien and Jonas, 2003). Similar to other fast-spiking neurons, vertical cell action potentials were narrow (half-width ~230 μs) and repolarized rapidly, consistent with an important role for K^+ conductances in shaping spike output.

A particularly striking feature of most vertical cells was the ability to sustain very high firing rates (up to 400-500 Hz) throughout the duration of depolarizing current steps. In fact, in several cells, particularly those in which initial spike rates were <~250 Hz, spike rates were higher at the end compared to the beginning of a 300 pA current step. Even cells with high initial spike rates often showed some acceleration of instantaneous spike frequencies after an initial drop in frequency at the start of current steps (see especially individual traces for “plateau and rebound spiking” cells in Figure 2.4A). The

biophysical mechanisms that underlie the maintenance (or acceleration) of high firing rates in vertical cells were not explored in this study, but it is interesting to speculate that the same conductances underlying the generation of plateau potentials in some vertical cells might also contribute to sustained high frequency firing by providing a depolarizing drive during excitatory input. Unfortunately, testing this hypothesis may have to await better tools to manipulate the conductances contributing to plateau depolarizations.

Synaptic properties of vertical cells

Excitatory synaptic inputs to vertical cells, which arise from auditory nerve fibers and axons of T-stellate cells of the ventral cochlear nucleus (Rubio and Juiz, 2004), exhibited short-term depression in response to repetitive stimulation. This is consistent with the dynamics of auditory inputs to fusiform neurons (Irie and Ohmori, 2008) and contrasts with strong short-term facilitation of parallel fiber synapses in the DCN molecular layer (Roberts and Trussell, 2010). Interestingly, on average, the depression of EPSC amplitudes in vertical cells was similar across a ten-fold range of stimulus frequencies (20 to 200 Hz). Although this in part reflects cell to cell variability in the extent of depression of excitatory inputs at the different stimulus frequencies, the lack of difference in synaptic depression at low or high input frequencies was observed for approximately half of the cells examined (see Figure 2.5C). Frequency-independent synaptic transmission has recently been described at vestibular nerve synapses in the vestibular nuclei (Bagnall et al., 2008) and at vestibular mossy fiber synapses onto granule cells in the cerebellum (Arenz et al., 2008), where frequency-independent transmission is proposed to support linear vestibular behaviors. Because changes in sound

intensity are encoded as increases or decreases in the spike rate of auditory afferents, the apparent frequency-independence of transmission of at least some auditory fibers onto vertical cells may preserve information regarding the intensity of auditory stimuli.

To our knowledge, this study is the first to directly examine vertical cell synaptic input to fusiform neurons. Paired whole cell recordings demonstrated that vertical cells made synapses onto fusiform cells with a moderate connection probability, but we were surprised to find that vertical cell-mediated unitary currents recorded from fusiform cells were usually small in amplitude, particularly in comparison to uIPSCs mediated by molecular layer cartwheel interneurons. Further, current-clamp recordings indicated that activity in a single presynaptic vertical cell is not usually sufficient to affect fusiform cell spike output. Instead, our experiments suggest that activity in multiple vertical cells must be coordinated to inhibit fusiform cells.

Using dual recordings, we also discovered that vertical cells synapse upon other vertical cells with high connection probability. Together with the low frequency of spontaneous inhibitory currents observed in vertical cells, which indicates vertical cells do not receive significant input from inhibitory neurons that are spontaneously active in DCN slices, most prominently cartwheel cells (Kim and Trussell, 2007), this high connection probability suggests that a major source of inhibition to vertical cells comes from other vertical cells. Thus, vertical cell-mediated inhibition may underlie the inhibitory responses to non-best frequency tones (inhibitory sidebands) recorded from vertical cells *in vivo* and could therefore potentially contribute to the narrow frequency tuning of vertical cells (Rhode, 1999; Spirou et al., 1999). However, whether connected vertical cells are usually tuned to different characteristic frequencies remains to be

examined. We should also note that it seems unlikely that vertical cell-mediated inhibition could underlie the lack of vertical cell responses to broadband noise, which has been suggested to arise from inhibition arising from "onset chopper" units that respond robustly to broadband sounds (Nelken and Young, 1994; Young and Davis, 2002), which are thought to be D-stellate neurons of the ventral cochlear nucleus (Smith and Rhode, 1989).

Implications for vertical cell function

Although heterogeneous, the intrinsic properties of vertical cells do not appear to account for the various tone-evoked response patterns observed *in vivo*, which include spiking responses classified according to the shapes of tone-evoked peristimulus spike time histograms as chopper (regular discharge pattern sustained throughout tone presentation), onset (spiking at tone onset) and "unusual" responses with elements of both onset and chopper responses (Shofner and Young, 1985). Rather, the regular, sustained firing responses in response to depolarizing current steps observed in all vertical cells are most consistent with the chopper response type. An interesting possibility is that inhibition provided by other vertical cells contributes to the onset and "unusual" spiking phenotypes observed in some vertical cells.

Together, vertical cell intrinsic spiking properties and excitatory synaptic inputs to vertical cells appear suited to support enhanced vertical cell activity in response to increasing rates of auditory input. Indeed, vertical cells recorded *in vivo* usually exhibit increasing firing rates in response to best frequency tones presented at increasing sound intensities for moderate sound levels (Joris, 1998; Rhode, 1999; Shofner and Young,

1985; Spirou et al., 1999). This ability to respond to increasing sound level has been hypothesized to contribute to the non-linear *in vivo* response properties of principal neurons, which exhibit predominantly inhibitory responses to moderate and high intensity sounds (Young and Davis, 2002). However, our data indicate that vertical cell-mediated inhibition is not as robust as previously suggested from *in vivo* studies. One possibility is that the strongly inhibitory responses seen in some principal neurons are due to coordinated tone-evoked activity in a population of vertical cells converging on those principal neurons. Another possibility is that vertical cell-mediated inhibition plays a more subtle role in shaping principal cell output in mouse DCN compared to cat. In fact, Type IV responses were not observed in a study that examined tone-evoked response properties of principal neurons in awake mice (Roberts and Portfors, 2008). Vertical cells also project axon collaterals into the ipsilateral VCN and are therefore thought to provide feedback inhibition to targets within the VCN (Lorente de No, 1981; Wickesberg et al., 1991; Zhang and Oertel, 1993c). Whether vertical cell synapses in the VCN have functional properties similar to those we have shown for the feed-forward inhibitory function of vertical cells within the DCN remains to be examined.

The ability of vertical cells to fire persistently for prolonged periods following hyperpolarizing or depolarizing current steps has not previously been noted in *in vivo* recordings. However, *in vivo* intracellular recordings in fusiform cells have shown that tone offset can be followed by long periods of hyperpolarization (Hancock and Voigt, 2002; Rhode et al., 1983). Whether persistent spiking lasting beyond sound offset could contribute to DCN function is not clear. However, because prolonged spiking activity might support periods of inhibition lasting beyond the duration of acoustic stimuli, it is

possible that persistent vertical cell activity might have a role in suppressing sounds that occur after an initial stimulus that strongly activates vertical cells. Although further work is needed to examine this possibility, such a function could potentially contribute to sensory adaptation or echo suppression.

Acknowledgments

This work was supported by NIH grants RO1DC0044050 (L.O.T.) and F31DC010120 (S.P.K.). We thank Dr. Sascha du Lac for providing the GlyT2-EGFP transgenic mice.

Figure 2.1

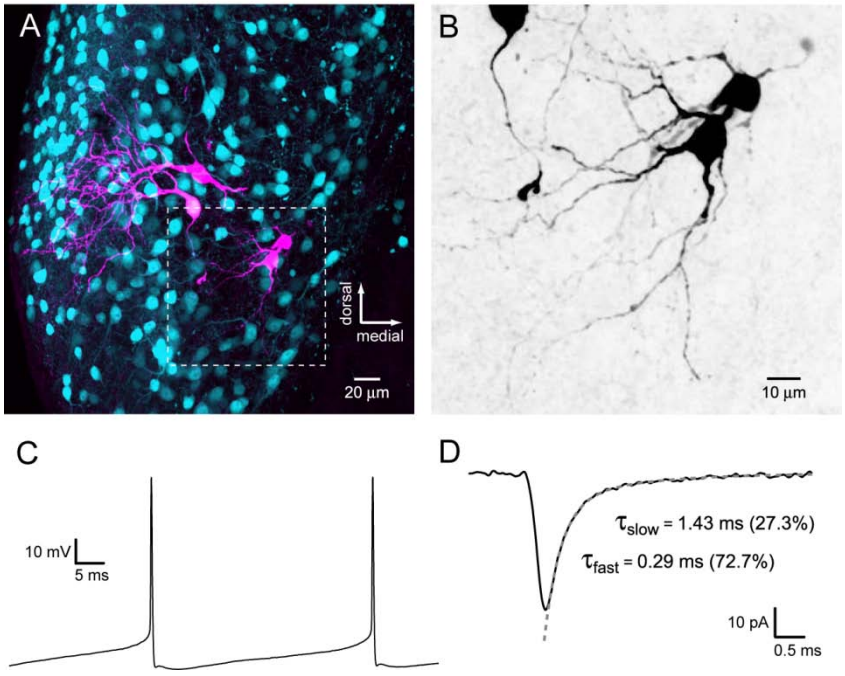

Figure 2.1. Targeting recordings of vertical cells in GlyT2-EGFP transgenic mice. (A) Maximum intensity confocal z-projection (50.4 µm in z-axis, 0.4 µm intervals) of fixed coronal slice from a GlyT2-EGFP mouse in which one fusiform (left, top), one cartwheel (left, lower), and two vertical cells (lower right) were filled with biocytin. GFP fluorescence in cyan. Biocytin labeling in magenta. The basal dendrites of the labeled fusiform cell and axon of the cartwheel cell were truncated in this slice. Prior to recordings, the labeled cartwheel cell and vertical cells exhibited strong GFP fluorescence. The fusiform cell did not express GFP. (B) Enlarged negative image of red fluorescence channel from boxed region in A. Note the round somatic morphology and smooth, relatively unbranched dendrites, typical of vertical cells. (C) Example voltage trace from a GFP(+) deep layer neuron (different cell than shown in B). Initial response to a 50 pA, 200 ms long current injection. Note the biphasic post-spike afterhyperpolarization. (D) Averaged spontaneous EPSC recorded at -70.2 mV from a GFP(+) deep layer neuron (average from 133 events occurring during 1 min of recording). Different cell than in B or C.

Figure 2.2

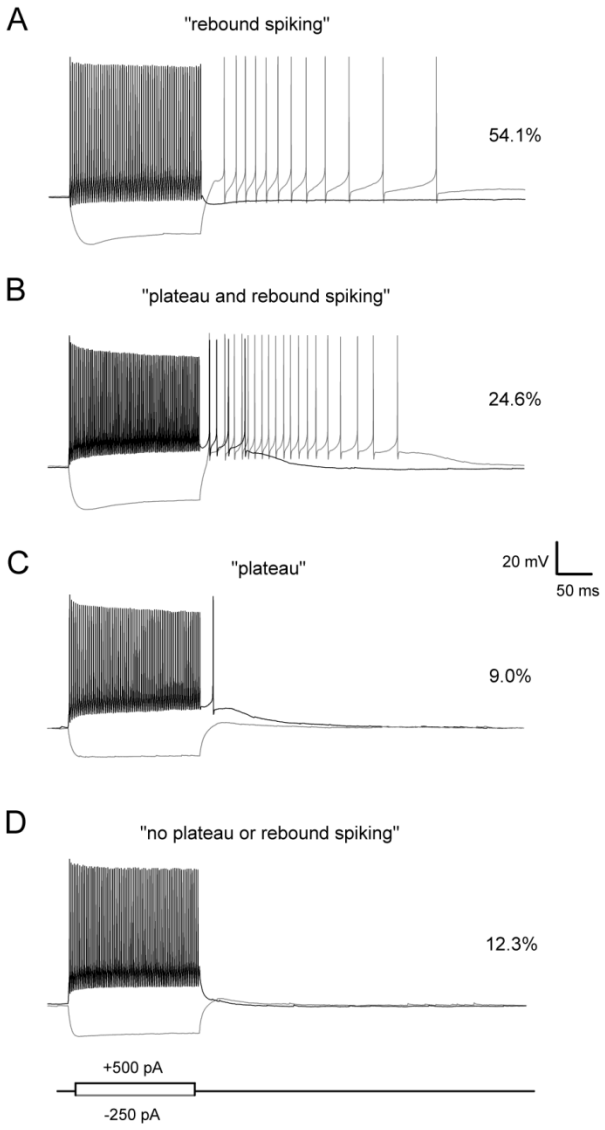

Figure 2.2. Heterogeneous spiking responses in vertical cells. (A-D) Example responses to hyperpolarizing (-250 pA, gray trace) and depolarizing (+500 pA, black trace) current injections (200 ms duration, see bottom of D) in A, “rebound spiking” (66/122 recorded vertical cells); B, “plateau and rebound spiking” (30/122); C, “plateau” (11/122); D, “no plateau or rebound spiking” (15/122) cells.

Table 2.1. Intrinsic membrane properties of vertical cells

	vertical cell subtype	n	mean	S.D.	range
Vrest (mV)	rebound spiking	27	-69.1	2.8	-64.7 to -74.5
	plateau and rebound spiking	11	-70.9	1.7	-67.1 to -74.7
	plateau	7	-70.7	4.8	-70.7 to -76.7
	no plateau or rebound spiking	9	-72.3	1.9	-69.5 to -75.0
Rinput (MΩ)	rebound spiking	27	163.7	53.8	93.6 to 286.5
	plateau and rebound spiking	11	149.0	37.2	101.5 to 211.1
	plateau	7	127.0	49.4	81.3 to 214.6
	no plateau or rebound spiking	9	141.3	32.0	93.8 to 184.4
Tau membrane (ms)	rebound spiking	27	11.5	4.6	6.8 to 22.9
	plateau and rebound spiking	11	10.3	2.4	6.7 to 13.6
	plateau	7	9.1	3.4	5.9 to 13.7
	no plateau or rebound spiking	9	9.8	1.9	7.7 to 12.7

all comparisons between vertical cell subtypes not statistically significant
except Vrest of "rebound spiking" and "no plateau or rebound spiking" cells ($p < 0.01$)

Table 2.2. Action potential properties of vertical cells

	vertical cell subtype	n	mean	S.D.	range
Threshold (mV)	rebound spiking	14	-56.0	5.6	-43.5 to -64.9
	plateau and rebound spiking	8	-54.2	6.6	-43.0 to -62.4
	plateau	6	-56.6	5.3	-49.4 to -63.0
	no plateau or rebound spiking	8	-58.1	4.4	-49.7 to -62.4
Height (mV)	rebound spiking	14	69.3	5.3	60.4 to 77.2
(peak - threshold)	plateau and rebound spiking	8	68.5	4.9	59.8 to 74.2
	plateau	6	71.6	5.7	65.4 to 79.8
	no plateau or rebound spiking	8	68.4	5.9	61.6 to 77.3
Half-height width (μs)	rebound spiking	14	227	29	188 to 286
	plateau and rebound spiking	8	220	22	179 to 244
	plateau	6	230	25	189 to 262
	no plateau or rebound spiking	8	232	23	197 to 274

no statistically significant differences between vertical cell subtypes

Figure 2.3

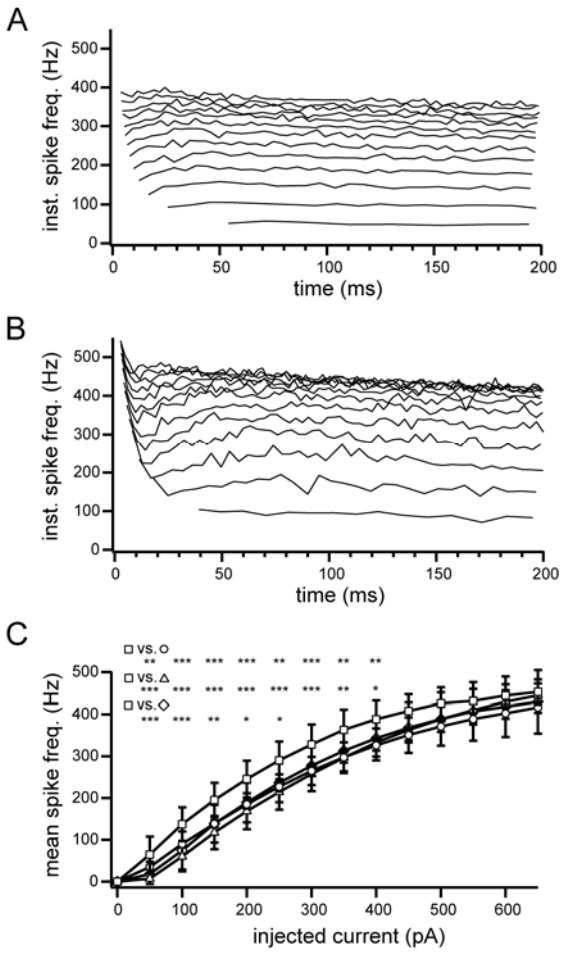

Figure 2.3. Input-output relationships in vertical cells. (A) Instantaneous spike frequencies during depolarizing current injections from +50 pA (bottom line) to +650 pA (top) in 50 pA increments in an example neuron. Current injection (200 ms) started at time zero. This cell was a "rebound spiking" neuron and was near the lower end of the observed range of mean spiking rates. (B) Same as in A, but for a cell that was near the upper end of the range for mean spike. "Plateau and rebound spiking" neuron. (C) Summary of mean frequencies (spikes occurring within the 200 ms duration of current injections). Symbols and error bars show mean ± S.D. of mean spike frequencies for "rebound spiking" (circles, n= 21), "plateau and rebound spiking" (squares, n= 12), "plateau (diamonds, n= 7) and "no plateau or rebound spiking" (triangles, n= 9) cells. Asterisks indicate statistical significance (*p< 0.05, **p< 0.01, ***p< 0.005).

Figure 2.4

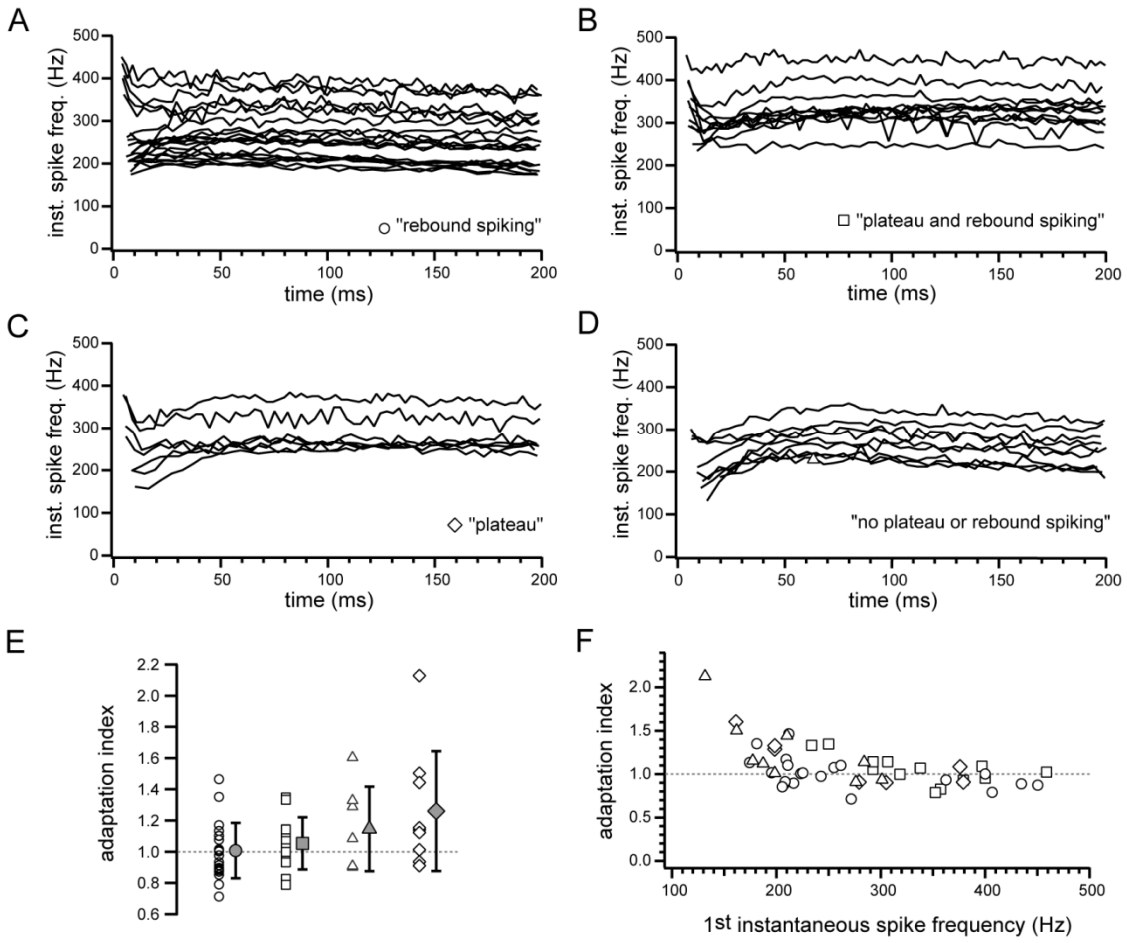

Figure 2.4. Sustained spike rates in vertical cells. (A-D) Plots of instantaneous spike frequencies over the duration of 200 ms current steps at 300 pA. Connected lines represent spike frequency measurements for individual cells. A, Data from 21 "rebound spiking" cells. B, "plateau and rebound spiking" cells (n= 13). C, "plateau" cells (n= 7). D, "no plateau or rebound spiking" cells (n= 9). (E) Summary of adaptation index measurements (mean instantaneous spike frequency of last 20 ms divided by that of first 20 ms of 200 ms step) for different vertical cell subtypes (symbols as in A-D) from data shown in A-D. Filled gray symbols show mean ± S.D. (F) Plot of adaptation index vs. first instantaneous spike frequency for data in A-D.

Figure 2.5

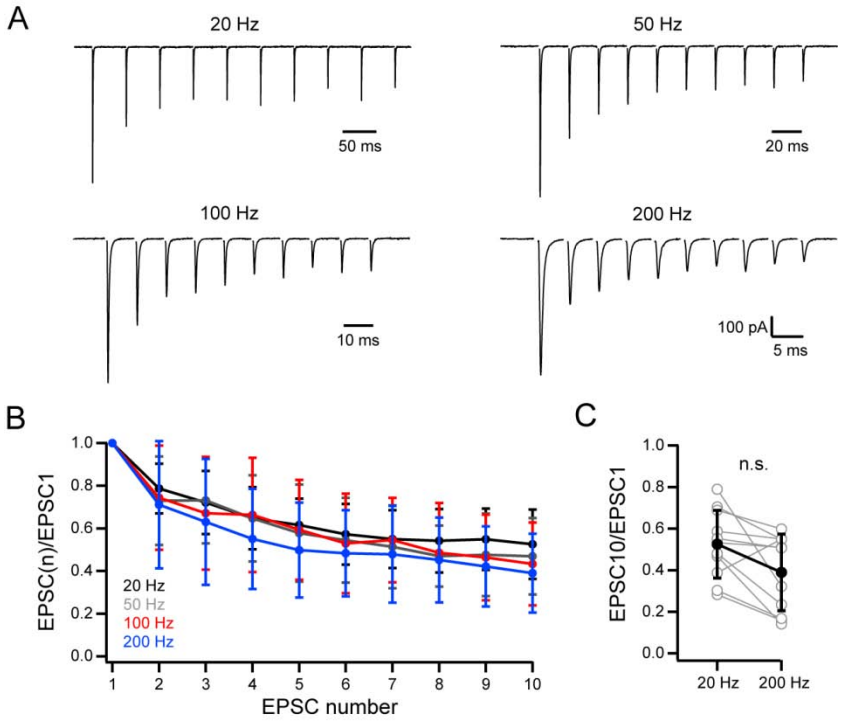

Figure 2.5. Short-term depression of excitatory inputs to vertical cells. (A) Example EPSCs recorded from a vertical cell in response to stimulus trains applied to auditory fibers at different frequencies. (B) Summary of ratio of EPSC peak amplitudes compared to the first stimulus-evoked EPSC over the course of stimulus trains for 11 cells that exhibited depression of EPSC amplitudes (out of 12 recorded vertical cells). Symbols and error bars show mean ± S.D. (C) EPSC10/EPSC1 ratios for 20 Hz and 200 Hz stimulus trains. Gray circles connected by lines show data from individual cells acquired at each stimulus frequency. Filled black circles and error bars show mean ± S.D. p= 0.08, paired t-test. All recordings for data in A-C were acquired with 50 μM D-APV, 0.5 μM strychnine, and 10 μM SR95531 in the bath solutions.

Figure 2.6

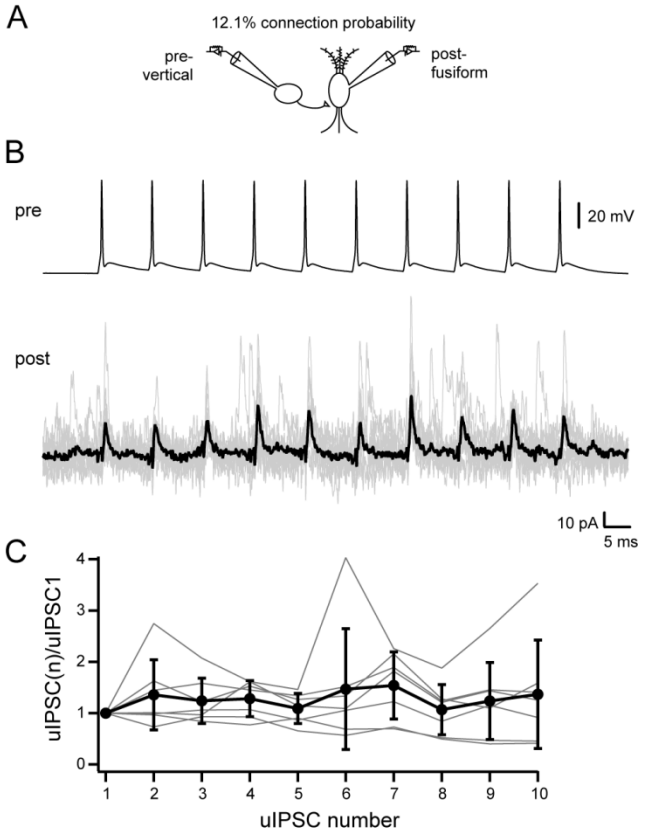

Figure 2.6. Paired recordings between vertical and fusiform neurons. (A) Schematic of paired recordings. In 11 out of 91 tested pairs, spiking in presynaptic vertical cells elicited detectable unitary IPSCs in postsynaptic fusiform neurons. (B) Example time-locked traces recorded simultaneously from a presynaptic vertical cell recorded in current-clamp mode (top, single sweep) and a postsynaptic fusiform cell held in voltage-clamp at -60.2 mV (bottom; gray traces are ten superimposed current sweeps, black trace is average of 20 sweeps). APs were elicited in the presynaptic vertical cell by 1 ms suprathreshold current injections applied ten times at 100 Hz (15 sec between trials). (C) Ratios of peak uIPSC amplitudes recorded in postsynaptic fusiform cells for each presynaptic vertical cell AP in a 100 Hz train compared to the first AP. Gray lines are data from individual cells. Black circles with error bars are mean ± S.D. (n= 7 pairs).

Figure 2.7

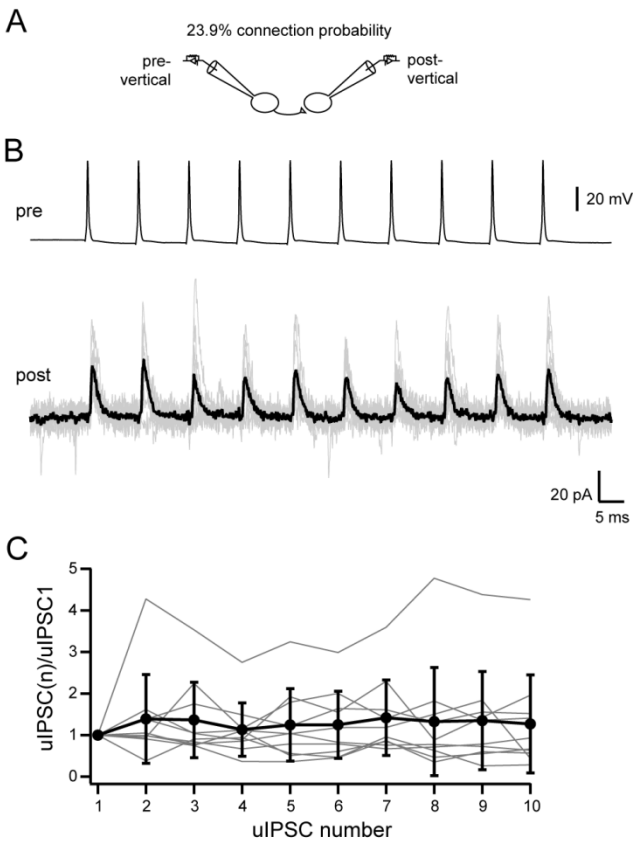

Figure 2.7. Paired recordings between vertical cells. (A) Schematic of recording configuration. Unidirectional connections were found in 15 out of 36 tested pairs and one pair was connected in both directions (reciprocal connection). In all but one pair, synapses were tested in both directions, yielding a connection probability of 23.9% (17 out of 71 tested connections). (B) Example time-locked traces recorded simultaneously from a presynaptic vertical cell recorded in current-clamp mode (top, single sweep) and a postsynaptic vertical cell held in voltage-clamp at -60.2 mV (bottom; gray traces are ten superimposed current sweeps, black trace is average of the ten individual sweeps). APs were elicited in the presynaptic vertical cell by 1 ms suprathreshold current injections applied ten times at 100 Hz (15 sec between trials). (C) Ratios of peak uIPSC amplitudes recorded in postsynaptic cells for each presynaptic AP in a 100 Hz train compared to the first AP. Gray lines are data from individual cells. Black circles with error bars are mean ± S.D. (n= 10 pairs).

Table 2.3. Properties of vertical cell unitary IPSCs recorded from fusiform cells

	n	mean	S.D.	range
peak conductance (nS)				
including failures	11	2.056	2.931	0.712 to 10.297
without failures	11	2.652	2.736	0.861 to 10.297
failure rate (%)	11	39.5	24.4	0 to 71.4
latency (ms)	8	0.59	0.20	0.31 to 0.85
τ decay (ms)	7	1.03	0.23	0.72 to 1.367

Table 2.4. Properties of vertical cell unitary IPSCs recorded from vertical cells

	n	mean	S.D.	range
peak conductance (nS)				
including failures	14	1.838	2.290	0.343 to 7.815
without failures	14	2.444	2.065	0.524 to 7.815
failure rate (%)	14	37.7	30.8	0 to 80
latency (ms)	14	0.58	0.15	0.33 to 0.84
τ decay (ms)	14	1.31	0.29	0.87 to 2.07

Figure 2.8

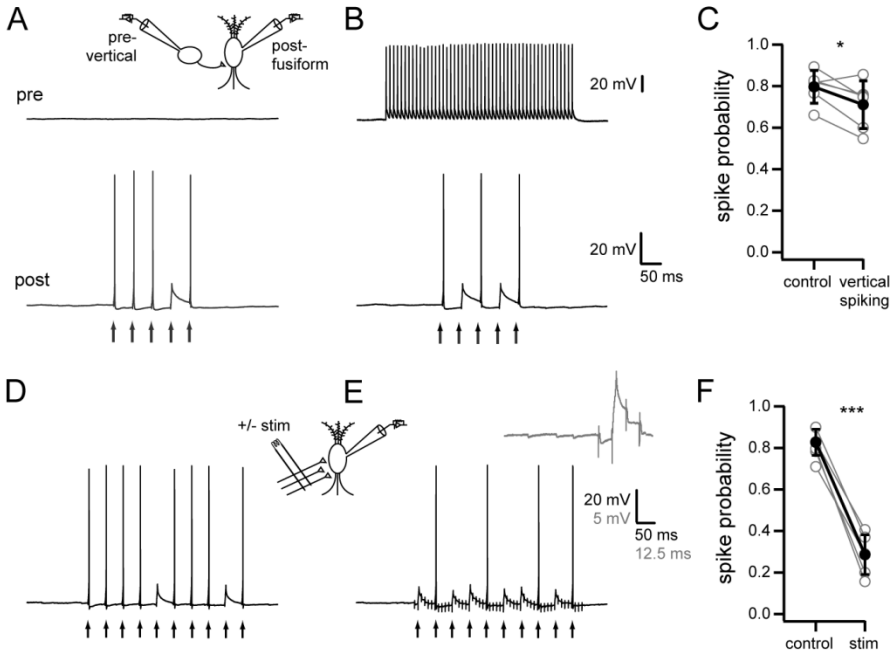

Figure 2.8. Effect of vertical cell-mediated inhibition on fusiform cell spike output. (A-B) Example traces from a simultaneous recording acquired from a synaptically connected vertical cell and fusiform cell pair (see inset) in which fusiform cell spikes were evoked by just-suprathreshold current injection (arrows) either when the presynaptic vertical cell was at resting V_m and did not fire spikes (control; example traces in A), or when a train of suprathreshold current steps were applied to elicit 50 APs at 100 Hz in the presynaptic vertical cell starting 50 ms prior to test injections into the fusiform cell (vertical spiking; example traces in B). Sweeps with presynaptic vertical cell spiking were interleaved with control sweeps. Identical test injections into the postsynaptic fusiform were used for both conditions and were constant throughout the experiment. (C) Summary of paired recording experiments as shown in A-B. Spike probabilities were determined for 25-30 trials in each condition and were calculated by dividing the number of observed spikes by the number of test injections. Gray circles connected by lines represent mean

spike probabilities in individual pairs under each experimental conditions. Black circles with error bars show mean ± S.D. for all tested pairs (n= 6 pairs). (D-E) Example voltage traces in a fusiform cell in which just-suprathreshold current injections (arrows) were used to elicit spikes without (D) or with extracellular stimulation of inhibitory fibers starting 10 ms prior to test injections (E). Inset between D and E shows recording configuration. Gray inset in E is expanded region of voltage trace showing first four extracellular stimuli and first intracellular current injection. Note small (~2 mV) IPSPs following stimulus artifacts. Control and stimulus conditions were interleaved. (F) Summary of experiments as in D-E. For each cell, mean spike probabilities were determined from 30 sweeps in each condition (gray circles). Black circles with error bars are mean ± S.D for the 6 cells. For data shown in F, three cells were recorded with and three cells were recorded without SR95531 (10 μM) in the bath solution. All recordings in A-F were acquired with D-APV (50 μM) and NBQX (10 μM) in the bath solutions.

CHAPTER 3. SPONTANEOUS SPIKING AND SYNAPTIC DEPRESSION UNDERLIE NORADRENERGIC CONTROL OF FEED-FORWARD INHIBITION

Sidney P. Kuo and Laurence O. Trussell

Neuroscience Graduate Program and Oregon Hearing Research Center and Vollum Institute, Oregon Health and Science University, Portland, OR 97239

Abstract

Inhibitory interneurons across diverse brain regions commonly exhibit spontaneous spiking activity, even in the absence of external stimuli. It is not well understood how stimulus-evoked inhibition can be distinguished from background inhibition arising from spontaneous firing. We found that noradrenaline simultaneously reduced spontaneous inhibitory inputs and enhanced evoked inhibitory currents recorded from principal neurons of the mouse dorsal cochlear nucleus (DCN). Together, these effects produced a large increase in signal-to-noise ratio for stimulus-evoked inhibition. Surprisingly, the opposing effects on background and evoked currents could both be attributed to noradrenergic silencing of spontaneous spiking in glycinergic interneurons. During spontaneous firing, glycine release was decreased due to strong short-term depression. Elimination of background spiking relieved inhibitory synapses from depression and thereby enhanced stimulus-evoked inhibition. Our findings illustrate a simple yet powerful neuromodulatory mechanism to shift the balance between background and stimulus-evoked signals.

Introduction

Neurons are rarely silent in the intact brain. Rather, intrinsic and network mechanisms interact to drive action potential firing, even in the absence of external stimuli. For example, multiple classes of inhibitory interneuron exhibit spontaneous spiking behavior *in vivo* (Gentet et al., 2010; Klausberger et al., 2003; Ruigrok et al., 2011) and *in vitro* (Parra et al., 1998). Postsynaptic targets of inhibitory neurons are therefore subject to constantly fluctuating inhibitory synaptic conductances which do not necessarily correspond to stimulus-evoked activity (Alger and Nicoll, 1980; Salin and Prince, 1996; Vincent and Marty, 1996). This background input may impose a tonic inhibition that shapes neuronal integration (Mitchell and Silver, 2003) and can even enhance stimulus encoding if its structure correlates with that of background excitatory inputs (Cafaro and Rieke, 2010). However, numerous studies have also highlighted the importance of stimulus-driven inhibition in controlling the output of target neurons. For example, the precise temporal relationship between afferent-evoked excitation and inhibition imposed by feed-forward inhibitory circuits can strongly regulate spike timing in postsynaptic cells (Mittmann et al., 2005; Pouille and Scanziani, 2001). Despite the prevalence of spontaneous activity in interneurons, few studies have addressed whether background spontaneous firing affects how stimulus-evoked signals are conveyed by inhibitory cells.

By altering neuronal excitability and/or synaptic transmission, engagement of neuromodulatory systems may provide a general way to adjust the relationship between spontaneous and evoked signals according to environmental and physiological context (Hurley et al., 2004). Noradrenaline (NA) in particular has been implicated in enhancing

sensory or stimulus-evoked firing with respect to background activity in several brain regions (Freedman et al., 1976; Hirata et al., 2006; Hurley et al., 2004; Kossl and Vater, 1989; Waterhouse and Woodward, 1980). In the auditory system, the brainstem cochlear nuclei are densely innervated by noradrenergic fibers (Jones and Friedman, 1983; Klepper and Herbert, 1991; Kossl et al., 1988; Kromer and Moore, 1976), but the functional roles of these inputs are not well understood.

Here, we examined how NA affects spontaneous and stimulus-evoked inhibition mediated by cartwheel interneurons of the DCN. Cartwheel cells fire spontaneously at moderate rates both *in vivo* (Davis et al., 1996b; Davis and Young, 1997; Portfors and Roberts, 2007) and *in vitro* (Golding and Oertel, 1997; Kim and Trussell, 2007; Manis et al., 1994) and provide strong, glycinergic input to DCN fusiform principal neurons (Mancilla and Manis, 2009; Roberts and Trussell, 2010). Within the molecular layer of the DCN, parallel fiber axons originating from DCN granule cells convey excitatory input from multiple sensory modalities to cartwheel cells as well as to fusiform cells (Oertel and Young, 2004). This shared input between cartwheel and principal cells forms the basis for a feed-forward inhibitory network (Roberts and Trussell, 2010) that powerfully filters the acoustic responses of principal neurons (Davis et al., 1996b; Davis and Young, 1997; Shore, 2005).

We found that NA enhanced inhibition elicited by parallel fiber stimulation while simultaneously reducing spontaneous inhibitory input to fusiform cells. This dual effect resulted in a large increase in the signal-to-noise ratio of parallel fiber-evoked feed-forward inhibition. Unexpectedly, the opposing effects of NA upon spontaneous and evoked inhibition were both due to noradrenergic elimination of cartwheel cell

spontaneous spiking. Under control conditions, cartwheel synapses were tonically depressed by background spiking activity. By shutting off spontaneous spiking, NA relieved cartwheel synapses from depression and thereby enhanced glycine release in response to parallel fiber stimulation. This indirect control of synaptic output through modulation of spontaneous activity may have distinct advantages over direct modulation of presynaptic release probability in spontaneously firing cells.

Methods

Slice preparation

All procedures used in the care and handling of animals were approved by the OHSU Institutional Animal Care and Use Committee. Parasagittal brainstem slices (210 μm) were prepared from postnatal day 17-23 heterozygous transgenic GIN (**G**FP-expressing **I**nhibitory **N**eurons) (Oliva et al., 2000) or GlyT2-GFP mice (Zeilhofer et al., 2005) and their wild-type littermates. Both transgenic lines were backcrossed into the C57BL/6J genetic background (Jackson Labs) and were maintained and genotyped as previously described (Roberts et al., 2008). No differences were observed across genotypes so data from all mouse strains were pooled. Slices were prepared then maintained for 1 hour in warm (~34°C) ACSF solution containing (in mM): 130 NaCl, 2.1 KCl, 1.7 $CaCl_2$, 1.0 $MgSO_4$, 1.2 KH_2PO_4, 20 $NaHCO_3$, 3 Na-HEPES, 11 glucose; bubbled with 5% CO_2/ 95% O_2, ~300 mOsm. Slices not transferred to the recording chamber immediately following the one-hour recovery period were maintained in the same solution at room temperature (~22°C) until use.

Electrophysiology

During recordings, slices were constantly perfused (~1-2 mL/min) with ACSF maintained at 33 ± 1°C. Cells were visualized on the stage of an upright microscope (Olympus BX51W) using infrared gradient contrast optics (Dodt et al., 2002) and a 60X magnification objective. Fusiform cells and cartwheel cells were identified based on location within the slice, somatic size and morphology, and characteristic responses to hyperpolarizing and depolarizing current injections (Golding and Oertel, 1997; Manis et al., 1994; Tzounopoulos et al., 2004; Zhang and Oertel, 1994). In loose cell-attached recordings, spontaneously active cartwheel cells could be easily identified by their irregular action potential firing patterns (Kim and Trussell, 2007). Additionally, EGFP expression in tissue from GIN (subset of GAD67-expressing cells labeled) or GlyT2-EGFP (all glycinergic neurons labeled) transgenic mice was often used to facilitate cell identification (Roberts and Trussell, 2008). For whole cell recordings, electrodes were filled with a solution containing (in mM): 113 K-Gluconate, 9 HEPES, 2.75 $MgCl_2$, 1.75 $MgSO_4$, 0.1 EGTA, 14 $Tris_2$-phosphocreatine, 4 Na_2-ATP, 0.3 Tris-GTP; osmolality adjusted to ~290 mOsm with sucrose, pH adjusted to 7.25 with KOH. All reported membrane potential values are corrected for a -10 mV junction potential. For loose cell-attached recordings, pipettes were filled with a modified ACSF solution containing (in mM): 142 NaCl, 2.1 KCl, 1.7 $CaCl_2$, 1.0 $MgSO_4$, 1.2 KH_2PO_4, 10 Na-HEPES, 11 glucose; ~300 mOsm, pH adjusted to 7.35 with NaOH. Patch pipettes (2-4 MΩ) were pulled from borosilicate glass (WPI). For loose cell-attached experiments, 10 µM NBQX, 50 µM D-APV, 0.5 µM strychnine, 10 µM SR95531 (gabazine) were added to all bath solutions to block excitatory and inhibitory synaptic transmission. Bath solutions for

whole cell recordings did not contain drugs unless specified otherwise. To stimulate parallel fibers, voltage pulses (10-30 V, 150-200 μsec) were applied via ACSF-filled double-barreled glass electrodes (lengthwise tip diameter ~5 μm; theta glass, WPI) that were positioned in the molecular layer >~100 μm from the soma of recorded cells. Paired recordings targeted nearby neurons (<50 μm intersomatic distance). In close agreement with previous results (Roberts and Trussell, 2010), we found functional cartwheel to fusiform cell synaptic connections in 35 out of 98 tested cartwheel-fusiform pairs (35.7 % connection probability).

Data acquisition and analysis

Recordings were acquired using a Multiclamp 700B amplifier and pClamp 10 software (Molecular Devices). Signals were digitized at 10-50 kHz using a Digidata 1322A (Molecular Devices) and low-pass filtered at 3-10 kHz. For all voltage-clamp experiments, series resistance (<20 MΩ) was compensated by 80% and membrane potential was held constant at -60 mV. To quantify changes in stimulus-evoked currents (Figures 1D, 6D, 8B), total outward charge was measured from averaged current traces (Figures 1, 6: 20 sweeps in each experimental condition; Figure 3.8, 13 to 33 sweeps per condition) by integrating all current within a window that started at the first zero current level crossing following stimulus onset and ending 20 ms after stimulus onset. Charge difference (Figure 1F, 6F, 8E) was measured from subtracted currents (see Figures 1E, 6E, 8D) over 20 ms windows that started 1 ms after stimulus onset. Spontaneous IPSCs occurring within 250 ms windows prior to parallel fiber stimulus application (15 sec inter-sweep interval) were detected using the template function event detection feature in

Axograph X. Root mean square (RMS) measurements for spontaneous currents were determined from current amplitude values for every point (50 kHz acquisition, 10 kHz filtering) within the same time windows used to detect sIPSCs. All data are reported as mean ± SEM. Unless otherwise stated, statistical significance ($p<0.05$) was tested using paired or unpaired Student's t-tests as appropriate.

Reagents

NBQX, D-APV, strychnine and gabazine were obtained from Ascent Scientific. All other drugs and chemicals were from Sigma Aldrich. Stocks of NA were prepared fresh from (+/-)-Noradrenaline (+)-bitartate powder each day. Bath solutions containing NA were protected from light to minimize oxidation. Final concentration of NA was 10 μM in all experiments except those in Figure S1 (50 μM NA). All drugs were applied via bath perfusion.

Results

Noradrenaline enhances feed-forward inhibition

We examined whether NA affects integration of excitatory and inhibitory signals conveyed through the molecular layer circuitry of the DCN. Whole-cell voltage-clamp recordings were acquired from fusiform cells in acute slices of mouse brainstem and synaptic currents were recorded in response to activation of parallel fibers by an extracellular stimulating electrode positioned in the DCN molecular layer (Figure 3.1A). Single stimuli typically elicited weak excitatory currents and small or undetectable inhibitory currents (see first stimulus, Figure 3.1B, top). Because parallel fibers exhibit

strong short-term facilitation (Roberts and Trussell, 2010; Tzounopoulos et al., 2004), brief stimulus trains (three stimuli at 20 Hz) were applied to recruit robust parallel fiber activity. When fusiform cells were clamped at -60 mV, intermediate to the reversal potentials for Cl^- conductances (-84 mV) and excitatory conductances (~0 mV), each stimulus elicited a sequence of inward current followed closely by outward current (Figure 3.1B), characteristic of direct activation of excitatory fibers followed by feed-forward recruitment of inhibitory inputs (Mittmann et al., 2005; Pouille and Scanziani, 2001). Both inward and outward components of the responses were larger for the second and third parallel fiber stimuli due to facilitation of excitatory inputs onto both fusiform and cartwheel cells (Roberts and Trussell, 2010). Consistent with activation of disynaptic inhibition, inward and outward components of the evoked responses were largely abolished by application of NBQX (Figure 3.1C).

When identical stimulus trains were applied in the presence of 10 μM NA, we observed a significant enhancement of the outward components of evoked currents in response to the second and third stimuli (Figure 3.1B, middle, D; measured as total outward charge, see Methods; stim2 control: 701±246 pA*ms, NA: 1809±561 pA*ms, $p<0.05$, n= 6; stim3 control: 596±203 pA*ms, NA: 1680±286 pA*ms; $p<0.01$, n=6). This effect could be clearly visualized by subtracting average control responses from average currents recorded in NA (Figure 3.1B, bottom). Quantification of total charge in such subtracted records demonstrated a large net increase in the charge following the second and third stimuli (Figure 3.1E; stim2 1158±421 pA*ms; stim 3 1271±261 pA*ms, $p<0.05$ and <0.005, respectively, one sample t-test comparison to 0 pA*ms). On average a small

reduction in the total charge was observed following the first stimulus (Figure 3.1E; -216±47 pA*ms, $p<0.05$, one sample t-test comparison to 0 pA*ms).

The enhancement of net outward synaptic current by NA could reflect an increase in inhibitory conductance and/or a decrease in excitatory conductance. NA did not have any effect on the peak amplitude (EPSC1 control: -203±39 pA, NA: -195±31 pA, $p=0.40$, $n=5$) or short-term facilitation (EPSC2/1 control: 1.73± 0.27, NA: 1.69±0.28; $p=0.59$; EPSC3/1 control 1.92±0.77, NA: 1.93±0.38, $p=0.93$, $n=5$) of evoked parallel fiber EPSCs recorded from fusiform cells (inhibitory transmission blocked with 10 μM gabazine, 0.5 μM strychnine) (Figure S1). Thus, NA specifically altered inhibitory input to fusiform cells.

NA increases signal-to-noise ratio of feed-forward inhibition

In addition to the enhancement of stimulus-evoked inhibitory postsynaptic currents (IPSCs), we also observed that NA sharply reduced spontaneous IPSCs (sIPSCs) recorded in fusiform cells (Figure 3.2). Application of NA (10 μM) significantly decreased both frequency (Figure 3.2B; mean frequency control: 93.0±8.2 Hz, NA: 15.3±3.9 Hz; $p<0.001$, paired t-test, $n=6$) and peak amplitude (Figure 3.2C; control 78.9±6.5 pA, NA 46.6±4.3 pA; $p<0.01$, paired t-test, $n=6$) of spontaneous events in all cells tested.

The opposing effects of NA upon spontaneous and parallel fiber stimulation-evoked IPSCs led to a dramatic shift in the balance between these two modes of

inhibitory input. In control, sIPSCs occurred frequently and often had amplitudes similar to those evoked by parallel fiber stimulation (Figure 3.3A, top). In the presence of NA, the near elimination of spontaneous IPSCs together with the enhancement of stimulus-evoked IPSCs resulted in a marked difference between stimulus-driven versus background currents (Figure 3.3A, bottom). To quantify the change in background input produced by NA, we measured root-mean-square (RMS) values of individual current sweeps over a 250 ms period just prior to parallel fiber stimulation (left side of Figure 3.3A). NA (10 μM) significantly reduced the RMS of background currents (Figure 3.3B; control: 33.06±4.45 pA, NA: 13.79±1.23 pA, $p<0.005$, n=6). We quantified the change in relative amplitudes between evoked and spontaneous currents by dividing evoked IPSC peak amplitudes by the RMS of background currents (signal-to-noise ratio). Signal-to-noise of the first parallel fiber stimulus was not significantly changed between control and NA (1.36±0.50 and 2.83±1.36, respectively; $p=0.16$), but NA application resulted in a 7-8-fold change in signal-to-noise ratios for the second and third stimuli in a train (stim2 control: 3.3±1.3, NA: 23.2±6.9, $p<0.02$; stim 3 control 2.8±0.7, NA: 22.1±3.9, $p< 0.005$; n=6; Figure 3.3C). These results indicate that in the presence of NA, feed-forward inhibition evoked by parallel-fiber activity dominates over spontaneous inputs.

Activation of α_2 adrenergic receptors eliminates cartwheel cell spontaneous spiking

DCN principal neurons receive inhibitory inputs from several subtypes of interneuron (Oertel and Young, 2004). However, the noradrenergic elimination of fusiform cell sIPSCs is probably due to effects of NA on the spontaneous firing of

presynaptic cartwheel cells. First, cartwheels are the most numerous molecular layer interneuron type (Lorente de No, 1981) and have a high probability of forming strong synaptic connections onto nearby fusiform cells (Mancilla and Manis, 2009; Roberts and Trussell, 2010). Second, >75% of cartwheel cells fire spontaneously under similar recording conditions to those used here (Kim and Trussell, 2007). Finally, cartwheel cells are distinguished from other DCN neurons by their ability to fire high-frequency (~200 Hz) bursts of action potentials termed complex spikes (Kim and Trussell, 2007; Manis et al., 1994; Zhang and Oertel, 1993a) and complex spike-like bursts of spontaneous IPSCs were frequently observed in all cells (Golding and Oertel, 1997; Roberts and Trussell, 2010).

We therefore investigated whether NA affects cartwheel cell spontaneous behavior using extracellular loose cell-attached recordings. Consistent with previous results (Kim and Trussell, 2007), 72.4% (63/87 cells) of cartwheel cells fired APs spontaneously in control conditions. Also in agreement with previous work (Golding and Oertel, 1997; Kim and Trussell, 2007), control spontaneous spiking was not regular but instead was characterized by brief periods of spiking activity separated by periods of quiescence, each of which could last from ~0.5 s up to several seconds (Figure 3.4A). Spiking periods consisted primarily of simple spikes occurring at a frequency of ~20-30 Hz (Figure 3.4B-C) and in 6/11 cells included one or two high-frequency (~200 Hz) complex spike bursts per spiking period ("complex spiking" Figure 3.4B-C). The mean firing rate in control was 13.6±2.0 Hz (range 4.5 to 25.9 Hz, n= 11).

NA application (10 μM) resulted in almost complete elimination of spontaneous spiking in all cartwheel cells tested (Figure 3.4A-B, D-F; spike rate reduced to 4.8±3.0%

of control, n= 6). This effect was reversed by the α_2-adrenergic receptor antagonist idazoxan (1 μM; Figure 3.4E-F; 101.9±7.3% control spike rate in NA + idazoxan, n= 5; not significantly different than 100 % control rate, p=0.80, one-sample t-test) and was mimicked by the α_2 agonists UK14304 (1 μM; 19.8±10.4% control rate, n= 8) and clonidine (5 μM; 14.8±13.0% control rate, n=4) (Figure 3.4F). In contrast, NA was equally effective at eliminating cartwheel spiking when applied alone, or in the presence of the α_1 antagonist prazosin (0.1 μM) or the β receptor antagonist propranolol (20 μM) (Figure 3.4F; NA reduced spike rate to 8.2±7.3%, n=4, and 0.8±0.8%, n=6, of control, respectively). Thus, NA silences cartwheel cell spontaneous spiking and this effect is mediated solely by α_2 adrenergic receptors.

NA does not directly affect synaptic transmission

NA could affect parallel fiber-evoked inhibition of fusiform cells through several potential mechanisms. NA is known to directly alter neurotransmitter release from multiple cell types by activating adrenergic receptors located on or near presynaptic axon terminals (Kondo and Marty, 1997; Leao and Von Gersdorff, 2002). We therefore examined whether direct enhancement of glutamate release from parallel fibers onto cartwheel cells and/or glycine release from cartwheel cell terminals could account for the observed increase in parallel fiber-evoked feed-forward inhibition of fusiform cells induced by NA.

To determine whether noradrenergic strengthening of parallel fiber inputs could contribute to enhanced recruitment of cartwheel cell activity, we made whole-cell recordings from cartwheel cells and measured EPSCs in response to parallel fiber

stimulation (inhibitory currents blocked with 10 μM gabazine, 0.5 μM strychnine)(Figure 3.5A-B). NA did not alter the peak amplitude (Figure 3.5C; EPSC1 in control: -382±105 pA, NA: -336±85 pA, p=0.30, n=6) or short-term facilitation (Figure 3.5D; EPSC2/EPSC1 control: 2.25±0.12, NA: 2.14±0.11, p=0.39, n=6; EPSC3/EPSC1 control: 2.96±0.23, NA: 2.75±0.14, p=0.19, n=6) of parallel fiber EPSCs. Thus, the increase in feed-forward inhibition of fusiform cells was not due to a change in excitatory input to cartwheel cells.

To test whether NA could act directly on cartwheel cell axon terminals to modulate glycine release, we acquired simultaneous whole-cell recordings from synaptically connected pairs of cartwheel and fusiform cells. Three simple spikes at 20-ms intervals were elicited by brief depolarizing current injections into presynaptic cartwheel cells held in current clamp and the resulting unitary IPSCs (uIPSCs) were recorded in postsynaptic fusiform cells held in voltage clamp (Figure 3.5E). NA application did not alter the peak amplitude (Figure 3.5F; uIPSC1 in control: 557±176 pA, NA: 552±187 pA, p=0.89, n=6 pairs) or short-term depression (Figure 3.5G; uIPSC2/uIPSC1 control: 0.55±0.02, NA: 0.59±0.01, p=0.10, n=6 pairs; uIPSC3/uIPSC1 control: 0.40±0.01, NA: 0.42±0.01, p=0.31, n=6 pairs) of uIPSCs. Thus, NA does not change spontaneous or evoked cartwheel cell-mediated inhibition of fusiform neurons by directly affecting release from cartwheel synapses.

Subthreshold changes in somatic membrane potential (V_m) can alter synaptic transmission (Alle and Geiger, 2006; Shu et al., 2006). Because NA likely exerted its effects on spontaneous spiking by hyperpolarizing cartwheel cells, we examined cartwheel synaptic output in three additional connected cartwheel and fusiform cell

pairs while holding the presynaptic cartwheel V_m at either -79.4±0.9 mV (V_{rest}) or -89.6±0.6 mV ($V_{hyperpol}$) using bias current injection in current-clamp (not shown). Both potentials were below threshold for spontaneous firing. Hyperpolarization of V_m did not affect uIPSC peak amplitude (uIPSC1 V_{rest} 834±346 pA, $V_{hyperpol}$ 802±332, p=0.39; uIPSC1 $V_{hyperpol}/V_{rest}$ 0.97±0.02) or short-term depression in response to trains of presynaptic action potentials (3 APs at 50 Hz) (uIPSC2/1 V_{rest} 0.57±0.02, $V_{hyperpol}$ 0.53±0.03, p=0.35; uIPSC3/1 V_{rest} 0.43±0.06, $V_{hyperpol}$ 0.44±0.03, p=0.79).

Noradrenergic enhancement of feed-forward inhibition requires α_2-adrenergic receptors

We wondered whether elimination of spontaneous cartwheel spiking might somehow contribute to the enhancement of feed-forward inhibition by NA. Because silencing of cartwheel cell spontaneous spiking was dependent on α_2-adrenergic receptors (Figure 3.4E-F), we tested whether α_2-receptors were similarly required for the noradrenergic enhancement of feed-forward inhibition. Current responses to parallel fiber train stimulation were recorded in fusiform cells in control conditions, then in NA (10 μM), followed by NA (10 μM) and idazoxan (1 μM) (Figure 3.6A). NA again strongly enhanced outward currents evoked by the second and third stimuli (Figure 3.6B; outward charge stim 2 control: 1425±397 pA*ms, NA: 3618±609 pA*ms, p<0.001, n=5; stim 3 control: 1158 pA*ms, NA: 4065±946 pA*ms, p<0.01, n=5). Idazoxan reduced the NA-induced enhancement of outward charge in all cells tested, resulting in a complete reversal of the NA effect on feed-forward inhibition for the second stimuli (outward charge in NA + idazoxan: 1953±526 pA*ms, comparison to control: p=0.097, n=5) and near complete reversal for the third stimulus (Figure 3.6B; 1665±419 pA*ms, comparison

to control: p=0.047, n=5). When averaged currents recorded during the baseline control period were subtracted from those recorded during co-application of NA and idazoxan, only a minor increase in the total current was revealed for each of the stimuli (Figure 3.6C-D; stim1: 193±159 pA*ms; stim 2: 610±225 pA*ms; stim 3: 572±175 pA*ms). This was in contrast to the large total charge difference following the second and third stimuli measured from currents obtained from subtraction of control traces from those obtained during NA application (Figure 3.6C-D; stim 1: 200±247 pA*ms; stim 2: 2279±263 pA*ms; stim 3: 2950±635 pA*ms). Thus, α_2-receptors were the primary adrenergic receptor subtype mediating the noradrenergic enhancement of feed-forward inhibition.

Spontaneous spiking depresses cartwheel cell synaptic transmission

The shared dependence on α_2 adrenergic receptors of noradrenergic modulation of cartwheel cell spontaneous firing (Figure 3.4) and feed-forward inhibition of fusiform cells (Figure 3.6) suggested a potential link between the two effects. Taking into account that our initial examination of cartwheel synapses onto fusiform cells demonstrated strong short-term depression at this synapse (Figure 3.5), we hypothesized the constant background spontaneous firing of cartwheel cells in control conditions would lead to persistently depressed cartwheel synaptic output. As a result of tonic synaptic depression, cartwheel-mediated IPSCs onto fusiform cells evoked by parallel fiber stimulation would be weakened in control conditions. However, the loss of spontaneous spiking in the presence of NA should permit cartwheel synapses to recover from depression and thus result in robust stimulus-evoked inputs to fusiform neurons.

As an initial examination of this hypothesis, we characterized synaptic depression at cartwheel synapses using simultaneous whole-cell recordings from connected pairs of cartwheel and fusiform neurons. Current injection was used to trigger an initial simple spike or complex spike burst (3-4 spikelets) in presynaptic cartwheel cells, which was then followed by a second simple spike at intervals between 50 ms to 15 seconds after the first simple/complex spike. The resulting uIPSCs were recorded in postsynaptic fusiform cells (example responses to initial presynaptic simple spike, Figure 3.7B; initial presynaptic complex spike, Figure 3.7C). These experiments revealed strong synaptic depression at short test intervals (intervals from 50-500 ms, depressed by 35.1±1.0% (initial simple spike) or by 69.4±0.8% (initial complex spike) of first uIPSC peak amplitude). The time courses of recovery from depression were well fitted by exponential functions with similar time constants for recovery (5.8±0.9 seconds and 5.5±0.9 seconds following an initial simple or complex spike, respectively; Figure 3.7D).

The relatively slow time course of recovery from depression at cartwheel to fusiform cell synapses indicated these synapses would likely be depressed during control conditions, since spontaneously active cartwheels typically exhibited spiking with mean interspike intervals <1 second (Figure 3.4C). To directly confirm that spontaneous spiking resulted in depression, additional recordings from connected cartwheel and fusiform pairs were performed in which constant bias current injection was used to induce presynaptic cartwheel cells to fire at various background rates (Figure 3.7E-F). These experiments demonstrated a clear relationship between presynaptic firing rate and postsynaptic uIPSC amplitude (mean spike rate range 0.7 to 13.8 Hz; uIPSC depressed from 38.0% to 89.9% of peak amplitude without background firing; Figure 3.7F). Thus,

cartwheel synapses were persistently depressed at the background firing rates observed under control conditions.

Modulation of spontaneous firing in a single presynaptic interneuron reproduces NA effect on feed-forward inhibition

If noradrenergic control of cartwheel background spiking accounts for the NA-induced changes in parallel fiber-evoked feed-forward inhibition then modulating cartwheel spontaneous spiking independent of NA should also alter feed-forward inhibition. To test this, simultaneous recordings were acquired from connected cartwheel-fusiform pairs while parallel fibers onto both cells were stimulated (Figure 3.8A). This configuration allowed us to control the firing rate of a presynaptic cartwheel using constant bias current injection while assessing any potential changes in the fusiform cell response to parallel fiber stimulation. In each experiment, stimulus position and strength was adjusted to elicit both stimulus-evoked spiking in the presynaptic cartwheel cell and feed-forward inhibition in the post-synaptic fusiform neuron.

Parallel fiber stimulus-evoked spiking in the presynaptic cartwheel was slightly changed in the absence of background spiking, with a lower probability of spiking on the first stimulus compared to the background spiking condition (compare Figure 3.8B, middle traces). Complex spikes were also sometimes more readily elicited by stimuli applied on a background of spontaneous firing. This can be attributed to differences in cartwheel excitability at the different levels of bias current injection.

More importantly, the outward component of the postsynaptic fusiform responses to the second stimulus in the train was significantly enhanced when the presynaptic

cartwheel did not spike spontaneously in all cartwheel-fusiform pairs tested (compare bottom traces in Figure 3.8B; summary for 1.4 to 6.6 Hz background presynaptic firing rates in Figure 3.8C; stim 2 mean outward charge with background firing: 1388±208 pA*ms, no background firing: 2520±366 pA*ms, $p<0.05$, n=4 pairs). Total charge measurements from traces created by subtracting averaged fusiform currents obtained during background spiking in patch-clamped presynaptic cartwheels from those recorded without presynaptic background firing (see example Figure 3.8D) demonstrated a clear enhancement of outward charge following the second stimulus (Figure 3.8E; stim 2 1173±357 pA*ms).

Thus, changing cartwheel spontaneous spiking activity by intracellular current injection alone was sufficient to alter parallel fiber-evoked feed-forward inhibition. In fact, the change in outward current following the second stimulus was remarkably similar to that observed previously in response to NA (compare Figures 1F, 6D, 8B). These results support the idea that NA enhances feed-forward inhibition by indirectly relieving cartwheel synapses from depression through elimination of spontaneous action potential firing in a small number of connected presynaptic cartwheel cells.

In contrast to the effects of NA, the response to the third stimulus was unchanged between the presynaptic background spiking versus no spiking conditions (Figure 3.8B; outward charge with background firing: 1149±494 pA*ms, no background firing: 1317±434 pA*ms, $p=0.14$, n=4 pairs). However, this likely reflected limitations of our experimental approach. In the paired recording experiments shown in Figure 3.8, parallel fiber stimuli were adjusted to evoke presynaptic cartwheel spikes reliably by the second stimulus in the train under both background spiking and no background spiking

conditions. Thus, synapses from the presynaptically recorded cartwheel cell were usually strongly depressed by the third stimulus in either condition, and therefore likely contributed a similar amount to the total current following the third stimulus both with and without background spiking. With NA application (Figures 1, 6), spontaneous rate in all presynaptic cartwheel cells, rather than a single neuron, should have been affected. The change in inhibitory input for both the second and third stimuli with NA was probably due to recruitment of multiple cartwheel cells with varying levels of stimulus-evoked parallel fiber input and/or spike thresholds.

Discussion

For diverse inhibitory cell types, stimulus-evoked action potential output occurs against a background of spontaneous spiking activity. Although background inhibitory inputs can contribute to information processing (Cafaro and Rieke, 2010; Mitchell and Silver, 2003), the presence of background activity raises the issue of whether stimulus-driven signals can be differentiated from those driven by spontaneous activity in postsynaptic targets.

We identified a neuromodulatory mechanism that robustly alters the balance between spontaneous and evoked inhibitory signals received by DCN principal neurons. By simultaneously reducing spontaneous inhibitory currents while increasing afferent-evoked inhibition, NA shifted the mode of inhibition of fusiform cells strongly in favor of inhibition driven by parallel fiber activity. This mechanism is distinct from other possible strategies for differentiating between evoked and background activity. These include coordinating stimulus-evoked activity among a population of presynaptic neurons

(Swadlow, 2002), encoding stimuli as changes in firing frequency in relation to background rates (Telgkamp and Raman, 2002), and presynaptic inhibition (Frerking and Ohliger-Frerking, 2006). These mechanisms could also potentially contribute to enhancement of signal-to-noise at the cartwheel to fusiform synapse, but their effectiveness might be limited for several reasons. First, cartwheel cells do not commonly share single excitatory input fibers, and even a single cartwheel cell can strongly inhibit postsynaptic fusiform neurons (Roberts and Trussell, 2010). Thus, activation of multiple cartwheel cells, which would depend on specific patterns activity in the granule cell population, is not necessary to affect fusiform output. Second, cartwheel cells spontaneous firing is not regular, but instead occurs in bursts, thus complicating firing rate-based representations of stimuli. Moreover, the temporal relationship between excitatory and inhibitory signals arising from parallel fiber activity might not be preserved if stimuli were simply encoded as a change in cartwheel cell firing rate. Finally, at hippocampal synapses presynaptic inhibition is proposed to function as a high-pass filter to differentiate high-frequency signals evoked by sensory stimuli from lower frequency background activity (Frerking and Ohliger-Frerking, 2006), but cartwheel cell spontaneous firing often includes high-frequency bursts of activity (i.e. complex spikes).

Indirect versus direct modulation of synaptic transmission

Presynaptic nerve terminals are common targets of neuromodulators . However, we found that the dual effects of NA upon spontaneous and evoked activity were both mediated by noradrenergic silencing of cartwheel cell spontaneous spiking, rather than a direct effect upon presynaptic release probability. By targeting cartwheel cell

spontaneous spiking, NA not only reduced spontaneous IPSCs in fusiform cells, but also indirectly strengthened stimulus-evoked cartwheel cell-mediated IPSCs by relieving cartwheel synapses from a chronically depressed state. If instead, NA had acted directly upon cartwheel terminals to enhance release probability independent of spontaneous firing, the result would likely be an enhancement of both spontaneous and stimulus-evoked output. By coordinating the strength of stimulus-evoked output with background firing rate, selective targeting of spontaneous spiking produced an enhancement of signal-to-noise ratio that would not likely be achieved by direct enhancement of release probability.

It is also informative to contrast our observations with less selective actions of neuromodulators in other brain regions. For instance, depolarization-induced release of endogenous cannabinoids from Purkinje cells suppresses both spontaneous firing and presynaptic release probability of molecular layer interneurons in the cerebellum (Kreitzer et al., 2002). Although background inhibitory input to Purkinje cell is reduced by these dual actions of endocannabinoids, evoked responses are similarly reduced due to the decrease in presynaptic release probability (Kreitzer et al., 2002).

Synaptic depression and spontaneous spiking

Our results are consistent with and extend previous studies demonstrating an important relationship between short-term synaptic depression and background firing rate. *In vitro* slice recordings have revealed suppression of postsynaptic currents by *in vivo* spontaneous activity patterns at the calyx of Held synapse (Hermann et al., 2007) and giant corticothalamic synapses between somatosensory cortex and thalamus (Groh et

al., 2008). *In vivo* studies have observed that spontaneous activity of thalamic neurons results in tonic depression of thalamocortical synapses in primary somatosensory (Castro-Alamancos and Oldford, 2002) and visual cortices (Boudreau and Ferster, 2005). Thus, depression of synaptic output by spontaneous patterns of spiking activity appears to be a common phenomenon. Our experiments show that selective control of background spike rate provides a powerful way to alter synaptic output at synapses that exhibit short-term depression. Neuromodulatory control of spontaneous firing may therefore represent a general mechanism to shift between distinct modes of signaling according to behavioral context (Castro-Alamancos and Oldford, 2002).

Inhibition of spontaneous firing by activation of α_2 adrenergic receptors

The elimination of spontaneous firing in cartwheel cells by activation of α_2 adrenergic receptors is consistent with the effects of α_2 receptors on other spontaneously active neurons (Hirono and Obata, 2006; Li and van den Pol, 2005; Solis and Perkel, 2006; Williams and North, 1985). α_2 adrenergic receptors generally mediate inhibitory actions of NA. A primary consequence of α_2 receptor activation in many cell types is the opening of G-protein-activated inwardly rectifying potassium channels (GIRKs) (Williams et al., 1985). Other effects include inhibition of voltage-gated calcium channels (Bean, 1989; Dunlap and Fischbach, 1981) and reductions in cyclic nucleotide gated (HCN) channel activity (Carr et al., 2007). The specific mechanism(s) underlying loss of spontaneous cartwheel cell firing were not examined in the present study, but previous studies have generally shown that depression of spontaneous activity by α_2 receptors is primarily a result of hyperpolarization due to GIRK channel activation (Arima et al.,

1998; Li and van den Pol, 2005; Williams et al., 1985; Williams and North, 1985). We therefore consider it likely that activation of GIRK channels underlies the loss of spontaneous spiking in cartwheel cells.

Implications for auditory processing

This study adds to growing evidence that the DCN molecular layer circuitry is subject to modifications by specific patterns of afferent activity (Fujino and Oertel, 2003; Tzounopoulos et al., 2004; Tzounopoulos et al., 2007) as well as extrinsic and intrinsic neuromodulatory systems (Bender et al., 2010; Zhao et al., 2009; Zhao and Tzounopoulos, 2011). Although the specific role of the molecular layer circuitry in auditory processing is not fully understood, the ability to flexibly adapt molecular layer output according to previous activity or physiological context may contribute importantly to DCN function (Oertel and Young, 2004). One prominent hypothesis regarding DCN function is that proprioceptive information conveyed by parallel fibers is integrated with spectral information from auditory inputs to contribute to sound localization (May, 2000; Oertel and Young, 2004; Sutherland et al., 1998). An additional proposal is that, by analogy to cerebellum-like electrosensory structures in weakly electric fish, the DCN molecular layer circuitry functions as an adaptive filter to cancel sounds that are not behaviorally relevant, such as self- or movement-generated noise (Bell et al., 2008; Oertel and Young, 2004). Importantly, both proposed functions rely upon the ability of activity in parallel fibers to recruit robust inhibition of principal neurons. By strongly enhancing parallel fiber stimulus-evoked inhibition, the actions of NA may contribute critically to the filtering of auditory signals by the cartwheel cell network. It will

therefore be important to determine under what conditions NA is released in the DCN. Similar to other brain regions, noradrenergic innervation of DCN appears to arise primarily from locus coeruleus (LC) (Klepper and Herbert, 1991; Thompson, 2003). LC neurons exhibit tonic spiking activity that is highest during awake states and absent during REM sleep. Additionally, firing in these neurons can be briefly elevated above tonic levels ("phasic" responses) when an animal attends to behaviorally relevant stimuli (Berridge and Waterhouse, 2003). How these activity patterns correspond to release of NA in the DCN remains to be investigated, but a reasonable assumption is that NA levels are elevated during vigilant states corresponding to high levels of LC activity. Thus, noradrenergic modulation of cartwheel cell output may permit selective filtering of auditory information during awake and attentive states.

Acknowledgements

We are grateful to Pierre Apostolides and Drs. Hai Huang, Haining Zhong and Craig Jahr for helpful discussions and to Elizabeth Brodeen-Kuo and Drs. Kevin Bender and John Williams for advice and suggestions on the manuscript. We thank Dr. Sascha du Lac for providing GIN and GlyT2-EGFP mice. This work was supported by NIH grants RO1DC0044050 (L.O.T.) and F31DC010120 (S.P.K.).

Figure 3.1

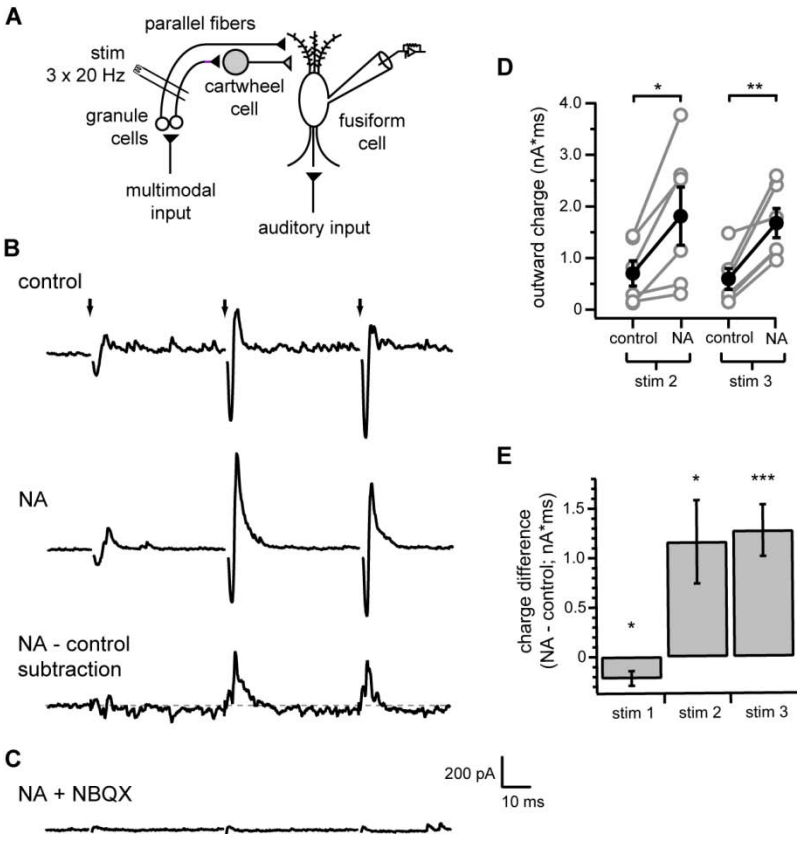

Figure 3.1. NA enhances parallel fiber-evoked feed-forward inhibition of DCN fusiform cells. (A) Simplified DCN circuit diagram. Black and gray triangles represent glutamatergic and glycinergic/GABAergic synaptic terminals, respectively. Recording and stimulus (stim) electrodes illustrate experimental configuration for B-G. (B) Example responses to identical parallel fiber stimulation (3 stimuli at 20 Hz, arrows) recorded from a fusiform cell in control conditions (top) or in 10 μM NA (middle). Bottom trace shows difference current calculated from subtraction of response in control from response in NA. Gray dotted line is zero current level. (C) NBQX eliminated both inward and outward components of evoked responses, confirming disynaptic nature of outward currents. Same cell as in B. (D) Summary of total charge of outward components (see Methods) of second and third responses in control and NA. Gray circles are data

from individual cells. Filled black circles with error bars represent mean ± SEM of outward charge measurements. NA significantly increased outward charge for both stimulus 2 (*$p<0.05$) and 3 (**$p<0.01$), n=6. (E) Summary of mean total charge measurements after each stimulus (20 ms window) determined from subtraction currents as shown in E. Charge difference significantly different from 0 pA*ms for all stimuli (stim1 *$p<0.05$, stim2 *$p<0.05$, stim3 ***$p<0.005$), one sample t-tests, n=6. In B-C, current traces are averages of 20 sweeps. Stimulus artifacts were removed from B, top and middle, and C for clarity. Scale bars apply to all current traces.

Figure 3.2

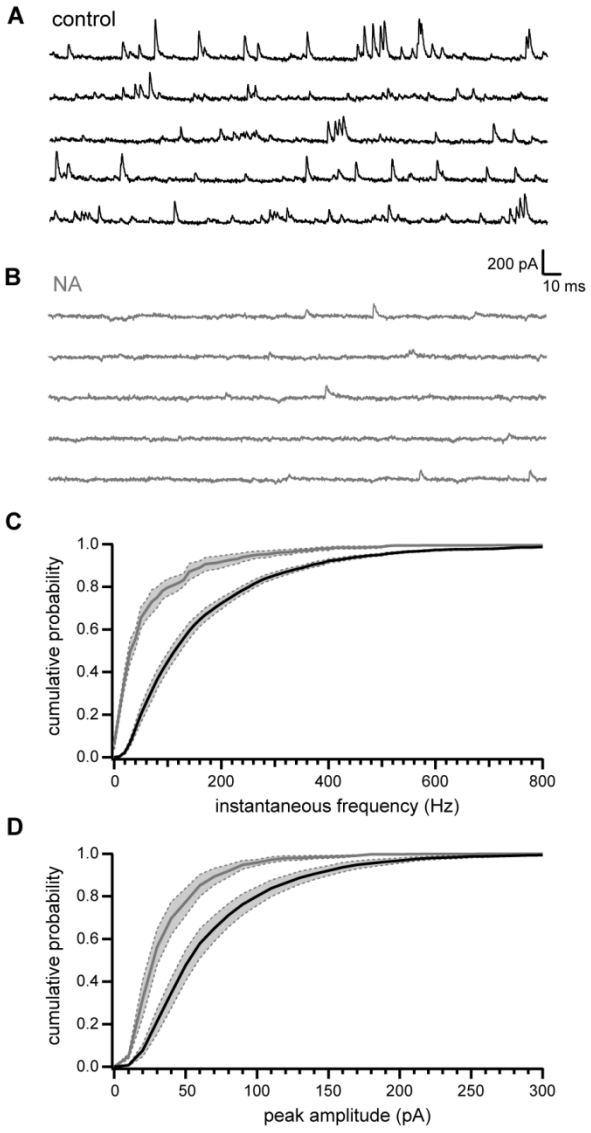

Figure 3.2. NA reduces spontaneous IPSCs recorded in fusiform cells. (A-B) Current traces recorded from an example fusiform cell in control conditions (black, A) and 10 μM NA (gray, B). Traces are from a different cell than that shown in Figure 1. (C) Cumulative probability histogram of inter-event instantaneous frequencies for fusiform cell sIPSCs. Black line and gray line are

mean sIPSC instantaneous frequencies in control and NA, respectively, n=6 cells. Dotted gray lines bounding shaded gray regions show SEM. Distributions are significantly different, $p<0.0001$, Kolmogorov-Smirnov test. (D) Same as C but for sIPSC peak amplitude measurements. Data in (B-C) from same cells as in Figure 1. Distributions are significantly different, $p<0.0001$, Kolmogorov-Smirnov test.

Figure 3.3

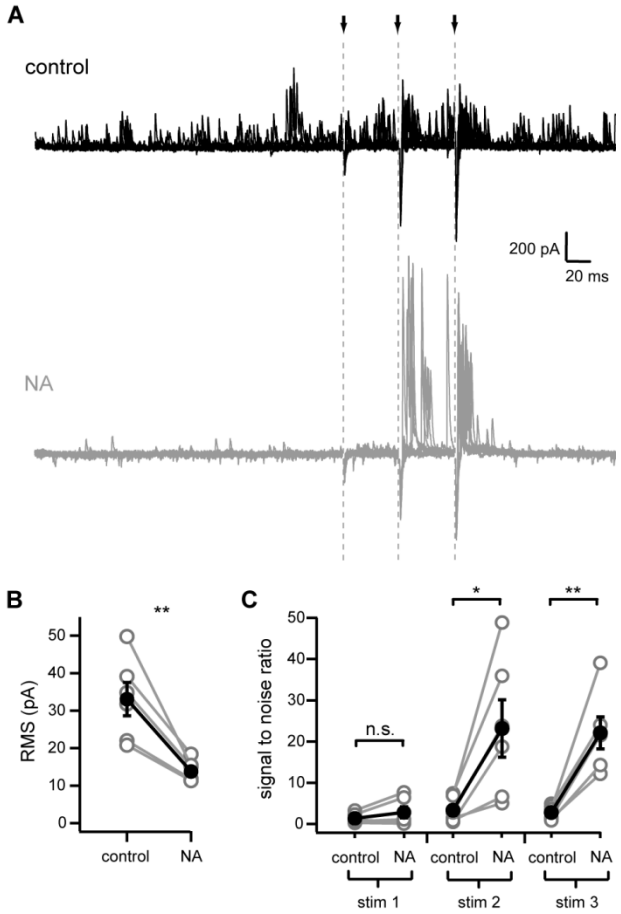

Figure 3.3. NA enhances signal-to-noise of parallel fiber-evoked inhibition. (A) Overlays of ten current traces recorded from a fusiform cell in control (black, top) and in 10 μM NA (gray, bottom). Arrows and gray dotted lines show times of parallel fiber stimulation. Same cell as in Figure 3.2A. Stimulus artifacts were removed for clarity. (B) RMS measurements in control and NA. Gray circles are data from individual cells. Filled black circles with error bars are mean±SEM. **p< 0.005, n=6. (C) Signal-to-noise ratios calculated by dividing peak amplitude of outward currents following each stimulus by RMS measurements. *p< 0.02, **p<0.005, n=6. Data from same cells shown in Figures 3.1 and 3.2.

Figure 3.4

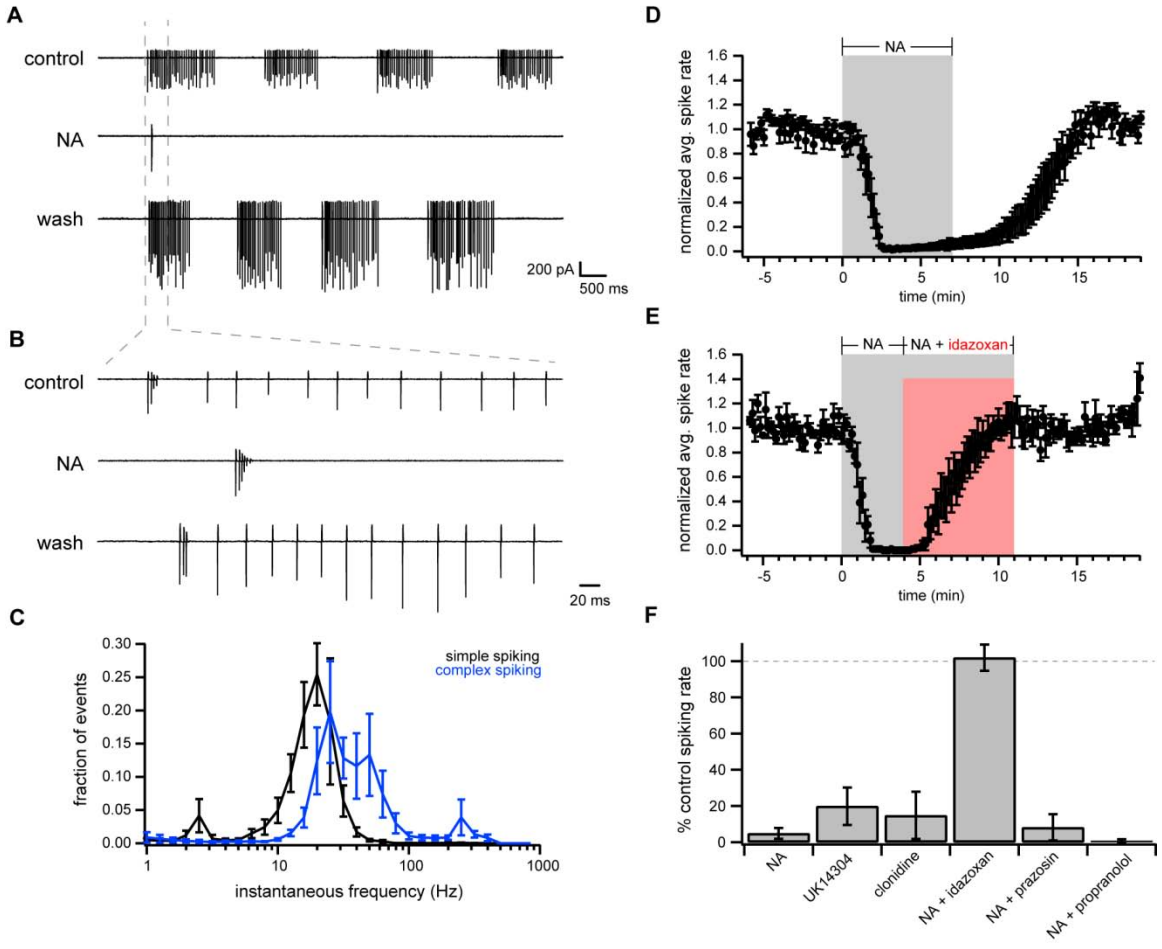

Figure 3.4. NA eliminates cartwheel cell spontaneous spiking via α_2 adrenergic receptors. (A) Example loose cell-attached recording from spontaneously spiking cartwheel in control (top), NA (10 μM; middle), and after washout of NA (bottom). (B) Region of traces from A within gray dotted lines with expanded time base. Note presence of both complex and simple spikes in this cell. (C) Normalized histogram of instantaneous spike frequencies from cartwheels with primarily simple spikes (simple spiking, black; defined as cells with <1% of interspike intervals >100 Hz, n= 5) and those with both complex and simple spikes (complex spiking, blue; >1% interspike intervals ≥100 Hz, n=6). (D) Time course of spontaneously cartwheel cell spike rate normalized to mean baseline rate. NA (10 μM) was bath applied during time demarcated by gray box. n=6.

(E) Time course of spontaneously spiking cartwheel cell responses to NA (10 μM; gray box) followed by co-application of NA with idazoxan (1 μM; light red box). n=5 cells. Filled circles and error bars in D-E are mean ± SEM. (F) Summarized data (mean ± SEM) for spontaneously spiking cartwheel responses with respect to baseline spike rate. NA data is from cells shown in D. NA + idazoxan data is from cells shown in E. UK14304: 1 μM, n=8; clonidine: 5 μM, n=4; prazosin: 0.1 μM, n=4; propranolol: 20 μM, n=6. All groups are not significantly different from NA group with the exception of NA + idazoxan ($p<0.0002$), which is not significantly different from 100% of control spike rate ($p=0.80$, one sample t-test).

Figure 3.5

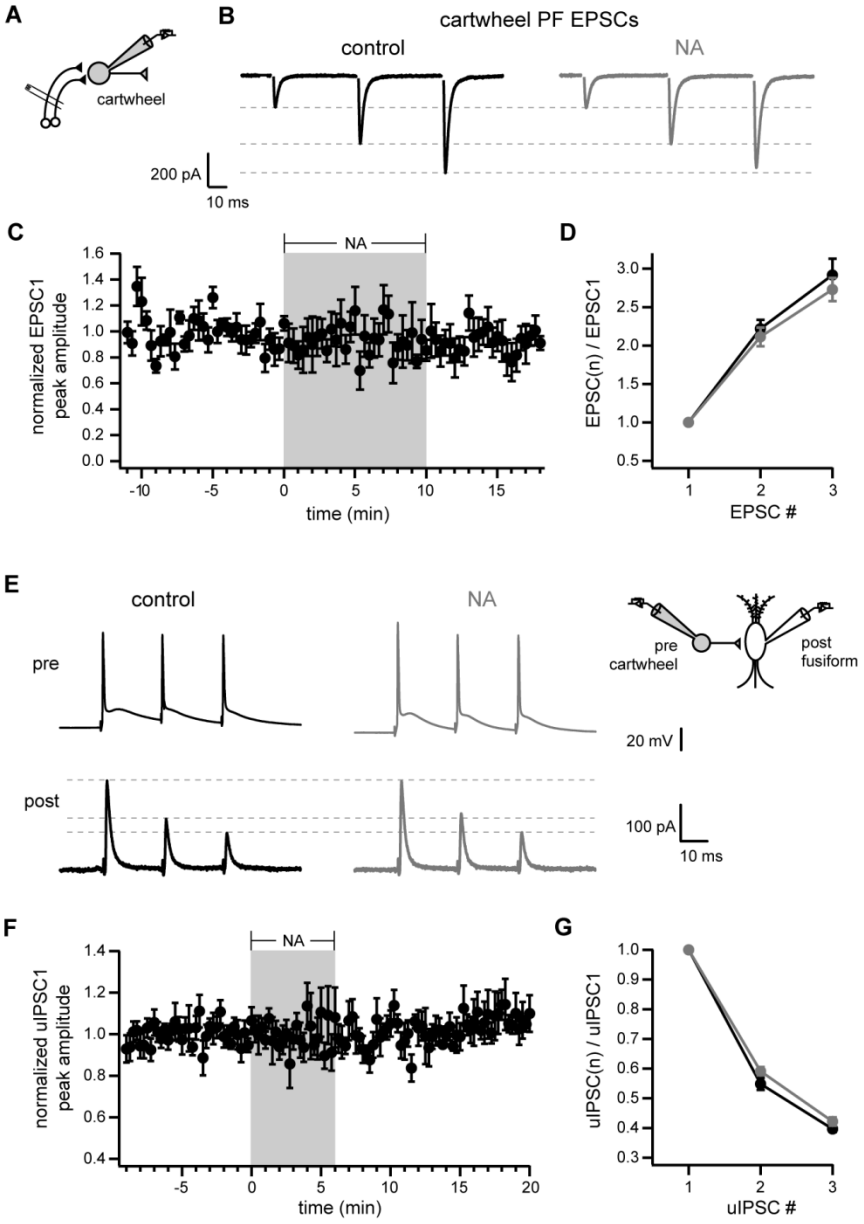

Figure 3.5. No direct effect of NA on parallel fiber or cartwheel synapses. (A) Experimental configuration for B-D. (B) Average current traces from example cartwheel cell in control (black, left) and 10 μM NA (gray, right). Stimulus artifacts were removed for clarity. (C) Time course of peak amplitudes of first PF EPSC normalized to mean baseline peak amplitude. NA (10 μM) bath applied during period outlined by gray box. (D) Ratios of EPSC peak amplitudes with respect to first EPSC. Black is control data, gray shows responses in NA. C-D, n=6. No significant

differences between control and NA. (E) Example simultaneous recordings from synaptically connected cartwheel (top, single voltage traces) and fusiform (bottom, averaged current traces). Brief, suprathreshold current injections were applied to presynaptic cartwheel to elicit train of three simple spikes at 50 Hz. Black traces (left) recorded in baseline control conditions. Gray traces (right) recorded in 10 μM NA. Inset shows recording configuration. (F) Time course of first uIPSC peak amplitude normalized to mean baseline uIPSC peak amplitude. 10 μM NA bath applied during gray box. (G) Ratios of uIPSC peak amplitudes with respect to first uIPSC. Black, control; gray, NA. F-G, n=6. No significant differences between control and NA.

Figure 3.6

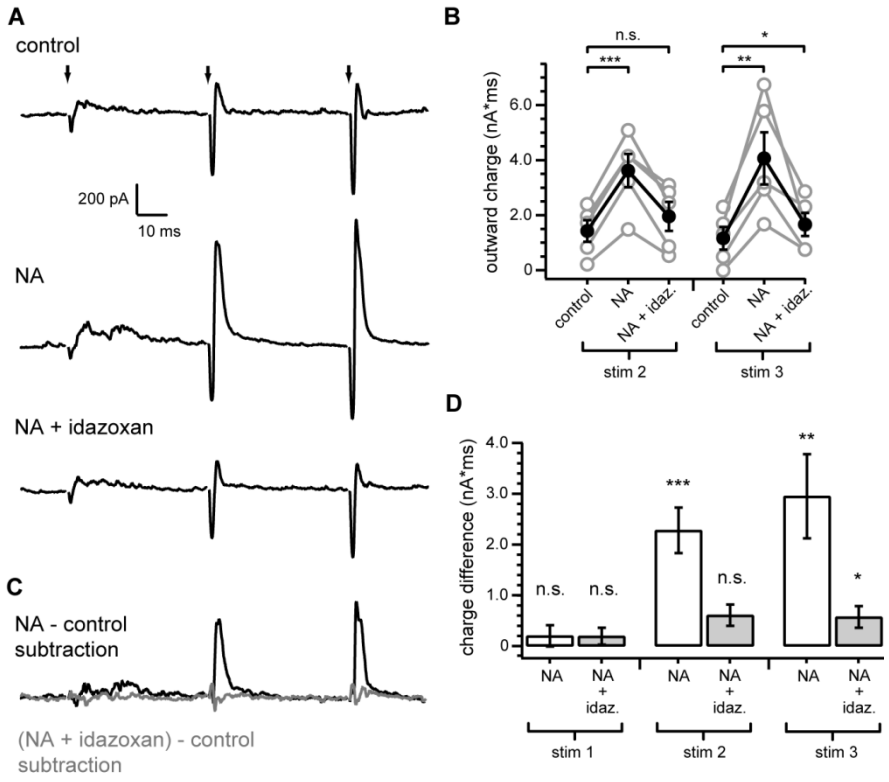

Figure 3.6. Noradrenergic enhancement of feed-forward inhibition requires α2 adrenergic receptors. (A) Top, example fusiform cell averaged response to train stimuli of parallel fiber inputs (3 stim at 20 Hz) (identical experimental configuration to Figure 1). Middle, response of same cell to identical stimulus, but in NA (10 μM). Bottom, subsequent response of same cell to same stimulus, with co-application of idazoxan (1 μM) and NA. (B) Summary of outward charge measurements for second and third stimuli. Gray circles are data from individual cells. Filled black circles with error bars show mean ± SEM. Outward charge after second stimulus was significantly increased from control in NA (***$p < 0.001$), but not in NA + idazoxan ($p=0.1$). Outward charge after third stimulus was significantly increased from control in NA (**$p<0.01$) and slightly, but significantly, increased in NA + idazoxan (*$p=0.047$), n=5. (C) Subtraction of response in control (A, top) from response in NA (A, middle) is shown in black. Subtraction of

response in control (A, top) from response in NA+ idazoxan (A, bottom) is shown in gray. (D) Summary of mean total charge measurements after each stimulus (20 ms window) from subtracted currents as shown in E. Charge difference measurements are significantly different from 0 pA*ms for stim2 NA (***$p<0.002$) and stim3 NA (**$p<0.01$) and NA + idazoxan (*$p<0.05$), but not for stim1 NA ($p=0.46$) and NA + idazoxan ($p=0.29$) or stim2 NA + idazoxan ($p=0.053$), one sample t-test, n=5. Stimulus artifacts in (A) were blanked for clarity. Current traces are averages from 20 consecutive sweeps. Scale bars apply to all current traces.

Figure 3.7

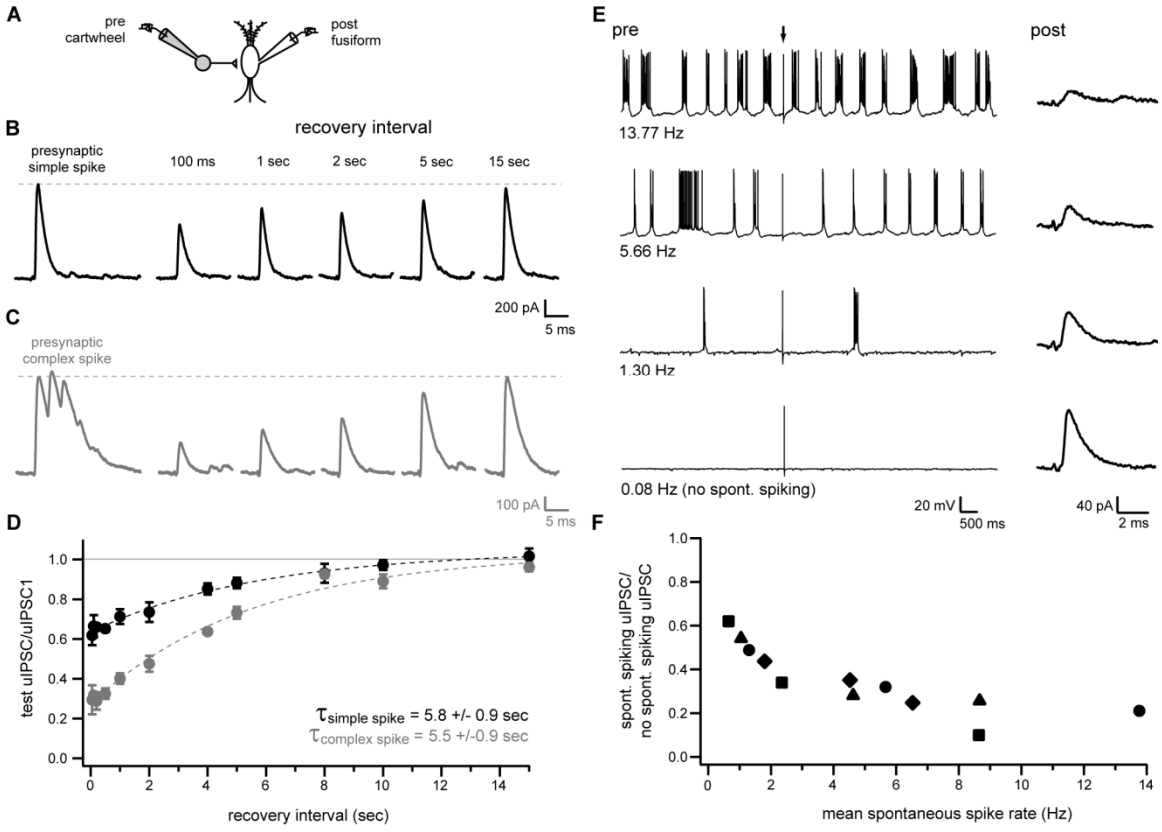

Figure 3.7. Depression of cartwheel synapses during spontaneous spiking. (A) Recording configuration for B-F. (B-C) Postsynaptic fusiform cell responses to simple (B, black) or complex (C, gray) spikes in presynaptic cartwheel cell (leftmost traces) and to subsequent presynaptic simple spikes elicited at various time intervals after the initial simple or complex spikes. Presynaptic spikes were elicited by brief, suprathreshold current injection. Presynaptic cartwheels were either not spontaneously active, or were held below threshold for spontaneous activity by steady bias current injection for the duration of experiments in B-D. Traces in B and C are from different pairs and are averages of 8-15 sweeps. (D) Summary of experiments as in B and C plotted as ratio of uIPSC peak amplitudes at different recovery intervals with respect to peak amplitude of response to initial simple spike (black circles; n=5 pairs except for 100 ms interval, n=4) or first spikelet of initial complex spike (gray circles; n=5 pairs except for 50 ms, 100 ms,

200 ms and 10 s intervals, n=4). Dotted lines are exponential fits to the data. (E) Left traces show example voltage records from a presynaptic cartwheel cell held at different mean spontaneous firing rates by steady bias current injection. Arrow indicates time at which brief intracellular current injection was applied to elicit a single simple spike. Right traces show average currents (12-19 sweeps) recorded from postsynaptic fusiform cell in response current injection-triggered simple spikes in presynaptic cartwheels (arrow; 12 seconds between injections) at the different presynaptic spontaneous firing rates. (F) Summary of experiments as shown in (E). Data for different spontaneous rates plotted as peak uIPSC amplitude with respect to uIPSC peak amplitude without background spontaneous firing (0.08 Hz condition). n=4 pairs (data points with shared symbols are from same pairs).

Figure 3.8

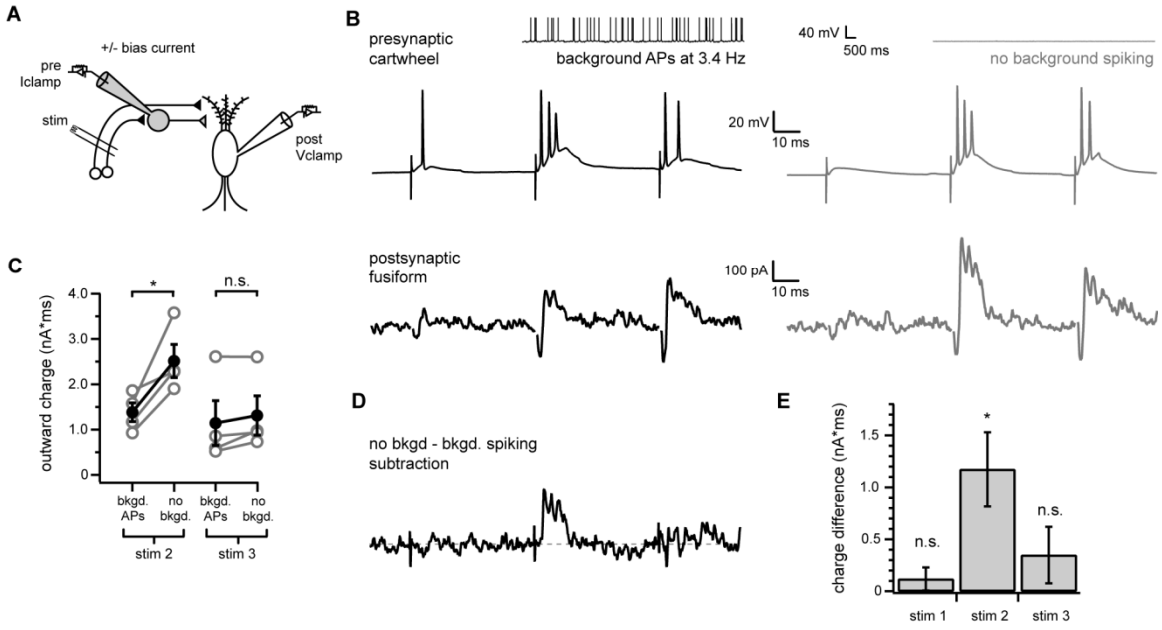

Figure 3.8. Modulation of cartwheel spontaneous spiking alters feed-forward inhibition of fusiform cells. (A) Experimental configuration. (B) Example traces from connected cartwheel-fusiform pair in response to train stimulation of parallel fiber inputs to both cells. The presynaptic cartwheel (top traces) was held in current clamp and steady bias current was applied to induce the cell to either spike spontaneously (black traces on left, see inset, mean background firing rate was 3.4 Hz), or to remain silent (gray traces on right) in the absence of parallel fiber stimulation. Bottom traces show average fusiform cell responses to parallel fiber stimulation measured in voltage clamp under either presynaptic firing condition. Note enhancement of outward component of fusiform response to second parallel fiber stimulus without background presynaptic spiking (gray trace) compared to responses during background presynaptic firing (black trace). Stimulus artifacts were removed from fusiform cell current traces for clarity. (C) Summary of outward charge measurements for second and third stimuli for experiments as shown in A, n=4 pairs. Gray circles show data for individual pairs. Filled black circles with error bars show mean±SEM for all pairs. The outward component of the response to the second parallel fiber

stimulus was significantly larger when presynaptic cartwheels were not spiking spontaneously ('no bkgd.') compared to when they were induced to fire spontaneously ('bkgd APs'), *p< 0.05. (D) Difference current from subtraction of fusiform current trace shown on left in B (presynaptic background APs) from trace shown in B, right (no background spiking condition). (E) Summary of mean total charge measurements after each stimulus (20 ms window) between no background and background spiking conditions determined from subtraction currents as shown in D. Charge difference significantly different from 0 pA*ms for stim2 (*p<0.05), but not stim 1 or stim 3 (p=0.36, 0.29, respectively), one sample t-test, n=4.

Figure 3.S1

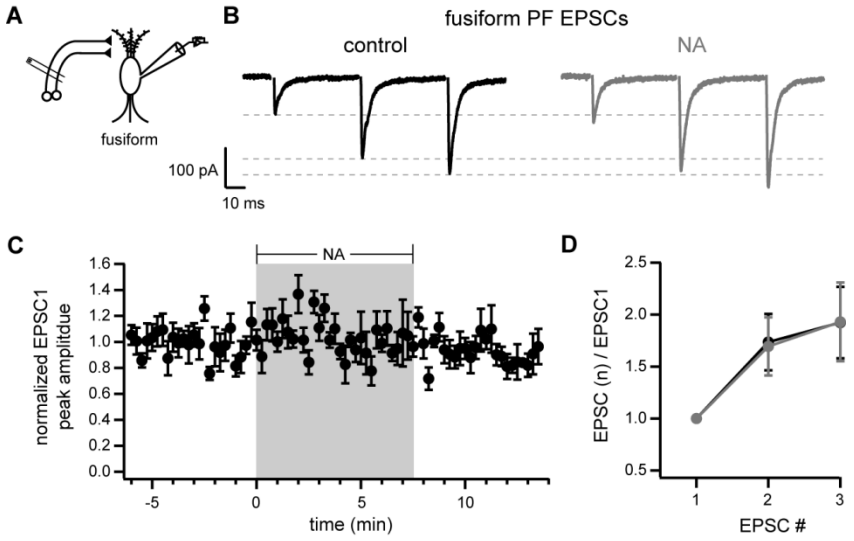

Figure 3.S1. Fusiform cell parallel fiber EPSCs not affected by NA. (A) Recording configuration. (B) Averaged current responses to parallel fiber stimulation (3 stimuli at 20 Hz) in an example fusiform cell in control (black, left) and in NA (gray, right). (C) Time course of peak amplitude of first PF EPSC normalized to mean baseline peak amplitude. NA (50 μM) was bath applied during time period demarcated by gray box. (D) Ratios of EPSC peak amplitudes with respect to first EPSC. Black is control data, gray shows responses in NA. n=5. No significant differences between control and NA.

SUMMARY AND CONCLUSIONS

The work presented in the preceding chapters was undertaken with the general goal of elucidating mechanisms of inhibitory synaptic transmission in the auditory brainstem cochlear nuclei. By examining the physiology of inhibitory synapses and inhibitory neurons in avian and mammalian auditory brainstem circuits, I sought to clarify some of the basic cellular properties that define how inhibition contributes to the encoding of acoustic signals at the earliest stage of auditory processing.

In Chapter 1, I examined inhibition in the chick auditory brainstem. A striking anatomical feature of the avian brainstem is that inhibitory input to functionally and anatomically distinct auditory nuclei primarily arises from a shared source, the ipsilateral superior olivary nucleus (Burger et al., 2005; Lachica et al., 1994). I discovered that inhibitory currents in the different divisions of the avian cochlear nuclei, nMag and nAng, as well as in downstream targets of nMag neurons in nLam, exhibited different time courses. Because the duration of postsynaptic currents has a critical role in determining the impact of inhibitory input, the kinetic differences observed here suggest potentially different roles for inhibition, despite a common origin in the SON. This is consistent with the distinct computational roles of the different brainstem nuclei in sound processing. The slow time course of inhibitory currents in from nMag neurons has previously been proposed to contribute to a tonic form of inhibition that enhances the ability of nMag neurons to faithfully relay temporal information to nLam (Lu and Trussell, 2000). The faster kinetics of inhibitory currents in nLam and a subset of nAng neurons may serve a more phasic role, although this will need to be explored further. Of note, inhibitory current kinetics ranged from fast to slow in nAng neurons, which is

consistent with potential diverse roles for nAng in auditory processing (Carr and Soares, 2002). An additional finding was that inhibitory currents in nAng were mediated by both glycine and $GABA_A$ receptors whereas, consistent with previous work, those in nMag and nLam were mediated solely by $GABA_A$ receptors (Funabiki et al., 1998; Lu and Trussell, 2000). Interestingly, immunohistochemical labeling for inhibitory neurotransmitters indicated that both GABA and glycine are present in nerve terminal-like structures in nAng, nMag and nLam. Thus, differential postsynaptic receptor expression likely contributed to the distinct pharmacology of inhibitory currents among the different nuclei.

In Chapters 2 and 3, I examined inhibition in the mouse DCN, which contrasts from the avian brainstem in that multiple, functionally distinct sources of inhibition converge upon DCN principal neurons. In Chapter 2, I studied vertical cells, which provide inhibition associated with auditory inputs in the deep layer of the DCN. In Chapter 3, I investigated inhibition mediated by cartwheel cells, which respond to multimodal sensory input and are part of the superficial molecular layer circuitry of the DCN.

Based upon *in vivo* evidence, vertical cells are proposed to provide powerful feed-forward inhibition that contributes to sound spectrum analysis in DCN principal cells (Young and Davis, 2002). Central to this hypothesis, vertical cells are thought to provide narrowly tuned inhibitory input that increases in strength in direct relation to sound level. From the patch-clamp recordings described in Chapter 2, vertical cell intrinsic spiking properties and excitatory synaptic inputs appear suited to produce sensitivity to sound intensity, which is encoded as changes in auditory nerve firing rate (Sachs and Abbas,

1974). However, paired whole-cell recordings revealed that although vertical cells form synaptic contacts upon fusiform cells with moderate connection probability, these connections were usually weak, particularly when compared to those between presynaptic cartwheel cells and fusiform neurons. Further experiments suggested that activity in multiple vertical cells is necessary to gate fusiform cell output.

The narrow frequency tuning of vertical cell activity is thought to arise primarily from the restriction of vertical cell dendrites to isofrequency bands within the tonotopic organization of auditory inputs to the DCN (Rhode, 1999). However, inhibition may also contribute since vertical cells exhibit inhibitory responses to non-characteristic frequency tones (Rhode, 1999; Spirou et al., 1999). Using paired recordings, I found that vertical cells form synaptic contacts upon other vertical cells with a high probability. Although not conclusive, this finding raises the possibility that inhibition from other vertical cells contributes to the narrow frequency tuning of vertical cells.

Finally, current-clamp recordings revealed that vertical cells exhibit a range of intrinsic firing properties. Unexpectedly, a large proportion (~35%) of vertical cells could fire persistently beyond the period during which they received excitatory input. Whether and how such behavior contributes to DCN output is unclear, but the diversity of spiking responses observed here suggests vertical cell behavior is more complex than previously recognized.

In Chapter 3, I examined the interaction between spontaneous and evoked inhibitory transmission mediated by cartwheel cells. Similar to many other inhibitory neuron types in the brain, cartwheel cells spike spontaneously both *in vivo* and *in vitro* ((Davis et al., 1996b; Kim and Trussell, 2007). This raises the issue of how stimulus-

evoked inhibitory signals mediated by cartwheel cells are differentiated from those arising from spontaneous activity. I found that noradrenaline could dramatically shift the balance between spontaneous and evoked cartwheel cell mediated inhibition in postsynaptic fusiform neurons, resulting in an enhanced signal to noise ratio for stimulus-evoked inhibition. Further, I demonstrated that a remarkably simple mechanism accounts for the alterations in both spontaneous and evoked inhibition. By eliminating cartwheel spontaneous spiking, NA not only strongly reduced spontaneous inhibitory input to fusiform neurons, but also allowed cartwheel synapses to recover from chronic synaptic depression and therefore enhanced glycine release in response to spiking elicited by parallel fiber stimulation. This mechanism may have general relevance for the regulation of spontaneous versus stimulus-evoked activity in other neurons. Although further experiments will be required to establish whether and how NA is released within the DCN, the work presented here adds to growing evidence that neuromodulatory inputs can powerfully regulate DCN function (Bender et al., 2010; Zhao and Tzounopoulos, 2011).

REFERENCES

Alger, B.E., and Nicoll, R.A. (1980). Spontaneous inhibitory post-synaptic potentials in hippocampus: mechanism for tonic inhibition. Brain Res *200*, 195-200.

Alle, H., and Geiger, J.R. (2006). Combined analog and action potential coding in hippocampal mossy fibers. Science *311*, 1290-1293.

Arenz, A., Silver, R.A., Schaefer, A.T., and Margrie, T.W. (2008). The contribution of single synapses to sensory representation in vivo. Science *321*, 977-980.

Arima, J., Kubo, C., Ishibashi, H., and Akaike, N. (1998). alpha2-Adrenoceptor-mediated potassium currents in acutely dissociated rat locus coeruleus neurones. J Physiol *508 (Pt 1)*, 57-66.

Awatramani, G.B., Turecek, R., and Trussell, L.O. (2004). Inhibitory control at a synaptic relay. J Neurosci *24*, 2643-2647.

Awatramani, G.B., Turecek, R., and Trussell, L.O. (2005). Staggered development of GABAergic and glycinergic transmission in the MNTB. J Neurophysiol *93*, 819-828.

Bagnall, M.W., McElvain, L.E., Faulstich, M., and du Lac, S. (2008). Frequency-independent synaptic transmission supports a linear vestibular behavior. Neuron *60*, 343-352.

Bagnall, M.W., Stevens, R.J., and du Lac, S. (2007). Transgenic mouse lines subdivide medial vestibular nucleus neurons into discrete, neurochemically distinct populations. J Neurosci *27*, 2318-2330.

Bean, B.P. (1989). Neurotransmitter inhibition of neuronal calcium currents by changes in channel voltage dependence. Nature *340*, 153-156.

Bell, C.C., Han, V., and Sawtell, N.B. (2008). Cerebellum-like structures and their implications for cerebellar function. Annu Rev Neurosci *31*, 1-24.

Bender, K.J., Ford, C.P., and Trussell, L.O. (2010). Dopaminergic modulation of axon initial segment calcium channels regulates action potential initiation. Neuron *68*, 500-511.

Berridge, C.W., and Waterhouse, B.D. (2003). The locus coeruleus-noradrenergic system: modulation of behavioral state and state-dependent cognitive processes. Brain Res Brain Res Rev *42*, 33-84.

Blackstad, T.W., Osen, K.K., and Mugnaini, E. (1984). Pyramidal neurones of the dorsal cochlear nucleus: a Golgi and computer reconstruction study in cat. Neuroscience *13*, 827-854.

Boord, R.L. (1968). Ascending projections of the primary cochlear nuclei and nucleus laminaris in the pigeon. J Comp Neurol *133*, 523-541.

Boudreau, C.E., and Ferster, D. (2005). Short-term depression in thalamocortical synapses of cat primary visual cortex. J Neurosci *25*, 7179-7190.

Burger, R.M., Cramer, K.S., Pfeiffer, J.D., and Rubel, E.W. (2005). Avian superior olivary nucleus provides divergent inhibitory input to parallel auditory pathways. J Comp Neurol *481*, 6-18.

Cafaro, J., and Rieke, F. (2010). Noise correlations improve response fidelity and stimulus encoding. Nature *468*, 964-967.

Carr, C.E., Fujita, I., and Konishi, M. (1989). Distribution of GABAergic neurons and terminals in the auditory system of the barn owl. J Comp Neurol *286*, 190-207.

Carr, C.E., and Konishi, M. (1990). A circuit for detection of interaural time differences in the brain stem of the barn owl. J Neurosci *10*, 3227-3246.

Carr, C.E., and Soares, D. (2002). Evolutionary convergence and shared computational principles in the auditory system. Brain Behav Evol *59*, 294-311.

Carr, D.B., Andrews, G.D., Glen, W.B., and Lavin, A. (2007). alpha2-Noradrenergic receptors activation enhances excitability and synaptic integration in rat prefrontal cortex pyramidal neurons via inhibition of HCN currents. J Physiol *584*, 437-450.

Castro-Alamancos, M.A., and Oldford, E. (2002). Cortical sensory suppression during arousal is due to the activity-dependent depression of thalamocortical synapses. J Physiol *541*, 319-331.

Chang, S.Y., and Kim, U. (2004). Ionic mechanism of long-lasting discharges of action potentials triggered by membrane hyperpolarization in the medial lateral habenula. J Neurosci *24*, 2172-2181.

Code, R.A., and Rubel, E.W. (1989). Glycine-immunoreactivity in the auditory brain stem of the chick. Hear Res *40*, 167-172.

Dasika, V.K., White, J.A., Carney, L.H., and Colburn, H.S. (2005). Effects of inhibitory feedback in a network model of avian brain stem. J Neurophysiol *94*, 400-414.

Davis, K.A., Ding, J., Benson, T.E., and Voigt, H.F. (1996a). Response properties of units in the dorsal cochlear nucleus of unanesthetized decerebrate gerbil. J Neurophysiol *75*, 1411-1431.

Davis, K.A., Miller, R.L., and Young, E.D. (1996b). Effects of somatosensory and parallel-fiber stimulation on neurons in dorsal cochlear nucleus. J Neurophysiol *76*, 3012-3024.

Davis, K.A., and Young, E.D. (1997). Granule cell activation of complex-spiking neurons in dorsal cochlear nucleus. J Neurosci *17*, 6798-6806.

Davis, K.A., and Young, E.D. (2000). Pharmacological evidence of inhibitory and disinhibitory neuronal circuits in dorsal cochlear nucleus. J Neurophysiol *83*, 926-940.

Ding, J., and Voigt, H.F. (1997). Intracellular response properties of units in the dorsal cochlear nucleus of unanesthetized decerebrate gerbil. J Neurophysiol *77*, 2549-2572.

Dodt, H.U., Eder, M., Schierloh, A., and Zieglgansberger, W. (2002). Infrared-guided laser stimulation of neurons in brain slices. Sci STKE *2002*, pl2.

Doucet, J.R., and Ryugo, D.K. (1997). Projections from the ventral cochlear nucleus to the dorsal cochlear nucleus in rats. J Comp Neurol *385*, 245-264.

Dugue, G.P., Dumoulin, A., Triller, A., and Dieudonne, S. (2005). Target-dependent use of co-released inhibitory transmitters at central synapses. J Neurosci *25*, 6490-6498.

Dunlap, K., and Fischbach, G.D. (1981). Neurotransmitters decrease the calcium conductance activated by depolarization of embryonic chick sensory neurones. J Physiol *317*, 519-535.

Ebihara, S., Shirato, K., Harata, N., and Akaike, N. (1995). Gramicidin-perforated patch recording: GABA response in mammalian neurones with intact intracellular chloride. J Physiol *484 (Pt 1)*, 77-86.

Egorov, A.V., Hamam, B.N., Fransen, E., Hasselmo, M.E., and Alonso, A.A. (2002). Graded persistent activity in entorhinal cortex neurons. Nature *420*, 173-178.

Erisir, A., Lau, D., Rudy, B., and Leonard, C.S. (1999). Function of specific K(+) channels in sustained high-frequency firing of fast-spiking neocortical interneurons. J Neurophysiol *82*, 2476-2489.

Evans, E.F., and Nelson, P.G. (1973). The responses of single neurones in the cochlear nucleus of the cat as a function of their location and the anaesthetic state. Exp Brain Res *17*, 402-427.

Fettiplace, R., and Fuchs, P.A. (1999). Mechanisms of hair cell tuning. Annu Rev Physiol *61*, 809-834.

Freedman, R., Hoffer, B.J., Puro, D., and Woodward, D.J. (1976). Noradrenaline modulation of the responses of the cerebellar Purkinje cell to afferent synaptic activity. Br J Pharmacol *57*, 603-605.

Frerking, M., and Ohliger-Frerking, P. (2006). Functional consequences of presynaptic inhibition during behaviorally relevant activity. J Neurophysiol *96*, 2139-2143.

Friauf, E., Aragon, C., Lohrke, S., Westenfelder, B., and Zafra, F. (1999). Developmental expression of the glycine transporter GLYT2 in the auditory system of rats suggests involvement in synapse maturation. J Comp Neurol *412*, 17-37.

Fujino, K., and Oertel, D. (2003). Bidirectional synaptic plasticity in the cerebellum-like mammalian dorsal cochlear nucleus. Proc Natl Acad Sci U S A *100*, 265-270.

Fukui, I., and Ohmori, H. (2003). Developmental changes in membrane excitability and morphology of neurons in the nucleus angularis of the chicken. J Physiol *548*, 219-232.

Fukui, I., Sato, T., and Ohmori, H. (2006). Improvement of phase information at low sound frequency in nucleus magnocellularis of the chicken. J Neurophysiol *96*, 633-641.

Funabiki, K., Koyano, K., and Ohmori, H. (1998). The role of GABAergic inputs for coincidence detection in the neurones of nucleus laminaris of the chick. J Physiol *508 (Pt 3)*, 851-869.

Gardner, S.M., Trussell, L.O., and Oertel, D. (1999). Time course and permeation of synaptic AMPA receptors in cochlear nuclear neurons correlate with input. J Neurosci *19*, 8721-8729.

Gardner, S.M., Trussell, L.O., and Oertel, D. (2001). Correlation of AMPA receptor subunit composition with synaptic input in the mammalian cochlear nuclei. J Neurosci *21*, 7428-7437.

Gentet, L.J., Avermann, M., Matyas, F., Staiger, J.F., and Petersen, C.C. (2010). Membrane potential dynamics of GABAergic neurons in the barrel cortex of behaving mice. Neuron *65*, 422-435.

Gittis, A.H., Moghadam, S.H., and du Lac, S. (2010). Mechanisms of sustained high firing rates in two classes of vestibular nucleus neurons: differential contributions of resurgent Na, Kv3, and BK currents. J Neurophysiol *104*, 1625-1634.

Godfrey, D.A., Kiang, N.Y., and Norris, B.E. (1975). Single unit activity in the dorsal cochlear nucleus of the cat. J Comp Neurol *162*, 269-284.

Golding, N.L., and Oertel, D. (1997). Physiological identification of the targets of cartwheel cells in the dorsal cochlear nucleus. J Neurophysiol *78*, 248-260.

Groh, A., de Kock, C.P., Wimmer, V.C., Sakmann, B., and Kuner, T. (2008). Driver or coincidence detector: modal switch of a corticothalamic giant synapse controlled by spontaneous activity and short-term depression. J Neurosci *28*, 9652-9663.

Grothe, B. (2003). New roles for synaptic inhibition in sound localization. Nat Rev Neurosci *4*, 540-550.

Hancock, K.E., and Voigt, H.F. (2002). Intracellularly labeled fusiform cells in dorsal cochlear nucleus of the gerbil. I. Physiological response properties. J Neurophysiol *87*, 2505-2519.

Henze, D.A., and Buzsaki, G. (2001). Action potential threshold of hippocampal pyramidal cells in vivo is increased by recent spiking activity. Neuroscience *105*, 121-130.

Hermann, J., Pecka, M., von Gersdorff, H., Grothe, B., and Klug, A. (2007). Synaptic transmission at the calyx of Held under in vivo like activity levels. J Neurophysiol *98*, 807-820.

Hirata, A., Aguilar, J., and Castro-Alamancos, M.A. (2006). Noradrenergic activation amplifies bottom-up and top-down signal-to-noise ratios in sensory thalamus. J Neurosci *26*, 4426-4436.

Hirono, M., and Obata, K. (2006). Alpha-adrenoceptive dual modulation of inhibitory GABAergic inputs to Purkinje cells in the mouse cerebellum. J Neurophysiol *95*, 700-708.

Howard, M.A., Burger, R.M., and Rubel, E.W. (2007). A developmental switch to GABAergic inhibition dependent on increases in Kv1-type K+ currents. J Neurosci *27*, 2112-2123.

Howard, M.A., and Rubel, E.W. (2010). Dynamic spike thresholds during synaptic integration preserve and enhance temporal response properties in the avian cochlear nucleus. J Neurosci *30*, 12063-12074.

Hudspeth, A.J. (1989). How the ear's works work. Nature *341*, 397-404.

Hurley, L.M., Devilbiss, D.M., and Waterhouse, B.D. (2004). A matter of focus: monoaminergic modulation of stimulus coding in mammalian sensory networks. Curr Opin Neurobiol *14*, 488-495.

Irie, T., and Ohmori, H. (2008). Presynaptic GABA(B) receptors modulate synaptic facilitation and depression at distinct synapses in fusiform cells of mouse dorsal cochlear nucleus. Biochem Biophys Res Commun *367*, 503-508.

Jonas, P., Bischofberger, J., and Sandkuhler, J. (1998). Corelease of two fast neurotransmitters at a central synapse. Science *281*, 419-424.

Jones, B.E., and Friedman, L. (1983). Atlas of catecholamine perikarya, varicosities and pathways in the brainstem of the cat. J Comp Neurol *215*, 382-396.

Joris, P., and Yin, T.C. (2007). A matter of time: internal delays in binaural processing. Trends Neurosci *30*, 70-78.

Joris, P.X. (1998). Response classes in the dorsal cochlear nucleus and its output tract in the chloralose-anesthetized cat. J Neurosci *18*, 3955-3966.

Kalloniatis, M., and Fletcher, E.L. (1993). Immunocytochemical localization of the amino acid neurotransmitters in the chicken retina. J Comp Neurol *336*, 174-193.

Kim, Y., and Trussell, L.O. (2007). Ion channels generating complex spikes in cartwheel cells of the dorsal cochlear nucleus. J Neurophysiol *97*, 1705-1725.

Kim, Y., and Trussell, L.O. (2009). Negative shift in the glycine reversal potential mediated by a Ca2+- and pH-dependent mechanism in interneurons. J Neurosci *29*, 11495-11510.

Klausberger, T., Magill, P.J., Marton, L.F., Roberts, J.D., Cobden, P.M., Buzsaki, G., and Somogyi, P. (2003). Brain-state- and cell-type-specific firing of hippocampal interneurons in vivo. Nature *421*, 844-848.

Klepper, A., and Herbert, H. (1991). Distribution and origin of noradrenergic and serotonergic fibers in the cochlear nucleus and inferior colliculus of the rat. Brain Res *557*, 190-201.

Kolston, J., Osen, K.K., Hackney, C.M., Ottersen, O.P., and Storm-Mathisen, J. (1992). An atlas of glycine- and GABA-like immunoreactivity and colocalization in the cochlear nuclear complex of the guinea pig. Anat Embryol (Berl) *186*, 443-465.

Kondo, S., and Marty, A. (1997). Protein kinase A-mediated enhancement of miniature IPSC frequency by noradrenaline in rat cerebellar stellate cells. J Physiol *498 (Pt 1)*, 165-176.

Konishi, M. (2003). Coding of auditory space. Annu Rev Neurosci *26*, 31-55.

Koppl, C., and Carr, C.E. (2003). Computational diversity in the cochlear nucleus angularis of the barn owl. J Neurophysiol *89*, 2313-2329.

Kossl, M., and Vater, M. (1989). Noradrenaline enhances temporal auditory contrast and neuronal timing precision in the cochlear nucleus of the mustached bat. J Neurosci *9*, 4169-4178.

Kossl, M., Vater, M., and Schweizer, H. (1988). Distribution of catecholamine fibers in the cochlear nucleus of horseshoe bats and mustache bats. J Comp Neurol *269*, 523-534.

Kotak, V.C., Korada, S., Schwartz, I.R., and Sanes, D.H. (1998). A developmental shift from GABAergic to glycinergic transmission in the central auditory system. J Neurosci *18*, 4646-4655.

Kreitzer, A.C., Carter, A.G., and Regehr, W.G. (2002). Inhibition of interneuron firing extends the spread of endocannabinoid signaling in the cerebellum. Neuron *34*, 787-796.

Kromer, L.F., and Moore, R.Y. (1976). Cochlear nucleus innervation by central norepinephrine neurons in the rat. Brain Res *118*, 531-537.

Lachica, E.A., Rubsamen, R., and Rubel, E.W. (1994). GABAergic terminals in nucleus magnocellularis and laminaris originate from the superior olivary nucleus. J Comp Neurol *348*, 403-418.

Leao, R.M., and Von Gersdorff, H. (2002). Noradrenaline increases high-frequency firing at the calyx of held synapse during development by inhibiting glutamate release. J Neurophysiol *87*, 2297-2306.

Lee, C.R., and Tepper, J.M. (2007). A calcium-activated nonselective cation conductance underlies the plateau potential in rat substantia nigra GABAergic neurons. J Neurosci *27*, 6531-6541.

Li, Y., and van den Pol, A.N. (2005). Direct and indirect inhibition by catecholamines of hypocretin/orexin neurons. J Neurosci *25*, 173-183.

Lien, C.C., and Jonas, P. (2003). Kv3 potassium conductance is necessary and kinetically optimized for high-frequency action potential generation in hippocampal interneurons. J Neurosci *23*, 2058-2068.

Lorente de No, R. (1981). The Primary Acoustic Nuclei (New York: Raven Press).

Lu, T., Rubio, M.E., and Trussell, L.O. (2008). Glycinergic transmission shaped by the corelease of GABA in a mammalian auditory synapse. Neuron *57*, 524-535.

Lu, T., and Trussell, L.O. (2000). Inhibitory transmission mediated by asynchronous transmitter release. Neuron *26*, 683-694.

Lu, T., and Trussell, L.O. (2001). Mixed excitatory and inhibitory GABA-mediated transmission in chick cochlear nucleus. J Physiol *535*, 125-131.

Lu, Y., Burger, R.M., and Rubel, E.W. (2005). GABA(B) receptor activation modulates GABA(A) receptor-mediated inhibition in chicken nucleus magnocellularis neurons. J Neurophysiol *93*, 1429-1438.

MacLeod, K.M., and Carr, C.E. (2005). Synaptic physiology in the cochlear nucleus angularis of the chick. J Neurophysiol *93*, 2520-2529.

MacLeod, K.M., and Carr, C.E. (2007). Beyond timing in the auditory brainstem: intensity coding in the avian cochlear nucleus angularis. Prog Brain Res *165*, 123-133.

MacLeod, K.M., Horiuchi, T.K., and Carr, C.E. (2007). A role for short-term synaptic facilitation and depression in the processing of intensity information in the auditory brain stem. J Neurophysiol *97*, 2863-2874.

Magnusson, A.K., Kapfer, C., Grothe, B., and Koch, U. (2005). Maturation of glycinergic inhibition in the gerbil medial superior olive after hearing onset. J Physiol *568*, 497-512.

Mancilla, J.G., and Manis, P.B. (2009). Two distinct types of inhibition mediated by cartwheel cells in the dorsal cochlear nucleus. J Neurophysiol *102*, 1287-1295.

Manis, P.B., Spirou, G.A., Wright, D.D., Paydar, S., and Ryugo, D.K. (1994). Physiology and morphology of complex spiking neurons in the guinea pig dorsal cochlear nucleus. J Comp Neurol *348*, 261-276.

Matsubayashi, H., Alkondon, M., Pereira, E.F., Swanson, K.L., and Albuquerque, E.X. (1998). Strychnine: a potent competitive antagonist of alpha-bungarotoxin-sensitive nicotinic acetylcholine receptors in rat hippocampal neurons. J Pharmacol Exp Ther *284*, 904-913.

Matute, C., and Streit, P. (1986). Monoclonal antibodies demonstrating GABA-like immunoreactivity. Histochemistry *86*, 147-157.

May, B.J. (2000). Role of the dorsal cochlear nucleus in the sound localization behavior of cats. Hear Res *148*, 74-87.

McCormick, D.A., Connors, B.W., Lighthall, J.W., and Prince, D.A. (1985). Comparative electrophysiology of pyramidal and sparsely spiny stellate neurons of the neocortex. J Neurophysiol *54*, 782-806.

Mitchell, S.J., and Silver, R.A. (2003). Shunting inhibition modulates neuronal gain during synaptic excitation. Neuron *38*, 433-445.

Mittmann, W., Koch, U., and Hausser, M. (2005). Feed-forward inhibition shapes the spike output of cerebellar Purkinje cells. J Physiol *563*, 369-378.

Monsivais, P., and Rubel, E.W. (2001). Accommodation enhances depolarizing inhibition in central neurons. J Neurosci *21*, 7823-7830.

Monsivais, P., Yang, L., and Rubel, E.W. (2000). GABAergic inhibition in nucleus magnocellularis: implications for phase locking in the avian auditory brainstem. J Neurosci *20*, 2954-2963.

Morisset, V., and Nagy, F. (1999). Ionic basis for plateau potentials in deep dorsal horn neurons of the rat spinal cord. J Neurosci *19*, 7309-7316.

Mugnaini, E. (1985). GABA neurons in the superficial layers of the rat dorsal cochlear nucleus: light and electron microscopic immunocytochemistry. J Comp Neurol *235*, 61-81.

Mugnaini, E., Warr, W.B., and Osen, K.K. (1980). Distribution and light microscopic features of granule cells in the cochlear nuclei of cat, rat, and mouse. J Comp Neurol *191*, 581-606.

Muller, C.M. (1987). gamma-Aminobutyric acid immunoreactivity in brainstem auditory nuclei of the chicken. Neurosci Lett *77*, 272-276.

Musicant, A.D., Chan, J.C., and Hind, J.E. (1990). Direction-dependent spectral properties of cat external ear: new data and cross-species comparisons. J Acoust Soc Am *87*, 757-781.

Nabekura, J., Katsurabayashi, S., Kakazu, Y., Shibata, S., Matsubara, A., Jinno, S., Mizoguchi, Y., Sasaki, A., and Ishibashi, H. (2004). Developmental switch from GABA to glycine release in single central synaptic terminals. Nat Neurosci *7*, 17-23.

Nelken, I., and Young, E.D. (1994). Two separate inhibitory mechanisms shape the responses of dorsal cochlear nucleus type IV units to narrowband and wideband stimuli. J Neurophysiol *71*, 2446-2462.

Oertel, D. (1999). The role of timing in the brain stem auditory nuclei of vertebrates. Annu Rev Physiol *61*, 497-519.

Oertel, D., Wu, S.H., Garb, M.W., and Dizack, C. (1990). Morphology and physiology of cells in slice preparations of the posteroventral cochlear nucleus of mice. J Comp Neurol *295*, 136-154.

Oertel, D., and Young, E.D. (2004). What's a cerebellar circuit doing in the auditory system? Trends Neurosci *27*, 104-110.

Oliva, A.A., Jr., Jiang, M., Lam, T., Smith, K.L., and Swann, J.W. (2000). Novel hippocampal interneuronal subtypes identified using transgenic mice that express green fluorescent protein in GABAergic interneurons. J Neurosci *20*, 3354-3368.

Ottolia, M., and Toro, L. (1994). Potentiation of large conductance KCa channels by niflumic, flufenamic, and mefenamic acids. Biophys J *67*, 2272-2279.

Parks, T.N., and Rubel, E.W. (1975). Organization and development of brain stem auditory nuclei of the chicken: organization of projections from n. magnocellularis to n. laminaris. J Comp Neurol *164*, 435-448.

Parks, T.N., and Rubel, E.W. (1978). Organization and development of the brain stem auditory nuclei of the chicken: primary afferent projections. J Comp Neurol *180*, 439-448.

Parra, P., Gulyas, A.I., and Miles, R. (1998). How many subtypes of inhibitory cells in the hippocampus? Neuron *20*, 983-993.

Payne, J.A., Rivera, C., Voipio, J., and Kaila, K. (2003). Cation-chloride co-transporters in neuronal communication, development and trauma. Trends Neurosci *26*, 199-206.

Pfeiffer, R.R. (1966). Classification of response patterns of spike discharges for units in the cochlear nucleus: tone-burst stimulation. Exp Brain Res *1*, 220-235.

Poronnik, P., Ward, M.C., and Cook, D.I. (1992). Intracellular Ca2+ release by flufenamic acid and other blockers of the non-selective cation channel. FEBS Lett *296*, 245-248.

Portfors, C.V., and Roberts, P.D. (2007). Temporal and frequency characteristics of cartwheel cells in the dorsal cochlear nucleus of the awake mouse. J Neurophysiol *98*, 744-756.

Pouille, F., and Scanziani, M. (2001). Enforcement of temporal fidelity in pyramidal cells by somatic feed-forward inhibition. Science *293*, 1159-1163.

Rhode, W.S. (1999). Vertical cell responses to sound in cat dorsal cochlear nucleus. J Neurophysiol *82*, 1019-1032.

Rhode, W.S., Greenberg, S. (1992). Physiology of the Cochlear Nuclei. In The Mammalian Auditory Pathway: Neurophysiology, A.N. Popper, Fay, R.R., ed. (New York: Springer Verlag).

Rhode, W.S., Smith, P.H., and Oertel, D. (1983). Physiological response properties of cells labeled intracellularly with horseradish peroxidase in cat dorsal cochlear nucleus. J Comp Neurol *213*, 426-447.

Rice, J.J., May, B.J., Spirou, G.A., and Young, E.D. (1992). Pinna-based spectral cues for sound localization in cat. Hear Res *58*, 132-152.

Roberts, M.T., Bender, K.J., and Trussell, L.O. (2008). Fidelity of complex spike-mediated synaptic transmission between inhibitory interneurons. J Neurosci *28*, 9440-9450.

Roberts, M.T., and Trussell, L.O. (2010). Molecular layer inhibitory interneurons provide feedforward and lateral inhibition in the dorsal cochlear nucleus. J Neurophysiol *104*, 2462-2473.

Roberts, P.D., and Portfors, C.V. (2008). Design principles of sensory processing in cerebellum-like structures. Early stage processing of electrosensory and auditory objects. Biol Cybern *98*, 491-507.

Rose, J.E., Brugge, J.F., Anderson, D.J., and Hind, J.E. (1967). Phase-locked response to low-frequency tones in single auditory nerve fibers of the squirrel monkey. J Neurophysiol *30*, 769-793.

Rubel, E.W., and Parks, T.N. (1975). Organization and development of brain stem auditory nuclei of the chicken: tonotopic organization of n. magnocellularis and n. laminaris. J Comp Neurol *164*, 411-433.

Rubio, M.E., and Juiz, J.M. (2004). Differential distribution of synaptic endings containing glutamate, glycine, and GABA in the rat dorsal cochlear nucleus. J Comp Neurol *477*, 253-272.

Ruigrok, T.J., Hensbroek, R.A., and Simpson, J.I. (2011). Spontaneous activity signatures of morphologically identified interneurons in the vestibulocerebellum. J Neurosci *31*, 712-724.

Ryugo, D.K., Haenggeli, C.A., and Doucet, J.R. (2003). Multimodal inputs to the granule cell domain of the cochlear nucleus. Exp Brain Res *153*, 477-485.

Ryugo, D.K., and May, S.K. (1993). The projections of intracellularly labeled auditory nerve fibers to the dorsal cochlear nucleus of cats. J Comp Neurol *329*, 20-35.

Sachs, M.B., and Abbas, P.J. (1974). Rate versus level functions for auditory-nerve fibers in cats: tone-burst stimuli. J Acoust Soc Am *56*, 1835-1847.

Saint Marie, R.L., Benson, C.G., Ostapoff, E.M., and Morest, D.K. (1991). Glycine immunoreactive projections from the dorsal to the anteroventral cochlear nucleus. Hear Res *51*, 11-28.

Salin, P.A., and Prince, D.A. (1996). Spontaneous GABAA receptor-mediated inhibitory currents in adult rat somatosensory cortex. J Neurophysiol *75*, 1573-1588.

Shofner, W.P., and Young, E.D. (1985). Excitatory/inhibitory response types in the cochlear nucleus: relationships to discharge patterns and responses to electrical stimulation of the auditory nerve. J Neurophysiol *54*, 917-939.

Shore, S.E. (2005). Multisensory integration in the dorsal cochlear nucleus: unit responses to acoustic and trigeminal ganglion stimulation. Eur J Neurosci *21*, 3334-3348.

Shore, S.E., and Zhou, J. (2006). Somatosensory influence on the cochlear nucleus and beyond. Hear Res *216-217*, 90-99.

Shu, Y., Hasenstaub, A., Duque, A., Yu, Y., and McCormick, D.A. (2006). Modulation of intracortical synaptic potentials by presynaptic somatic membrane potential. Nature *441*, 761-765.

Smith, A.J., Owens, S., and Forsythe, I.D. (2000). Characterisation of inhibitory and excitatory postsynaptic currents of the rat medial superior olive. J Physiol *529 Pt 3*, 681-698.

Smith, P.H., and Rhode, W.S. (1985). Electron microscopic features of physiologically characterized, HRP-labeled fusiform cells in the cat dorsal cochlear nucleus. J Comp Neurol *237*, 127-143.

Smith, P.H., and Rhode, W.S. (1989). Structural and functional properties distinguish two types of multipolar cells in the ventral cochlear nucleus. J Comp Neurol *282*, 595-616.

Smith, P.H., Spirou, G.A. (2002). From the Cochlea to the Cortex and Back. In Integrative Functions in the Mammalian Auditory Pathway, D. Oertel, Fay, R.R., Popper, A.N., ed. (New York: Spring Verlag).

Soares, D., and Carr, C.E. (2001). The cytoarchitecture of the nucleus angularis of the barn owl (Tyto alba). J Comp Neurol *429*, 192-205.

Soares, D., Chitwood, R.A., Hyson, R.L., and Carr, C.E. (2002). Intrinsic neuronal properties of the chick nucleus angularis. J Neurophysiol *88*, 152-162.

Solis, M.M., and Perkel, D.J. (2006). Noradrenergic modulation of activity in a vocal control nucleus in vitro. J Neurophysiol *95*, 2265-2276.

Spirou, G.A., Davis, K.A., Nelken, I., and Young, E.D. (1999). Spectral integration by type II interneurons in dorsal cochlear nucleus. J Neurophysiol *82*, 648-663.

Spirou, G.A., and Young, E.D. (1991). Organization of dorsal cochlear nucleus type IV unit response maps and their relationship to activation by bandlimited noise. J Neurophysiol *66*, 1750-1768.

Sullivan, W.E., and Konishi, M. (1984). Segregation of stimulus phase and intensity coding in the cochlear nucleus of the barn owl. J Neurosci *4*, 1787-1799.

Sutherland, D.P., Glendenning, K.K., and Masterton, R.B. (1998). Role of acoustic striae in hearing: discrimination of sound-source elevation. Hear Res *120*, 86-108.

Swadlow, H.A. (2002). Thalamocortical control of feed-forward inhibition in awake somatosensory 'barrel' cortex. Philos Trans R Soc Lond B Biol Sci *357*, 1717-1727.

Takahashi, T., Moiseff, A., and Konishi, M. (1984). Time and intensity cues are processed independently in the auditory system of the owl. J Neurosci *4*, 1781-1786.

Telgkamp, P., and Raman, I.M. (2002). Depression of inhibitory synaptic transmission between Purkinje cells and neurons of the cerebellar nuclei. J Neurosci *22*, 8447-8457.

Thompson, A.M. (2003). Pontine sources of norepinephrine in the cat cochlear nucleus. J Comp Neurol *457*, 374-383.

Trussell, L.O. (1999). Synaptic mechanisms for coding timing in auditory neurons. Annu Rev Physiol *61*, 477-496.

Turecek, R., and Trussell, L.O. (2001). Presynaptic glycine receptors enhance transmitter release at a mammalian central synapse. Nature *411*, 587-590.

Tzounopoulos, T., Kim, Y., Oertel, D., and Trussell, L.O. (2004). Cell-specific, spike timing-dependent plasticities in the dorsal cochlear nucleus. Nat Neurosci *7*, 719-725.

Tzounopoulos, T., Rubio, M.E., Keen, J.E., and Trussell, L.O. (2007). Coactivation of pre- and postsynaptic signaling mechanisms determines cell-specific spike-timing-dependent plasticity. Neuron *54*, 291-301.

Vincent, P., and Marty, A. (1996). Fluctuations of inhibitory postsynaptic currents in Purkinje cells from rat cerebellar slices. J Physiol *494 (Pt 1)*, 183-199.

Voigt, H.F., and Young, E.D. (1990). Cross-correlation analysis of inhibitory interactions in dorsal cochlear nucleus. J Neurophysiol *64*, 1590-1610.

von Bartheld, C.S., Code, R.A., and Rubel, E.W. (1989). GABAergic neurons in brainstem auditory nuclei of the chick: distribution, morphology, and connectivity. J Comp Neurol *287*, 470-483.

Warchol, M.E., and Dallos, P. (1990). Neural coding in the chick cochlear nucleus. J Comp Physiol [A] *166*, 721-734.

Waterhouse, B.D., and Woodward, D.J. (1980). Interaction of norepinephrine with cerebrocortical activity evoked by stimulation of somatosensory afferent pathways in the rat. Exp Neurol *67*, 11-34.

Wickesberg, R.E., Whitlon, D., and Oertel, D. (1991). Tuberculoventral neurons project to the multipolar cell area but not to the octopus cell area of the posteroventral cochlear nucleus. J Comp Neurol *313*, 457-468.

Wickesberg, R.E., Whitlon, D., and Oertel, D. (1994). In vitro modulation of somatic glycine-like immunoreactivity in presumed glycinergic neurons. J Comp Neurol *339*, 311-327.

Williams, J.T., Henderson, G., and North, R.A. (1985). Characterization of alpha 2-adrenoceptors which increase potassium conductance in rat locus coeruleus neurones. Neuroscience *14*, 95-101.

Williams, J.T., and North, R.A. (1985). Catecholamine inhibition of calcium action potentials in rat locus coeruleus neurones. Neuroscience *14*, 103-109.

Yang, L., Monsivais, P., and Rubel, E.W. (1999). The superior olivary nucleus and its influence on nucleus laminaris: a source of inhibitory feedback for coincidence detection in the avian auditory brainstem. J Neurosci *19*, 2313-2325.

Yau, H.J., Baranauskas, G., and Martina, M. (2010). Flufenamic acid decreases neuronal excitability through modulation of voltage-gated sodium channel gating. J Physiol *588*, 3869-3882.

Young, E.D. (1980). Identification of response properties of ascending axons from dorsal cochlear nucleus. Brain Res *200*, 23-37.

Young, E.D., and Brownell, W.E. (1976). Responses to tones and noise of single cells in dorsal cochlear nucleus of unanesthetized cats. J Neurophysiol *39*, 282-300.

Young, E.D., and Davis, K.A. (2002). Circuitry and Function of the Dorsal Cochlear Nucleus. In Integrative Functions in the Mammalian Auditory Pathway, D. Oertel, Popper, A.N., and Fay, R.R., ed. (New York: Springer Verlag).

Zafra, F., Aragon, C., Olivares, L., Danbolt, N.C., Gimenez, C., and Storm-Mathisen, J. (1995). Glycine transporters are differentially expressed among CNS cells. J Neurosci *15*, 3952-3969.

Zeilhofer, H.U., Studler, B., Arabadzisz, D., Schweizer, C., Ahmadi, S., Layh, B., Bosl, M.R., and Fritschy, J.M. (2005). Glycinergic neurons expressing enhanced green fluorescent protein in bacterial artificial chromosome transgenic mice. J Comp Neurol *482*, 123-141.

Zhang, S., and Oertel, D. (1993a). Cartwheel and superficial stellate cells of the dorsal cochlear nucleus of mice: intracellular recordings in slices. J Neurophysiol *69*, 1384-1397.

Zhang, S., and Oertel, D. (1993b). Giant cells of the dorsal cochlear nucleus of mice: intracellular recordings in slices. J Neurophysiol *69*, 1398-1408.

Zhang, S., and Oertel, D. (1993c). Tuberculoventral cells of the dorsal cochlear nucleus of mice: intracellular recordings in slices. J Neurophysiol *69*, 1409-1421.

Zhang, S., and Oertel, D. (1994). Neuronal circuits associated with the output of the dorsal cochlear nucleus through fusiform cells. J Neurophysiol *71*, 914-930.

Zhao, Y., Rubio, M.E., and Tzounopoulos, T. (2009). Distinct functional and anatomical architecture of the endocannabinoid system in the auditory brainstem. J Neurophysiol *101*, 2434-2446.

Zhao, Y., and Tzounopoulos, T. (2011). Physiological Activation of Cholinergic Inputs Controls Associative Synaptic Plasticity via Modulation of Endocannabinoid Signaling. J Neurosci *31*, 3158-3168.